

**ASSESSMENT OF SPATIO-TEMPORAL
VARIABILITY OF STREAMBED HYDRAULIC
CONDUCTIVITY: A CASE STUDY IN THE
PAVANJE RIVER, INDIA**

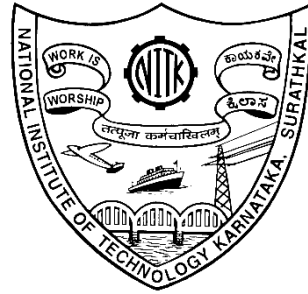
Thesis

Submitted in partial fulfilment of the requirements for the degree of

DOCTOR OF PHILOSOPHY

by

SUJAY RAGHAVENDRA N



DEPARTMENT OF APPLIED MECHANICS AND HYDRAULICS
NATIONAL INSTITUTE OF TECHNOLOGY KARNATAKA,
SURATHKAL, MANGALORE - 575025

October - 2019

D E C L A R A T I O N

I hereby *declare* that the Research Thesis entitled “Assessment of spatio-temporal variability of streambed hydraulic conductivity: A case study in the Pavanje river, India”, which is being submitted to the National Institute of Technology Karnataka, Surathkal in partial fulfilment of the requirements for the award of the Degree of Doctor of Philosophy in Water Resources Engineering is a *bonafide report of the research work carried out by me*. The material contained in this Research Thesis has not been submitted to any University or Institution for the award of any degree.

145036AM14F03, SUJAY RAGHAVENDRA N

Department of Applied Mechanics and Hydraulics
National Institute of Technology Karnataka, Surathkal

Place: NITK-Surathkal

Date:

C E R T I F I C A T E

This is to certify that the Research Thesis entitled “Assessment of spatio-temporal variability of streambed hydraulic conductivity: A case study in the Pavanje river, India” submitted by Sujay Raghavendra N (Register Number: 145036 AM14F03) as the record of the research work carried out by him, is *accepted as the Research Thesis submission* in partial fulfilment of the requirements for the award of degree of **Doctor of Philosophy**.

Prof. Paresh Chandra Deka
(Research Guide)

Prof. Amba Shetty
(Chairman - DRPC)

ACKNOWLEDGMENT

It gives me immense pleasure and innate satisfaction to express my deep sense of gratitude and indebtedness to my revered Prof. Paresh Chandra Deka to whom I owe what I have learnt in the field of Hydrology and Water Resources Engineering. His expert guidance, training and encouragement throughout has made this work possible.

My sincere thanks are due to William F. Hansen, Professional Hydrologist, US Forest Service for providing many useful insights regarding experimentation and interpretation of the results. I also owe my thanks to Dr. Sudheer Ch, Scientist D, Ministry of Environment, Forest and Climate Change, New Delhi for his valuable advice and timely guidance throughout the entire research work.

I thank Prof. Amba Shetty, Head, Department of Applied Mechanics and Hydraulics, NITK Surathkal for supporting this work. Additionally, I extend heartfelt thanks to my Research Progress Assessment Committee members for their critical evaluation and constructive comments over the research work.

I would also like to acknowledge my colleagues as well as my friends Manu D.S, Sreedhara B.M, Gireesh Mailar, Harish Kumar S, Geetha Kuntoji, Parameshwar Hiremath, Surajit Deb Barma, Abhishek Pathak, Jayakesh K, Krishnamurthy, Bhuvanamitra, Virupaksha Hebbal and Vignesh Bhat at the National Institute of Technology Karnataka for their assistance with general laboratory practices, experimentation, and encouragement throughout my tenure.

I hereby feel privileged lot and thank the Almighty for giving me a chance to recapitulate and show gratitude to the people for shaping my life in the most struggling as well as learning years.

Additionally, I would like to thank my Parents for believing in me and encouraging me to pursue a doctoral degree. They have been with me throughout my career and without them; I would not have been where I am. I profusely thank my beloved wife Latha K, sister Kumuda Anupama N and her family for their unconditional support and love during the entire period of my research work.

Also, I express my sincere thanks to all the faculty members, staff, and research scholars of the Department of Applied Mechanics and Hydraulics, N.I.T.K Surathkal for their kind co-operation, continuous support and constant encouragement.

Place: NITK, Surathkal

Sujay Raghavendra N

Date:

ABSTRACT

The hydro-geological properties of streambeds together with the hydraulic gradients determine the fluxes of water, energy and solutes between the stream and underlying aquifer system. Uncertainty in stream-aquifer interactions arises from the inherent complex-nested flow paths and spatio-temporal variability of streambed hydraulic properties. The estimation and modeling of streambed hydraulic conductivity (K_s) is an emerging interest due to its connection to water quality, aquatic habitat, and groundwater recharge.

Fragmenting streams with dams, diversions, and less frequently road culverts disrupt the longitudinal connectivity and capacity of a stream. Dam induced sedimentation affects hyporheic processes and alters substrate pore space geometries in the course of progressive stabilization of the sediment layers. The present study reports the spatial and temporal variability of streambed hydraulic conductivity along the stream reach obstructed by two Vented Dams in sequence. A detailed field investigation of streambed hydraulic conductivity using Guelph Permeameter was carried out in an intermittent stream reach of the Pavanje river basin located in the mountainous, forested tract of Western Ghats of India. Arriving at realistic statistical and spatial inference based on in-situ data collected is challenging, considering the possible sediment sources, processes, and complexity. Statistical tests such as Levene's and Welch's t-tests were employed to check for various variability measures. The strength of spatial dependence and the presence of spatial autocorrelation among the streambed K_s samples were tested by using Moran's I statistic. The measures of central tendency and dispersion pointed out reasonable spatial variability in streambed K_s distribution throughout the study reach during two consecutive years 2016 and 2017. The streambed was heterogeneous with regard to hydraulic conductivity distribution with high- K_s zones near the backwater areas of the vented dam and low- K_s zones particularly at the tail water section of vented dams. Dam operational strategies were responsible for seasonal fluctuations in sedimentation and modifications to streambed substrate characteristics (such as porosity, grain size, packing etc.), resulting in heterogeneous streambed K_s profiles. The channel downstream of vented dams contained significantly more cohesive deposits of fine sediment due to the overflow of surplus suspended

sediment-laden water at low velocity and pressure head. The statistical test results accept the hypothesis of significant spatial variability of streambed K_s but refuse to accept the temporal variations. Advanced geo-statistical techniques offer a wide range of univariate or multi-variate interpolation procedures such as kriging and variogram analysis that could be applied to these complex systems. The deterministic and geo-statistical approaches of spatial interpolation provided virtuous surface maps of streambed K_s distribution. The Moran's I index approved the presence of spatial dependence in the heterogeneous streambed K_s samples. Interpolation maps of Inverse Distance Weighting (IDW) and Radial Basis Functions (RBF) were more accurate than the krigged surface maps; however, the prediction uncertainty was lower around the sampled values in ordinary kriging estimates compared to deterministic methods.

In-situ measurement of streambed hydraulic conductivity all along the length of the stream may not be an ideal and cost-effective way. Hence, the soft computing approaches could be applied to induce a rule based relationship for estimating the values of streambed hydraulic conductivity at unmeasured locations using representative georeferenced neighborhood data. The artificial intelligence (AI) based spatial modeling schemes were tested to predict the spatial patterns of streambed hydraulic conductivity. The geographical coordinates (i.e., latitude and longitude) of the sampled locations from where the in-situ hydraulic conductivity measurements were made were used as model inputs to predict streambed K_s over spatial scale using artificial neural network (ANN), adaptive neuro fuzzy inference system (ANFIS) and support vector machine (SVM) paradigms. The statistical measures computed by using the actual versus predicted streambed K_s values of individual models were comparatively evaluated. The AI based spatial models provided superior spatial K_s prediction efficiencies with respect to both the strategies/schemes considered. The SVM model was found to predict reasonably accurate streambed K_s patterns.

CONTENTS

<i>Abstract</i>	i
<i>Contents</i>	iii
<i>List of Tables</i>	vi
<i>List of Figures</i>	vii
1. INTRODUCTION	1
1.1 General.....	1
1.2 Composition and structure of streambed.....	2
1.3 Factors affecting streambed hydraulic conductivity.....	5
1.4 Significance of streambed hydraulic conductivity estimation.....	6
1.5 Modeling spatial processes using geostatistical analysis.....	6
1.6 Modeling spatial processes using artificial intelligence paradigms	7
1.7 Vented Dam and its impacts on streambed.....	7
1.8 In-situ measurement of hydraulic conductivity using GUELPH permeameter.....	9
1.9 Scope of the present study.....	9
1.10 Organization of the Thesis.....	10
2. LITERATURE REVIEW	12
2.1 General.....	12
2.2 Influence of geological and hydrological factors on streambed hydraulic conductivity.....	12
2.2.1 Impacts of streambed composition and sediment properties.....	12
2.2.2 Impacts of stream morphology and basin topography.....	15
2.2.3 Impacts of stream stage and velocity.....	16
2.2.4 Impacts of stream water temperature and viscosity.....	18
2.3 Influence of anthropogenic activities on streambed hydraulic conductivity.....	20
2.3.1 Impacts of land use change and urbanization.....	20
2.3.2 Effects of engineering structures across or within a river/stream.....	22

2.4	Influence of biological factors on streambed hydraulic conductivity.....	25
2.5	Laboratory and in-situ methods of estimating streambed hydraulic conductivity.....	27
2.6	Statistical and geo-statistical techniques employed for the assessment of spatio-temporal variability of streambed hydraulic conductivity.....	29
2.7	Summary of literature review.....	36
2.8	Research gaps identified based on literature review.....	37
2.9	Problem formulation.....	38
2.10	Objectives of the study.....	39
3.	STUDY AREA AND DATA COLLECTION.....	40
3.1	General.....	40
3.2	Pavanje river basin.....	40
3.3	Selection of study reach.....	42
3.4	Field experiments and data collection.....	42
3.5	GUELPH Permeameter.....	45
3.5.1	Experimental procedure of GUELPH Permeameter.....	46
3.6	Grain size analysis.....	47
4.	METHODOLOGY.....	48
4.1	General.....	48
4.2	Statistical analysis.....	48
4.2.1	Normality tests.....	48
4.2.2	Test for equality of variances.....	51
4.3	Geostatistical analysis.....	53
4.3.1	Spatial autocorrelation: Moran's I.....	53
4.3.2	Spatial interpolation schemes: Deterministic approach.....	54
4.3.3	Spatial interpolation schemes: Geostatistical approach.....	55
4.4	Artificial Intelligence Paradigms.....	57
4.4.1	Artificial Neural Network.....	57
4.4.2	Adaptive Neuro-Fuzzy Inference System.....	58

4.4.3	Support Vector Machine.....	59
4.5	Strategies for spatial modeling using AI Paradigms.....	64
4.6	Performance evaluation measures.....	67
5.	RESULTS AND DISCUSSION.....	69
5.1	General.....	69
5.2	Analysis of streambed hydraulic conductivity values from in-situ GUELPH permeameter test.....	69
5.3	Variability of streambed hydraulic conductivity along the study reach.....	72
5.3.1	Results of Statistical analysis.....	72
5.3.2	Results of Geostatistical analysis.....	79
5.4	Discussion on influence of vented dams on the variability of streambed K_s	94
5.5	Results of AI based spatial models for K_s prediction.....	95
5.5.1	Performance of ANN prediction models.....	95
5.5.2	Performance of ANFIS prediction models.....	96
5.5.3	Performance of SVM prediction models.....	97
5.5.4	Comparative evaluation of AI models.....	98
5.6	Summary.....	105
6.	CONCLUSIONS & RECOMMENDATIONS.....	106
6.1	General.....	106
6.2	Conclusions.....	106
6.3	Contributions from the Study.....	108
6.4	Limitations and future scope.....	108
	REFERENCES.....	110

LIST OF TABLES

Table 2.2.1 Hydraulic conductivity of various unconsolidated sedimentary materials.....	13
Table 2.2.2 Soil classification based on saturated hydraulic conductivity values.....	14
Table 2.6.1 Statistical and Geo-statistical techniques for the assessment of variations of streambed hydraulic conductivity.....	30
Table 3.4.1 Channel configuration and streambed characteristics at the study reach.....	43
Table 5.2.1 Descriptive statistical analysis of field-scale streambed hydraulic conductivity (K_s) (cm/day).....	70
Table 5.3.1 Comparison among various Normality Tests for checking normal distribution.....	74
Table 5.3.2 Test results of Levene's and Welch's t-tests.....	79
Table 5.3.3 Performance evaluation of IDW and RBF interpolation methods.....	84
Table 5.3.4 Parameters of semivariogram models fitted to K_s data.....	87
Table 5.5.1 Performance indices of ANN modeling.....	95
Table 5.5.2 The optimal ANFIS architectures.....	96
Table 5.5.3 Performance indices of ANFIS modeling.....	96
Table 5.5.4 The optimal SVM architectures.....	97
Table 5.5.5 Performance indices of SVM modeling.....	98
Table 5.5.6 Comparative evaluation of AI models with respect to test phase.	99

LIST OF FIGURES

Figure 1.1 Generalized schematic of streambed, hyporheic and aquifer interaction.....	4
Figure 1.2 Factors affecting streambed hydraulic conductivity.....	5
Figure 1.3 A view of Vented Dams across the Pavanje River; (a) Downstream of a unregulated Vented Dam (b) Downstream of a regulated Vented Dam (c) View of both upstream and downstream of a regulated Vented Dam (d) Pair of grooves incised within the piers to stack the timber panels for flow regulation.....	8
Figure 3.1 Study Area - an intermittent stream of Pavanje River.....	41
Figure 3.2 Experimental sampling scheme.....	44
Figure 3.3 GUELPH Permeameter.....	46
Figure 4.1 Multi-layer Perceptron (MLP) Neural Network architecture	57
Figure 4.2 ANFIS architecture.....	59
Figure 4.3 Nonlinear SVM with Vapnik’s ϵ -insensitive loss function...	62
Figure 4.4. Network architecture of SVM.....	64
Figure 4.5 Spatial modeling scheme – Strategy 1.....	66
Figure 4.6 Spatial modeling scheme – Strategy 2.....	66
Figure 5.1 D50 and Mean K_s values at transects along the study reach.	71
Figure 5.2 Box and whisker plots summarizing K_s measurements of the study reach. The intrabox dots denote medians, triangles denote outliers, whiskers represent minimum and maximum values, and the box edges denote 25 th and 75 th percentiles...	73
Figure 5.3 Histograms constructed from streambed K_s samples of the year 2016.....	75
Figure 5.4 Histograms constructed from streambed K_s samples of the year 2017.....	76
Figure 5.5 Empirical CDF curve of the K-S test and the Q-Q plot of the 2016 K_s data.....	77

Figure 5.6	Empirical CDF curve of the K-S test and the Q-Q plot of the 2017 K_s data.....	78
Figure 5.7	Moran's I Spatial Correlogram for streambed K_s patterns of segment 1 which is the downstream of vented dam 1. The dots indicate the values of Moran's I at a significance level of 0.05.....	80
Figure 5.8	Moran's I Spatial Correlogram for streambed K_s patterns of segment 2 which is the streambed between vented dam 1&2.	81
Figure 5.9	Moran's I Spatial Correlogram for streambed K_s patterns of segment 3 which is the upstream of vented dam 2.....	81
Figure 5.10	Moran's I Spatial Correlogram for streambed K_s patterns considering the entire study reach.....	82
Figure 5.11	The local Moran's I scatterplot for streambed K_s patterns. The upper-right and lower-left quadrants of the scatter plot indicate positive spatial association of values that are higher and lower than the sample mean, respectively. The lower-right and upper-left quadrants include samples that exhibit negative spatial association or spatial outliers; i.e., these sampled values convey little similarity to their neighboring ones.....	83
Figure 5.12	Streambed K_s patterns interpolated through IDW and RBF methods with respect to 2016 K_s data.....	85
Figure 5.13	Streambed K_s patterns interpolated through IDW and RBF methods with respect to 2017 K_s data.....	86
Figure 5.14	Pentaspherical model for streambed K_s samples of 2016....	88
Figure 5.15	Circular model for streambed K_s samples of 2016.....	88
Figure 5.16	Exponential model for streambed K_s samples of 2017.....	89
Figure 5.17	Pentaspherical model for streambed K_s samples of 2017....	89
Figure 5.18	Krigged Streambed K_s patterns for the year 2016.....	91
Figure 5.19	Krigged Streambed K_s patterns for the year 2017.....	92

Figure 5.20 Taylor Diagrams for performance evaluation of Interpolation methods.....	93
Figure 5.21 Scatter plots of the Strategy 1 – ANN, ANFIS and SVM models during the test period.....	100
Figure 5.22 Scatter plots of the Strategy 2 – ANN, ANFIS and SVM models during the test period.....	101
Figure 5.23 Taylor diagrams plotted for comparative evaluation of the Strategy 1 – ANN, ANFIS and SVM models of test phase...	102
Figure 5.24 Taylor diagrams plotted for comparative evaluation of the Strategy 2 – ANN, ANFIS and SVM models of the test phase.....	103
Figure 5.25 Plot of RRMSE and NSE statistic of all the AI models.....	104

CHAPTER 1

INTRODUCTION

1.1 General

Soil water movement along different pathways and how long water resides in diverse soil zones are important and determine the quantity of recharge and quality of groundwater. The vertical downward flow of subsurface water is mainly controlled by gravity and the water movement in soils (homogeneous and heterogeneous) depends on hydraulic conductivity, suction potential and soil characteristics (Fox and Durnford, 2003; Menció et al., 2014). Soil hydraulic properties are highly nonlinear functions known to exhibit marked spatial variability in geologic media at various scales of observation. For instance, the hydraulic conductivity of a specific layer or substrate may control the net water movement rates and exchange among surface and groundwater systems. Streambed hydraulic conductivity is a key physical parameter, controlling the water fluxes across the stream–aquifer interface. It is highly influenced by streambed substrate characteristics (e.g., structure, effective porosity, grain size, packing), streambed alteration processes (e.g., aggradation, degradation, sedimentation, colmation, and erosion), and the configuration of stream channel geometry, floodplain connection, and streambed morphology (e.g., dunes, anti-dunes, pool-riffle sequences) (Schumm et al., 1984; Schneidewind et al., 2015). The streambed hydraulic conductivity affects the groundwater residence time and the potential for processes such as filtration, mixing, chemical interchange, decomposition, and solute transport. Variations in groundwater residence,

inflow and outflow rates could be associated with the hydraulic resistance of the clogging layer at the wetted perimeter of a streambed and river channel morphology (Katsuyama et al., 2010). The potential of groundwater recharge through streambed depends on the topography of the area, the velocity and depth of river stage and the hydro-geologic setting of the underlying aquifer.

1.2 Composition and structure of streambed

The streambed composition of various materials varying from bed load to fine-grained sediments does not exhibit constant properties or conditions of stable equilibrium, as they are subjected to alternate wet and dry conditions, swelling and shrinks, dispersion and flocculation, cracking, compaction, aggregation, experience bio-chemical changes, and structural rearrangements in channel adjustments (Reid and Frostick, 1987; Rehg et al., 2005). Bed sediments originate from soil and dead plant material brought into the water body by erosion or direct deposition, and from organic matter produced in the water body itself. Differences in material sources and types are also due to hydrologic position and scale, such as from higher gradient channels in the headwaters to low gradient valley rivers. The in-channel or near-channel degradation, therefore, could alter streams essentially into high water table swamps in a braided channel form to lower water table systems with increased drainage due to gullyng (Trimble, 2008). The heterogeneity in hyporheic and streambed substrates could be because of spatial variations in stream velocity (e.g., across-channel); streambed alteration processes (e.g., aggradation, degradation, sedimentation, colmation and erosion); the configuration of channel geometry, floodplain connection, streambed morphology (e.g., dunes, step pools, anti-dunes, reattachment bars, pool-riffle sequences, etc.) and, natural and anthropogenic disturbances (Springer et al., 1999; Zhou et al., 2014; Tonina et al., 2016).

The subsurface flow patterns and the stream–aquifer interactions via hyporheic zone are considerably more complex to characterize. It is not hard to imagine that most rivers dominated by gravel substrates have a permeable bed and a hyporheic zone with high porosity composed by gravels beneath it, and an intensive interaction exists between free surface flow and subsurface flow (Gordon et al., 2004). However, when dealing with

interactions between surface water, hyporheic zone and groundwater, spatial and temporal variability of water fluxes within the streambed exists and is related to channel bed morphology, relic valley materials, hydraulic properties (such as hydraulic conductivity, porosity), the roughness of stream substrate, and geo-hydrological processes (Kalbus et al., 2006; Valerio et al., 2010; Fleckenstein et al., 2010). Figure 1.1 presents a generalized schematic of streambed, hyporheic and aquifer interaction. The illustration (A) represents a gully form of a channel with terrace (not floodplain) with more gradient and narrow flood plain. It is a losing stream as the water table is below the channel. Illustration (B) represents a bankfull channel with floodplain connection having a lesser gradient and possibly sinuous upstream. The paleochannel and valley sediments would have a similar form as present bank full channel, just displaced somewhat within the bounds of the floodplain. Illustration (C) represents a gaining stream with riparian vegetation. The presence of riparian (streamside) vegetation directly influences a stream's physical, chemical, and biological diversity and composition. Illustration (D) represents a partially gaining and partially losing stream. This condition is common in mountainous/hilly terrains.

Depending on the amplitude of topographic variations, geometric and hydraulic properties of the streambed; the travel time, length, and depth of the groundwater flow path vary significantly from the points of recharge or collection to the points of discharge or dispersal (Tóth, 1962). Substrate modification may also be altered by runoff from impermeable surfaces, farming or clear-cutting of erodible or unstable landforms, or mining of channel substrates (Casas-Mulet et al., 2018). There are probably many such examples of local or area wide circumstances that have altered landforms that contribute to the variability of channel substrates and hydraulic conductivity. Some forces involved seem less extreme, such as wind-blown soils leaving loess deposits, tree blowdown or autumn leaf fall that could accumulate and clog channel substrates. Hurricanes, monsoons, floods, earthquakes, volcanism, plate tectonics, and severe wildfires are a few examples of extreme forces that could modify landscapes, stream morphology, and substrate materials (Schumm et al., 1984; Rosgen, 1996).

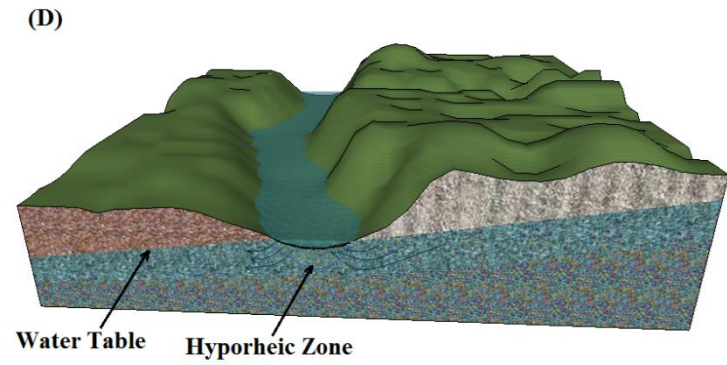
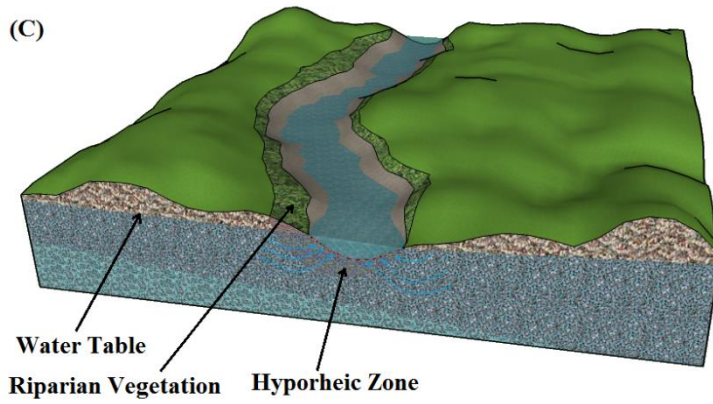
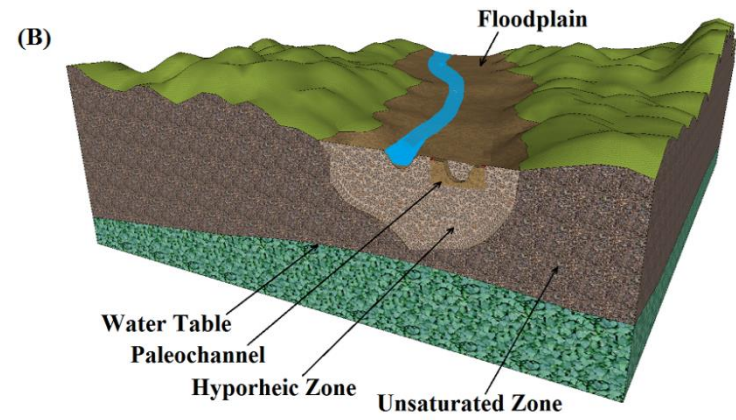
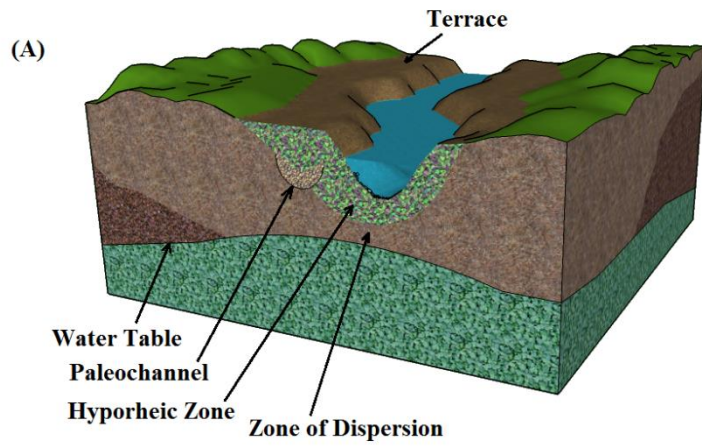


Figure 1.1 Generalized schematic of streambed, hyporheic and aquifer interaction.

1.3 Factors affecting streambed hydraulic conductivity

The factors responsible for spatio-temporal variability of streambed hydraulic conductivity could be broadly categorized into geological, hydrological, anthropogenic and biological factors (refer Figure 1.2). Exact boundaries and the influence of most of the factors is seldom sufficiently known due to the spatial and temporal complexity. Diverse geological histories and climatic conditions influence landscape and stream conditions resulting in the highly variable conditions. Most variables are categorized under hydrogeological factors such as floods, stream morphology, sediment sources and composition, and depth to impermeable sediment or bedrock (Partington et al., 2017). Biotic influences contribute to complexity such as large wood, leaves, root systems, colmation (clogging of the substrate with organic particles), and benthic macroinvertebrates. Anthropogenic disturbances such as flow regime modification by dams, artificial ditching, river channelization, and land use changes may also influence streambed structure and conductance.

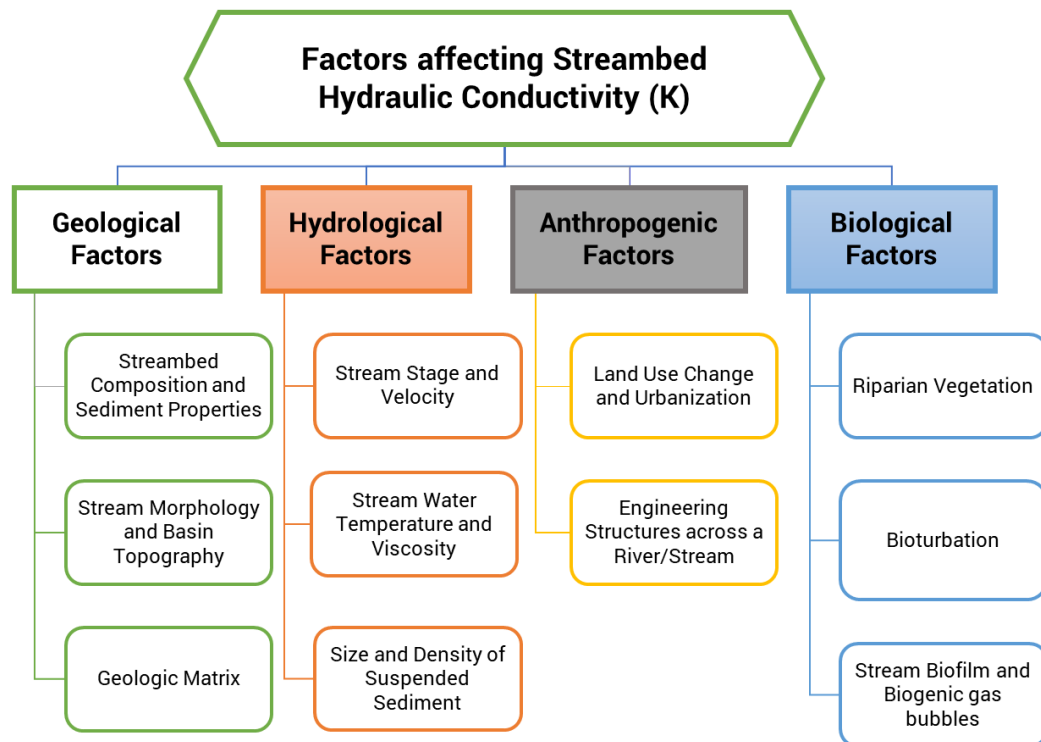


Figure 1.2 Factors affecting streambed hydraulic conductivity

1.4 Significance of streambed hydraulic conductivity estimation

Streams, rivers, wetlands, and lakes are seldom isolated, but typically hydraulically coupled or connected to some extent with underlying groundwater reservoir, with water passing back and forth with the flow interaction pattern mostly dependent on rainfall inputs, water head changes, and streambed conductance (Castro and Hornberger, 1991). The estimation and modeling of streambed hydraulic conductivity (K_s) is an emerging interest due to its connection to water quality, solute transport, and groundwater recharge. Detailed characterization of streambed may be beneficial and significant in improving our understanding of streambed hydraulic conductivity and its role in the mechanism of pollutant filtering via hyporheic zone and groundwater recharge or discharge. Determination of streambed hydraulic conductivity is important for studies designed to quantify base flow component of runoff (Cey et al., 1998; Gunduz, 2007); to quantify the impact of pumping wells on stream flow (Zume and Tarhule, 2008); to simulate regional ground water flow balances (Arnold et al., 2000); and to quantify solute transport, retention, and exchange with ground water.

1.5 Modeling spatial processes using geostatistical analysis

Geostatistical analysis refers to a set of models or tools for statistical analysis of continuous spatial data. Spatial data could be classified into three main categories namely, the spatial point data, geostatistical data, and lattice data. Spatial point data refers to a spatial process that is observed at a set of locations and the locations themselves are of interest. Geostatistical data refers to the observation of a spatial process that varies continuously at a few points e.g., mineral/soil properties at various locations. Lattice data refers to a spatial process that is observed on a regular or irregular grid. The first step in statistical data analysis is to verify three data features: dependency, distribution and stationarity. Geostatistics works best when the input data is best fitting to a Gaussian distribution. The geostatistical analyst of ArcGIS provides a variety of exploratory data analysis tools such as Kriging to accomplish the spatial modeling tasks that are aimed at understanding and modeling spatial variability.

1.6 Modeling spatial processes using artificial intelligence paradigms

Artificial intelligence (AI) based approaches are increasingly being used nowadays for the purpose of determining spatial patterns of soil processes or ecological variables (Kirkwood et al., 2016; Leuenberger and Kanevski, 2015). These models have found enormous applications in various fields such as geography, geosciences, demography etc. They are found applicable for spatial modeling of land use dynamics, spatial (environmental) processes that are non-stationary, soil nutrient dynamics, air pollution exposure modeling etc. (Forkuor et al., 2017; Grekousis et al., 2013; Reid et al., 2015). The AI based models are known to model any spatial parameter based on their inherent ability to learn complex input-output relationships even without considering any of the influencing physical factors. Dense (in-situ) sampling of any soil/ecological parameter at locations of interest may not be an ideal and cost-effective way. Hence, soft computing based approaches could be applied to induce a rule based relationship for estimating/ predicting the values of a parameter at unmeasured locations using representative geo-referenced neighborhood data. There exist several studies using artificial intelligence (AI) algorithms for predicting soil parameters such as cation exchange capacity, hydraulic conductivity, soil organic carbon, microbial diversity over spatial scales (Ghorbani et al., 2015; Dai et al., 2014; Twarakavi et al., 2009).

1.7 Vented Dam and its impacts on streambed

A Vented Dam (Figure. 1.3) is a type of low head, storage dam, which consists of a number of gateways called 'vents' throughout the stretch of the dam to regulate and stabilize the streamflow during low flow periods (Shetkar and Mahesha, 2011a,b). 'Stop-log' type of gates is employed to block the flow in Vented Dams. A number of long, rectangular, timber panels are stacked vertically between two piers, one and above the other in the grooves incised within the piers of the vented dam. The ditch between a pair of stop-logs is stuffed with fine mud to prevent water leakage that occurs amid a couple of timber panels. A series of Vented Dams are constructed along the Pavanje river reach across the third and fourth order streams for controlling and storing the surface runoff contributed

from base flow. These Vented Dams are ‘seasonal structures’ which come into operation only after monsoon retreats. During the rainy season, the vents are unregulated offering no obstruction to the flood. These Vented dams retard runoff and control sedimentation during their operation (Gowda and Mayya, 2015). The water stored in the vented dams will be used for irrigation by local farmers during the post monsoon and winter periods (October to January). The stream dries up every summer (in the months of February to May).



Figure 1.3 A view of Vented Dams across the Pavanje River; (a) Downstream of a unregulated Vented Dam (b) Downstream of a regulated Vented Dam (c) View of both upstream and downstream of a regulated Vented Dam (d) Pair of grooves incised within the piers to stack the timber panels for flow regulation

The existence of hydraulic structures such as vented dams alter the natural river flow and, as a result, affect both suspended sediment and bed load transport, leading to

adjustments such as the localized growth or erosion of deposits and changes to the carrying capacity and functions of a river. It is observed that vented dams produce changes in sediment grain size distribution, bed forms, bed slope, and riparian vegetation. They indeed affect specific stream channel responses resulting in an irregular distribution of sediment supply and therefore the streambed conductance over surface layers could vary on spatial scales.

1.8 In-situ measurement of hydraulic conductivity using GUELPH permeameter

A portable field instrument, the Guelph permeameter (GP), is a promising tool for measuring field-saturated hydraulic conductivity in remote watersheds. The procedure involves measuring the consistent rate of water flow into saturated stream sediments from a cylindrical well hole, in which a constant depth (head) of water is maintained. The measurements are made when a ‘bulb’ of saturated soil is formed around the auger hole due to flow along both vertical (gravity) and lateral (capillary) directions. The instrument can be easily carried, assembled, and operated by a single person. The measurements could be made in the range of 15 - 75 cm below the soil surface within 30 to 120 minutes, depending on the soil type (Permeameter, G.U.E.L.P.H, 2012).

1.9 Scope of the present study

Fragmenting streams with dams, diversions and sometimes culverts disrupt the longitudinal connectivity of a stream (Chen, 2004; Fanelli and Lautz, 2008). The head of water behind dam adds hydraulic pressure to increase hydraulic conductivity (K_s), but if very fine sediments and organics settle as a result into the bed substrates, the K_s may be reduced. Most of the existing research focus on how in-stream structures affect the hyporheic exchange of water and heat between the surface flow and the underlying aquifer system. The hyporheic solute exchange and flux are likely to be influenced by longitudinal streambed profile and other geomorphic factors leading to heterogeneity and anisotropy of streambed K_s (Ryan and Boufadel, 2006; Song et al., 2007; Tonina and Buffington, 2009). Liu et al. (2018) studied the dynamic processes of hyporheic exchange in a riparian zone

downstream of the Xin'an river dam and found that dams also induce thermal heterogeneity in the subsurface via infiltration. Studies have shown that intense hyporheic exchange exists in the vicinity of in-stream structures (Hester and Doyle, 2008) and the streambed hydraulic conductivity and depth of alluvium are the key factors that determine hyporheic residence time (Tonina and Buffington, 2011). The study by Rana et al. (2017) determined that a series of in-stream structures have the potential to increase transient storage than a single structure. The effect of in-stream structures on the variability of streambed hydraulic conductivity at reach scale is seldom considered, analyzed or known.

Hence, this study is intended to inform broadly on the spatial and temporal patterns of K_s along a dynamic streambed over relatively short distances (relative to the vented dams) and short time period (relative to the frequent high magnitude events). How does streambed K_s vary along the reach, upstream and downstream of a vented dam? Additionally, the premise of whether the streambed K_s has increased due to the hydraulic pressure exerted by head of water behind vented dams, or else declined due to settlement of very fine sediments and organics into the bed substrate is verified. Each situation may pose varying complexities to consider, and call for representative studies.

In-situ measurement of streambed hydraulic conductivity all along the length of the stream may not be an ideal and cost-effective way. Hence, the soft computing approaches could be applied to induce a rule based relationship for estimating the values of streambed hydraulic conductivity at unmeasured locations using representative georeferenced neighborhood data. The artificial intelligence (AI) based spatial modeling schemes were tested to predict the spatial patterns of streambed hydraulic conductivity. The applicability of several AI approaches were tested and comparatively evaluated.

1.10 Organization of the Thesis

The thesis is organized into six chapters.

Chapter 1 provides a brief overview on the composition and structure of streambed, factors that influence streambed hydraulic conductivity and its role in stream-aquifer interaction.

The relevance of geostatistical and artificial intelligence systems for spatial modeling of soil processes are discussed. It also includes the scope of proposed investigation.

Chapter 2 provides a detailed review of literature related to the variability of streambed hydraulic conductivity across diverse landscapes and stream systems. It includes a summary of available laboratory and in-situ methods of estimating streambed hydraulic conductivity. The statistical and geostatistical methods employed for spatial interpolation of streambed K_s are qualitatively evaluated in this chapter. Based on the identified research gaps, the formulated research objectives are presented.

Chapter 3 presents the description of the study area which includes the details of physiographic, geologic and climatic features of the Pavanje river basin. A brief description on field experiments carried out for data collection and the experimental procedure of Guelph permeameter are also reported.

Chapter 4 discusses, in detail, the statistical and geostatistical methods employed to evaluate the in-situ determined streambed K_s data. The details of implemented spatial modeling schemes and theoretical overview of artificial intelligence approaches considered are also included in this chapter.

Chapter 5 presents the results of statistical analysis of streambed K_s data along with the spatial interpolation maps obtained through geostatistical approaches. The performance of AI based spatial modeling schemes for the prediction of streambed K_s are also presented.

Chapter 6 reports conclusions drawn based on the research insights gained from the experimental study findings along with the limitations of the study and future scope.

CHAPTER 2

LITERATURE REVIEW

2.1 General

This chapter discusses, in detail, various geological, hydrological, anthropogenic, and biological factors that influence streambed hydraulic conductivity and summarize the available laboratory and in situ methods of estimating streambed hydraulic conductivity (K_s). The statistical and geostatistical methods employed for spatial interpolation of streambed K_s are qualitatively evaluated. The review focuses on the current status and trend of streambed hydraulic conductivity research. However, due to the complexity of this subject, it is unlikely to present all the factors concerning streambed hydraulic conductivity and its connections between streams and groundwater. Due to the limited amount of research on this subject, and also the variability across landscapes and stream systems, it is inappropriate to try to describe all the conditions that may be encountered, but it is hoped that this review will help inform broadly on the subject.

2.2 Influence of geological and hydrological factors on streambed hydraulic conductivity

2.2.1 Impacts of streambed composition and sediment properties

The geology and hydrology based physical properties and factors are sometimes difficult to separate, but geology includes earth forming and modifying events over

substantial time periods that have led to the base landforms and landscapes now present. The geologic factors that primarily influence streambed hydraulic conductivity are sediment particle size, substratum heterogeneity, longitudinal variations in impervious surfaces such as bedrock and sills, bed material depth, channel geometry, variations in hydraulic radius, and roughness due to natural and anthropogenic modifications (Jackson, 1981; Stewardson et al., 2016). The other influencing factors that are uncommon include events such as consolidation or alteration of sediments through time, volcanic, tectonic, earthquakes, folding, and fracturing and shearing of bedrock materials (King and Wood, 1994; Dale et al., 2005).

Tables 2.2.1 and 2.2.2 provide representative values of hydraulic conductivity for various unconsolidated sedimentary materials and soils interfacing with permeability classes which are sometimes applied in the discussion. The range of hydraulic conductivity varies over several orders of magnitude for each sediment particle size class, reflecting variability that might be caused by settling, clogging of fine mineral or organic particles, compaction due to the weight of eroded materials, etc. Hence, the determination of K_s is not that simple or precise, due to uncertainty in stream–aquifer interactions resulting from the inherent complex-nested flow paths and particle size differences in substrate layers that pose difficulty to make generalizations.

Table 2.2.1 Hydraulic conductivity of various unconsolidated sedimentary materials

Substrate Particle Type	Hydraulic Conductivity (m/sec)
Gravel	3×10^{-4} to 3×10^{-2}
Fine Sand	2×10^{-7} to 2×10^{-4}
Medium Sand	9×10^{-7} to 5×10^{-4}
Coarse Sand	9×10^{-7} to 6×10^{-3}
Silt, Loess	1×10^{-9} to 2×10^{-5}
Till	1×10^{-12} to 2×10^{-6}
Clay	1×10^{-11} to 4.7×10^{-9}
Un-weathered Marine Clay	8×10^{-13} to 2×10^{-9}

Source: Domenico and Schwartz (1990)

The fundamental fluvial processes through time have implications applicable for measuring and modeling streambed K_s . The well-sorted, younger, fresh sediment deposits are likely to have a greater hydraulic conductivity than the formerly entrenched valley deposits due to more frequent and more irregular vertical and lateral changes in texture. As time passes, the colluvial and alluvial deposits in the valleys with repeated wetting and drying cycles tend to settle, coalesce, and develop into soils with vegetation development and more recognizable horizons. Alluvial fan deposits at valley floors are stratigraphically complex, commonly displaying a high degree of heterogeneity in their sediment properties indicated by the variance of K_s (Hamill and Bell, 2013).

Table 2.2.2 Soil classification based on saturated hydraulic conductivity values

Permeability of Soil (according the relative permeability)	Approximate range of saturated hydraulic conductivity (m/sec)	Examples of soil types
Highly impermeable	$< 10^{-10}$	Clays with low and medium and high plasticity
Impermeable	from 10^{-8} to 10^{-10}	Gravel loams, gravel clays and sandy clays, loams with low and medium plasticity
Lowly (poorly) permeable	from 10^{-6} to 10^{-8}	Sandy loams, loamy sands and clayey sands, loamy gravels and clayey gravels
Permeable	from 10^{-4} to 10^{-6}	Sands and gravels containing fine-grained fraction (5 – 15 %)
Highly permeable	$> 10^{-4}$	Sands and gravels without or with very low fine grained fraction (<5%)

Source: ISO/TS.17892-11 (2004)

The interaction of stream–aquifer interface via hyporheic zone is often influenced by colmation (a process of plugging of the streambed substrate pores by the settling of the suspended colloidal matter leading to consolidation of the hyporheic zone and minimization the bed hydraulic conductivity). Clogged streambed sediments are characterized by tight packing and a compact texture, with a low porosity. Colmation results in a low permeability sediment layer, known as a colmatage (Brunke, 1999). If the

diameter of clogging particles is larger than pore throats of the porous medium, the particulate matter gets entrapped at pore constrictions at various depths resulting in decreased hydraulic conductivity of the porous medium. Finer-grained riverbed is more vulnerable to external clogging than coarse-grained (Rosenberry et al., 2010). The colmation/decolmation of porous media by accretion/erosion of organic and inorganic particulate matter reduces/increases the hydraulic conductivity of the porous media depending on the geometry of the porous medium. The clogging layer does not seem to be stable over the long term, because of seasonal hydrostatic pressure variations. During the rising stage of storm or flood events, the relatively abrupt shift in stream power may entrain and move particles so that the initial hydraulic conductivity of the streambed substrates could be regained by reworking the subsurface sediment structure and decolmation (Baveye et al., 1998).

2.2.2 Impacts of stream morphology and basin topography

The braided streams occur in rivers when the threshold level of sediment load significantly exceeds the single thread channel capacity resulting in the infilling or aggradation of the channel and to some extent valley surface with the development of multiple channels, often sinuous and low habitat. The braided pattern is anticipated to present the highest diversity and extent of surface and subsurface exchanges facilitating high hydrological connectivity and aquifer recharge (Tockner et al., 2009). Anastomosed channels are fairly common in tropical and subtropical low gradient systems such as marine terraces and broad valley floodplains. Anastomosed channels are braided, but stabilized in place by well-vegetated settings such as rushes and sedges or dense bottomland with often fine grain substrates; however, the gravel beds are sometimes exposed by avulsions (i.e., flow diversions) that cause the formation of new channels on the floodplain (Makaske, 2001). Extensive cohesive deposits of fine sediments across portions of floodplains having a low hydraulic conductivity add to the variability of conditions found in some anastomosed sections (Heritage et al., 2009).

In a meandering-river system, at zones where point bar accumulations of water washed sediments are accumulated, the stream water table interaction is favored with

potential ramifications for groundwater-aquifer recharge (Ward and Trimble, 2003). Nowinski et al. (2011) studied the meander-scale changes in hydraulic conductivity of an alluvial aquifer adjacent to a stream and reports the temporal patterns of hydraulic conductivity. The lower initial hydraulic conductivity zones become further less permeable due to the hyporheic transport of fine materials that are flushed from upstream decolimated areas. Straight channels are characterized by increased channel gradients, entrenchment (i.e., limited floodplain), high stream power, and erosion-resistant banks (Schumm et al., 1984; Makaske, 2001). Without high gradient, natural straight channels are unusual without some geological control such as shear lineament. Alternate bars or side bars may still exist, but be poorly formed as a consequence of steeper gradients and higher velocities. The porosity and K_s of individual bars vary across the length of bar deposits, and those with gravel deposits are expected to have higher K_s in potential recharge zones during floods (Bridge, 2003; Obana et al., 2014). Recharge from the straight river channels may be larger locally because of a fractured, sheared geology or due to coarse surficial deposits of higher K_s (Matsuda, 2004).

Streambed topography often controls the distribution of water level and substrate changes that contribute to seepage forces and alteration of K_s . The fluvial and glacial systems produce fractal distributions of recharge, discharge, and associated subsurface flow patterns (Wörman et al., 2007). Streambed facets, substrates, and bedforms control reach-scale hyporheic pore water flows. The K_s tends to increase with the amplitude of bedforms within the reach (Stewardson et al., 2016). The spatial patterns of hyporheic flow are often controlled by bed topography and channel hydraulics (Harvey and Bencala, 1993; Tonina and Buffington, 2011).

2.2.3 Impacts of stream stage and velocity

Stream stage and velocity has implications on stream power and its ability to entrain, move, redistribute, and deposit channel particles. Spatially, high gradient segments of stream channel such as riffles may be narrower with coarser substrates and a high velocity of flow, while lower gradient pool segments common to sinuous bends are wider and deeper with a tendency to accumulate finer materials with lower K_s values. Natural

disturbances could sometimes promote change and rejuvenation as the fine bed material is scoured away when disturbed during torrential flows or periods of groundwater influx that helps to backflush fines, resulting in an increase in the hydraulic conductivity (Hannula and Poeter, 1995; Hatch et al., 2010). However, it is difficult to generalize these changes for all substrates, as some become embedded and compacted through time, may be stabilized by vegetation and do not easily break up during high flows. There is a substantial difference in the erosion capacity between clean and sediment-laden waters.

Flood events could induce temporal changes in streambed elevation and particle size composition, influencing the bed's hydraulic properties and stream-aquifer fluxes during and after an event. Simpson and Meixner (2012) observed preferential entrainment of bed load, both coarse and fine sediments during the rising phase of flood hydrographs leading to overall bed coarsening and increase in vertical hydraulic conductivity. The introduction of large wood to stream systems adds complexity, diverts flow and energy, improves habitat, and alters the local substrate composition (Lassette and Harris, 2001). Blasch et al. (2007) while modeling two sequential streamflow events, observed that the hydraulic conductivity of the streambed surface layer changed by about four orders of magnitude due to sediment redistribution from one event to the next. The rate of streamflow loss to the unsaturated zone beneath depends primarily on the stream stage, vertical hydraulic conductivity, and geometry of the streambed (Simonds and Sinclair, 2002). In the case of stream disconnected from water table (i.e., losing stream), Wang et al. (2014) observed a linear relationship between the vertical seepage rate and streambed hydraulic conductivity. The vertical seepage rate had a linear relation with stream water depth during laminar (low Reynolds number) flows and exponential relation during turbulent flows.

In gaining reaches of the stream, Chen et al. (2013) observed a decreasing trend of streambed hydraulic conductivity due to the upward winnowing of fine substrate from the deeper sediment cores; however, in losing reaches, hydraulic conductivity of deeper sediment cores increased due to silting of fine substrate in the porous top layers of the streambed. Rosenberry and Pitlick (2009) observed quite a dissimilar kind of situation where the magnitude of vertical hydraulic conductivity varied on the subject of seepage

direction, the gaining stream reach holding a higher K_s than the losing stretch. This contrasting characteristic is site specific and may be attributed by the composition, weight of substrate materials and vibrations that compact and settle substrates, reducing or enhancing hydraulic conductivity. Of course, these circumstances would not be found everywhere and difficult to generalize, as sometimes fine materials from landslides bury channels, with coarse channel materials buried and possibly providing a conduit for high flow.

2.2.4 Impacts of stream water temperature and viscosity

The density and viscosity of water are temperature sensitive variables. The hydraulic conductivity of a porous medium depends upon the density (ρ) and dynamic viscosity of the fluid (μ) involved and also on the average size and shape of the pores in a porous medium. The relationship between water temperature, density, and viscosity are not linear, and as the water temperature approaches freezing, the density and viscosity increases (Prince, 1984); however, the density decreases if the temperature falls below 4 °C as ice forms and floats on the surface. In fact, permeability is directly proportional to the unit weight of the fluid concerned and is inversely proportional to its viscosity (Hamill and Bell, 2013). The effects of stream water temperature changes on viscosity and hydraulic conductivity of streambeds are cited in literature extensively (Constantz et al., 1994, 2008; Su et al., 2004; Cardenas and Wilson, 2007a,b; Constantz, 2008; Irvine et al., 2015; Gerecht et al., 2011). In a streambed, the vertical and horizontal distribution of temperature is a function of both the advective and conductive heat transport process (Soares et al., 2012). Constantz et al. (1994) suggest that high infiltration rates cause rapid convection of heat to the streambed. In a system where the stream recharges the aquifer, the streambed could experience daily fluctuations in temperature that are attenuated and delayed with distance and depth from the surface water body (Cardenas and Wilson, 2007a). Cox et al. (2007) articulate that the parameters such as water temperature variation, scour, and clogging of the streambed influences the hydraulic conductivity of the streambed and observed a variation of 41% in K_s seasonally due to temperature variations alone. To evaluate the effect of water temperature on streambed vertical hydraulic

conductivity, Dong et al. (2014) conducted in situ permeameter tests in Clear Creek, NE, USA, where the coarser sandy sediments had a greater increase in the extent of the vertical hydraulic conductivity value per 1 °C increase in water temperature than sediments composed of silt and clay layers.

The streambed temperature will be highly variable in the case of a losing stream, but it will be relatively stable with little fluctuation in the case of a gaining stream (Lee et al., 2013). Stream thermal regimes are affected by outside influences such as air temperature, solar radiation, and heat loss as a result of evaporation. The instream geomorphic influences which facilitate heat transfer are processes such as hyporheic exchange of water, groundwater inputs from the adjacent water table, as well as the ability of the substrate to subdue heat exchange (Hester and Doyle, 2008). The hydro-geomorphic processes that drive changes in sediment texture are fine-scale granulometric variables such as oxygen, interstitial space, and organic matter translocation (McKenzie-Smith et al., 2006) along with the sources of sediments, weathering, particle breakup from tumbling, chemicals, freezing, etc. Hatch et al. (2010) from their experiments noticed that a 30% decrease in fluid viscosity would yield a commensurate increase in hydraulic conductivity of the streambed. The temperature of water entering the soil changes as it moves through the unsaturated zone before entering the water table producing variations in soil temperature and water viscosity which could have a direct impact on hydraulic conductivity (Dong et al., 2014). Ronan et al. (1998) spotted increased infiltration rates beneath an ephemeral stream and recognized the water viscosity effects on hydraulic conductivity from increased stream temperature. Lu et al. (2012) discusses the impact of temperature on the estimates of hydraulic conductivity and verified the inverse relationship of K_s value with the kinematic coefficient of viscosity. Beneficial to many streams and aquatic habitats, extreme temperature swings are limited and moderated by flow through hyporheic zone substrates relative to their capacity to absorb and dissipate heat over time. Groundwater influx to streams also contributes cool waters that help to moderate temperature extremes.

2.3 Influence of anthropogenic activities on streambed hydraulic conductivity

2.3.1 Impacts of land use change and urbanization

Urbanization, industrialization, and changes in the land use pattern have resulted in local changes in weather patterns that in some instances may approach irreversible disturbances to the hydrological processes. The increase in the impervious area associated with urban development affects the hydrologic cycle and consequently, there is an enhanced risk of channel instability and urban flooding (Niehoff et al. 2002). Urbanization often increases the discharging of pollutants to streams and water bodies from a variety of point and non-point sources. Physical changes as a result of soil compaction and vegetation losses within riparian zones may also alter water quality and hydrologic functions. The uncontrolled discharge of domestic, commercial and industrial wastewater to nearby ponds or rivers has the potential to cause major ecological and sustainability problems for the river inhabitants (Yule et al. 2015). Deforestation increases the runoff two to six times over what would occur naturally, reduces the vegetation transpiration, raises the water table, accelerates soil erosion, bank instability, and channel adjustments. Deforestation also affects the normal stream nutrient cycling, leaching, and transportation processes, some of which are desirable for ecological function (Biggs et al. 2002; Iwata et al. 2003). Due to deforestation, at landscape scales, the dense canopies, stabilizing root systems and increased filtering associated with stream buffers are destroyed, exposing streams to increased solar energy, erosion and pollutants. Excessive snagging and removal of large wood and aquatic plants from the channel could initiate bed level lowering as well as impact habitat diversity (Erskine and Webb 2003). Thomas et al. (2004) found greater siltation and exposure in deforested streams contributing to the development of a fine-grained, organic-rich stream bed with increased presence to dominance or infilling by aquatic vegetation.

As demonstrated in the field studies of river contamination, riverbeds play a vital role in the transport, filtering, and fate of contaminants in river systems (Jang and Liu 2005;

Barth et al. 2007; Gates et al. 2009; Sehgal et al. 2012). Contaminants may enter and leave the bed of the river by a variety of mechanisms (Zhu et al. 2014). Diffuse (non-point) sources of contaminants such as activities or actions which expose soils to erosion and connect to lotic waters sometimes transport sediments along with pollutants. Point sources of pollution are directly discharged wastes or wastewater from the industry, domestic use, community or urban releases from waste storage ponds or lagoons, and by the use of agrochemicals during irrigation and return flows (Nie et al. 2012). As long as the concentration of the contaminants is higher in the recipient water than in the pore water of the sediments, the net mass transport is directed into the sediments. Hence, the sediments act as a sink of contaminants (Forsman 2000), sometimes taking time for contaminant breakdown or continuing dilution of concentration as mixing occurs. However, contaminated sediment erosion and transport is a mechanism to consider if a breakdown does not occur. The hydraulic conductivity and porosity of the contaminated streambed sediments are the result of both erosion and depositional processes that take place in streams or rivers to produce a unique set of pore space geometries in the course of progressive adjustment and stabilization of the sediment layers through time (Messina and Biggs 2016). Weathering effects, which encourage for chemical breakdown of contaminated sediments, allow for settling and sediment embeddedness with trends to decrease particle size and the hydraulic conductivity of the streambed.

Intensive pumping of groundwater near streams has the potential to disconnect the aquifer from stream water inputs or changing the flow fields from the stream to the pumped aquifer system. The aquifer configuration and type of sediments in the stream channel controls the recharge rate of the underlying water table (Wang et al. 2011). Various types of other anthropogenic activities also influence streams, streambeds and groundwater interactions; including hydrologic modifications associated with wetland draining, stream ditching, channel straightening, channel dredging and realignment for transport, dikes or dams of various types and intensities of flow alteration, culverts and bridges, dispersion of mine tailings into streams or lakes, mining of instream materials such as sand, gravels, etc. These anthropogenic activities could alter the chemistry, channel morphology and function, streambed substrate, particle size, composition, hydraulic conductivity,

groundwater connectivity, flow permanence and other factors that affect water, sediment and pollutant movement (Jiang et al. 2010). Extensive best practices or professional guides have been prepared for many circumstances and anthropogenic activities to help prescribe reasonable approaches for protection of water quality, and it is likely that some of these measures such as forested stream buffers (Welsch 1991) may benefit in maintaining stream-aquifer connectivity and function.

2.3.2 Effects of engineering structures across or within a river/stream

Erection of hydraulic structures are often designed specifically to alter the natural flow of water and as a result, affect sediment and pollutant transport, leading to adjustments such as the localized growth or erosion of deposits and changes to the carrying capacity and functions of a river (Skalak et al. 2009). Fragmenting streams with dams, diversions and less frequently road culverts disrupt the longitudinal connectivity and capacity of a stream. It is known that after the construction of a dam, dike, weir or a barrage, accretion starts upstream in response to the grade shift with lower stream velocity, whereas retrogression takes place downstream due to inefficient energy dissipation by the discharge of clean water from elevation. Another effect of aggradation is the increase in tortuosity, sinuosity or even braiding of the channel upstream due to the loss in gradient and ability to transport sediment. The tendency for increasing tortuosity could be illustrated, by comparing the unaffected reference stream sinuosity and meander belts with sections affected by structures (Allan and Castillo 2007). In general, the larger and higher the dam, the greater the influence, while small or instream structures may produce only localized effects. Proper design and placement of small structures such as J-hooks and cross vanes could be used to reduce near bank stresses, effects of localized excessive sediment accumulations near bridges and habitat benefits (Rosgen 2001). Meandering alterations in low gradient systems may lead to adjustments or diversion of flow such as outflanking of hydraulic structures. Flow avulsion may not only be caused by diverting flow into a meandering channel that lacks capacity, but also if the river shifts its course to join other low-lying rivers. These kinds of changes indeed alter the affected stream-groundwater connections.

The tail-water releases of waters below the dam downstream are appreciably affected by the clean water effect, as these waters are hungry for sediment to the extent that stream degradation, bank and point bar erosion are typically significant. The channel gradient increases somewhat and this may extend over a considerable length downstream near large structures. The dam structure reduces the dominant discharge of a river and its fluctuations. The downstream channel tends to straighten, thus reducing the meander tendency (Mazumder 2004). Dams decrease the pollution effect considerably in the downstream part by lowering the pollution load coming from the source (Tahmiscioğlu et al. 2007). Downstream channels with lower than normal flows, may be invaded by vegetation and loose channel capacity, leading to increased flooding during severe floods. Regular channel maintenance flows every year or two as capable are prescribed to help reduce vegetation encroachment and maintain channel capacity, even though degradation is a potential for some sections. Measures to help maintain sediment transport through dams is sometimes employed to help reduce these effects.

The function of constructed embankments or levees along the flow of a river is to restrict access to the floodplain through a physical barrier or through channel adjustments in morphology that generally increases the stage and the velocity of the flood flow. With the increased velocity and potential for degradation, the total silt carried downstream to other low gradient areas or to the sea/ocean by an embanked river would be more than that of an unbanked river. Other conditions being the same, unless deposited before the basin outlet, the rate of extension of the delta with more sediment delivered would be greater. Greater extension of the delta with an increase to base-level may cause portions (i.e., lower gradient) of the embanked river to rise and result in building up of the river bed. Hydraulic changes to rivers do not always produce the effects desired and are seldom permanent changes. In the case of stable rivers, embankments may raise the flood level but are less likely to induce a change in the river bed configuration (Garde and Raju 2010). Embankments may be supplemented by other flood control measures such as storage reservoirs, diversion of the river, soil conservation practices, etc. Failure of these structures sometimes causes much more damage than would have naturally occurred, and that is why flood preparation and managing of water controls previous and during eminent hazards are

important elements to consider. The net effects of these structures to stream and groundwater interchange are seldom considered, analyzed or known.

Bed load transport in mountainous streams varies with the geology, gradient, sources of material, flow intensity, stream power, and the riverbed structure. Corrugated metal culverts can be worn and damaged under high bedload transport conditions, suggesting bridges may be needed and cost effective for sustainable passage (Hansen 1987). Dams or similar structures are likely to capture this load and may be a reason to avoid structures in high gradient systems. Zhang et al. (2010) articulates that the bed load transport rate varies in a range of 3-4 orders of magnitude in a mountain stream at the same place and under unaffected flow discharge, with the presence or absence of a step-pool system. Check dams are sometimes used to augment habitat, stabilize mountainous streams and landslide hazards. A point to remember is the higher the check dams, more hydrologically unstable they are. Located, designed and installed inappropriately may cause more issues than leaving the stream alone. The construction of check dams can produce changes in channel cross-sectional geometry, grain-size distribution, bed forms, bed slope and riparian vegetation. Sediment and/or bedload retention behind check dams can facilitate localized channel widening or narrowing, armoring and/or incision downstream (Wohl 2010). On watersheds with coarse soil textures, check dams may be particularly effective due to greater sediment retention and formation of a permeable bed, with a better mix of substrate materials to add diversity (Polyakov et al. 2014). Low rise check dams have some benefit for grade control such as in gully systems (Rosgen 1994). Spur dikes, deflectors, groins, rock vanes, cross vanes and J hooks are transverse structures that extend into or across the stream from the bank and reduce erosion by deflecting flows away from the bank and reducing bank stress (Rosgen 2001). Generally, two or three rock vanes (discontinuous, redirective structures) are constructed along the outer bank of a bend in order to redirect flows near the bank towards the centre or thalweg of the channel. By designing structures to maintain a channel thalweg helps to reduce this potential for diversion. Some structures such as gabions can settle or move if not adequately anchored or keyed into channel, slope or position. Continuing update and review of anthropogenic modifications and instream structures are needed to consider their effects to manage flows, flood damage, aquatic

passage, habitat, stream morphology and stability, sediment and bedload transport, water quality and stream-aquifer interactions.

2.4 Influence of biological factors on streambed hydraulic conductivity.

The removal of riparian (streamside) vegetation may lead to a reduction in bank stability and contribute to failure if soils are unstable. Activities that reforest or replace vegetation losses or allow for partial removal and regrowth are best to maintain stability as a general rule or best management practice. Vegetation removal may result in bank erosion or failure and stream siltation of fine sediments locally or downstream. The siltation generally reduces the number and capacity of pool sites, hydraulic conductivity due to finer materials and increases habitat homogeneity (leading away from pollution intolerant macroinvertebrates toward tolerant species). On slopes, over about 35%, special measures such as directional felling or adjusting logging systems may be needed to selectively fell, log or thin stream sides.

Riparian ecosystems are biologically active zones of diversity and productivity, and also often act as a sink for nutrients or pollutants from runoff waters (Sabater et al. 2000). Trees and shrubs physically constrain and retain the soil near the stream banks, thereby protecting the streambed and limiting the scouring effect of running water. In regions with high organic matter accumulation (e.g., leaf litter buried in alluvial deposits) an actively growing biofilm might clog sediment or soil pore spaces and thereby reduce the hydraulic conductivity of the streambed (Chestnut and McDowell, 2000). Biofilms predominantly develop on small sediment particles because of their large surface areas. Biofilms have a low porosity and therefore result in localized areas of low K_s . Riparian vegetation helps to provide shade and cooler air temperatures that contribute to the cooler and consistent stream water temperatures. In cold weather circumstances, heavily vegetated stream buffers may locally help to capture snow or retain warmth to buffer the heat exchange. The nutrient buffer capacity of riparian zones depends on the complex combination of landscape and hydro-geomorphologic variables (Gu et al. 2007; Garrett et al. 2012). The

presence of roots in riparian and channel substrates can contribute to subsurface flow conduits or underground blockages. In addition, the presence and burial of wood debris within sediment deposition events can also add to substrate complexity and function (Lassette and Harris, 2001; Erskine 2002). Wood that remains saturated has limited ability to decompose, while wood frequently exposed to air and associated macro and microorganism will decompose faster, increasing opportunity for voids, settling and localized water passageways (Lassette and Harris, 2001). Song et al. (2010) provide evidence of bioturbation activities which could result in increasing the streambed hydraulic conductivity profiles.

Tremendous complexity exists in fluvial systems and factors such as stream flow patterns; channel form; transport processes; and the distribution of riparian vegetation or woody debris that affect specific stream channel responses resulting in an irregular distribution of sediment supply (Abt et al. 1994). Organic sediment is derived from decaying accumulations of leaves, woody debris, algae, floras, and/or other organic material that develops falls or is delivered into streams (such as foliage). The microbial and macroinvertebrates attached to the debris or other inert matter contribute to the breakdown and processing of organic matter. Organic sediment transport through a fluvial system varies by location and season and is more difficult to quantify when compared to that of mineral sediment movement (Wynn and Mostaghimi, 2006). Organic and timber debris are sometimes more notable in bedrock and boulder-bed streams; it crafts a part of the stream geomorphology and permits a stabilizing effect. Streambeds buried or dominated by very fine sediments and nutrient accumulation, exposed to the sun, and with little flow disturbance have increased risk of clogging due to algal blooms. In contrast, sediment-starved streams may be incapable of accumulating organic materials or providing diverse habitats for benthic organisms (Quinn et al. 2009). Aquatic plants or periphyton may shield the shoreline, or streambed substrates, consume nutrients and contaminants from the water and may help stabilize the streambed sediments. They may also limit normal hyporheic water, particle mobilization or transport and add roughness to reduce flow velocity which would promote finer particle settling.

The activities and response of various organisms that live in streambed hyporheic zone have the potential to breakdown clogged substrates and bioremediate contamination for the improvement in the groundwater quality relative to its future uses without added treatment (Whelan 2007). Sediment reworking by macroinvertebrates as well as others such as fish spawning may increase the K_s of river bed locally. Chemical processes within the hyporheic zone may result in mineral dissolution or precipitation, which will increase and decrease water density and K_s seasonally. Hyporheic zones usually support a variety of substrate habitats that may accommodate, depending on water quality, a variety of invertebrate species including ostracods, copepods, amphipods, tardigrades, nematodes, oligochaete worms, rotifers and early instars of aquatic insects. These fauna and flora within the hyporheic zone are significant contributors to organic and nutrient cycling in streambeds (Clarkin 2008).

2.5 Laboratory and in-situ methods of estimating streambed hydraulic conductivity

Streambed Hydraulic Conductivity (K_s) measurements have been performed using a variety of techniques. Instream methods of determining K_s include slug tests (Duwelius 1996; Cey et al. 1998; Springer et al. 1999; Ryan and Boufadel 2007), in-situ permeameter tests (Lindgren and Landon 2000; Rosenberry 2000; Chen 2004, 2005; Chen et al. 2008; Genereux et al. 2008; Huang et al. 2014; Jiang et al. 2015) and seepage flux measurements using seepage meters coupled with measurement of hydraulic gradient through the streambed (Landon et al. 2001; Murdoch and Kelly 2003; Rosenberry 2008; Rosenberry et al. 2012). In addition, streambed samples can be collected for grain-size analysis and K_s could be estimated from pedo-transfer functions based on grain-size distribution (Boadu 2000; Song et al. 2009). Although field permeameters and seepage meters coupled with hydraulic gradient measurements determine vertical hydraulic conductivity (K_v), the slug tests measure horizontal hydraulic conductivity (K_h); and the hydraulic conductivity (K_s) values from grain-size methods are non-directional (isotropic). Reynolds et al. (2000) employed positive-head tension infiltrometer (TI) and single-ring pressure infiltrometer (PI) and classical undisturbed soil core (SC) methods for measuring K_s of single-grain sand,

structured loam, and cracking-clay loam soils. Cardenas and Zlotnik (2003) experimented with multilevel constant-head injection tests and multilevel slug tests to gather streambed hydraulic conductivity values. Piezo-Seep meter provided improved estimates of vertical saturated hydraulic conductivity, specifically in streambeds of medium to coarse textured sediments in the study conducted by Kelly and Murdoch (2003). Accurate evaluation of soil hydraulic conductivity, soil sorptivity, and matrix flux potential could be made in all types of soils using Guelph permeameter (Reynolds and Elrick 1985; Fares et al. 2000; Kodešová et al. 2010; MacDonald et al. 2012). For highly permeable gravel beds, Yamada et al. (2005) developed a packer test system based on Hvorslev's equation (Hvorslev 1951) for the in-situ estimation of streambed hydraulic conductivity. Laboratory determined values may be more precisely measured, but rarely agree with field measurements. Field methods are generally more reliable than laboratory methods due to the closer approximation to natural conditions and lower disturbance while sampling. (Scott 2000).

In addition, field sampling of streambed and valley bottom materials may exhibit variability of particle sizes resulting from various types of erosion and deposition processes of materials associated with vertical and lateral accretion, colluvial, splay, alluvial fan, and deltas (Happ et al. 1940; Trimble 2008). Piping in certain types of fine grained soil and weathered substrate materials can lead to rapid movement of water and sediments underground. An understanding of the geology, climate and hydrology forces of recent and past, and ample sampling of substrates should help to reveal and quantify the potential and/or presence of the variances caused by these variables. Decisions on how to conduct sampling for research and interpretations using in-situ or laboratory readings may be an iterative process that applies to the specific circumstances and intent.

Other methods such as those described by Garrett et al. (2012) on end member analysis of water chemistry, and others who use radionucleotides or fluorescent dyes in tracing water flow rates or transfer are examples of alternative methods (Abbott et al. 2016). Using fluorescent dyes, visual responses are possible, but fluorimeters can detect and quantify low concentrations in the parts per billion (ppb) range, well below visualization concentrations (Baker and Lamont-Black 2001). A constant injection rate

study of a known fluorescent dye concentration and monitoring concentrations downstream or in the hyporheic zone with fluorimeter at various levels could help define levels of dilution and rates of flow or exchange in layers (Holland et al. 2004). Applying hydrogeology and well-driller techniques of timed pumping or injecting water into wells with monitoring water levels in well or adjacent wells may also prove helpful in defining some of the local hydraulic conductivity processes. A sampling of coarse channel substrates with various methods of freezing materials (or freeze coring) has also been used to help remove relatively undisturbed samples for particle size analysis (Everest et al. 1980; Ulrich et al. 2015). Coating non-cored, relatively undisturbed frozen samples with paraffin may facilitate follow-up with laboratory testing for hydraulic conductivity.

2.6 Statistical and geo-statistical techniques employed for the assessment of spatio-temporal variability of streambed hydraulic conductivity

Previous studies have found a significant spatial and temporal variability in the valley and streambed sediments (Hannula and Poeter 1995; Reynolds et al. 2000; Landon et al. 2001; Hatch et al. 2010). Statistical measures are frequently used to design a sampling network and describe field data in terms of measures of central tendency and variability. Table 2.6.1 provides a detailed information regarding the statistical techniques employed in the literature of streambed hydraulic conductivity assessment. Presently, there are a variety of procedures for generating interpolated hydraulic conductivity (K_s) fields from a sparse set of K_s measurements. Geostatistical spatial characterization of a specified variable involves the generation of maps and predicting values of that particular variable at numerous unsampled locations. These methods are best used with care and consideration of geology, hydrology, soil and topographic properties associated with the conditions as the distribution of particles, substrates, channel morphology, etc. are not necessarily random populations, but often affected by recognizable factors such as valley type, channel gradient, sinuosity, entrenchment and stream type (Clément and Piégay 2005).

Table 2.6.1 Statistical and Geo-statistical techniques for the assessment of variations of streambed hydraulic conductivity.

Reference & Test site	Statistical Measures	Geo-statistical Measures	Applications	Implications
Chen (2004) Republican, Platte and Little Blue Rivers	Measures of Central Tendency and Variability Kruskal-Wallis test		The <i>Kruskal-Wallis</i> test to determine the significance of the difference of K_v values between two test sites of the same river and between the test sites of two rivers.	The <i>Kruskal-Wallis</i> test indicated a significant statistical difference of the K_v values between the Republican and Little Blue Rivers and between the Platte and Little Blue Rivers but found no such significant statistical difference between the Platte and Republican Rivers. Little Blue River is a smaller size hydrologic unit.
Chen (2005) Platte River, USA	Shapiro-Wilk test Kruskal-Wallis test	Variogram fitted using the least squares methods	<i>Shapiro-Wilk</i> test to check whether a sample is from a normally distributed population. <i>Kruskal-Wallis</i> test to determine the similarities of the K_v values from the test sites.	K_v values of the Platte River in south-central Nebraska showed a normal distribution. A positive correlation was observed between K_v and the water depth which produced Periodicity of K_v values across the channel.
Ryan and Boufadel (2007) Indian Creek, Philadelphia	Kolmogorov–Smirnov test	Variogram analyses	The K_v measurements at each depth were checked for Gaussian distribution. The combined data set deviated from the Gaussian distribution. The normal distribution of K_v (95% confidence level) at each depth was tested by Kolmogorov–Smirnov test.	Variogram analyses across the stream suggested symmetry – (in the upper layers of thalweg) and fractality - (in the lower layers). The variogram of $\ln K_v$ of the upper layer sediments suggests that fine sediments get trapped along the stream edge with low velocity and pressure head.

Genereux et al. (2008) West Bear Creek, North Carolina	Measures of Central Tendency and Variability	Exponential-semivariogram models Contour maps	Contour maps brought out anisotropic aspects of the K_s distribution without an anisotropic interpolation routine. The streambed K_s upstream and downstream of a small beaver dam were analyzed.	Slightly bimodal distribution of the K_s was observed via histogram plotting. Higher K_s in the center of the channel indicated gateway for water and chemical fluxes through the streambed. The average streambed K_s was about 23% lower on the upstream of the dam.
Leek et al. (2009) Touchet River, USA	<ul style="list-style-type: none"> · Kolmogorov–Smirnov (K-S) test · Wilcoxon rank-sum test · median two-sample test 		<i>K-S, Wilcoxon rank-sum, median two-sample</i> tests determine the differences in empirical cumulative distribution function (CDF), mean, and median of K_s between the two study sites and two depth intervals at each site.	All the three tests approved the similarities in empirical CDF, mean, or median among certain depth intervals. On the other hand, the spatial patterns of K_s in channel sediments varied from one depth interval to another. Gaining and losing zones based on vertical hydraulic gradient varied among different depth intervals, suggesting the complexities of the water flow regime.
Hatch et al. (2010) Fourth-order stream of Pajaro River, USA	Cross Plots Ranges of K_v		Relationships between streambed hydraulic conductivity, discharge, and seepage rate were demonstrated through ‘Cross plots’.	Local-scale variations in streambed seepage due to streambed topography was observed. The cross plot suggested a hysteresis relationship between streambed conductivity versus seepage rate. During higher discharge periods, increased K_s and seepage rates were observed due to bed scouring, however, as the discharge reduces, the sediment deposition progresses decreasing the seepage and K_s of bed.

Chen (2011) Platte River, USA	<ul style="list-style-type: none"> · Kruskal–Wallis test · Mann–Kendal test 	<p><i>Kruskal–Wallis</i> test to determine whether the K_v values from the three depth ranges have the same mean.</p> <p><i>Mann–Kendal</i> test to detect the trend of K_v for channel sediments from the shallow to the deep part.</p>	<p>The results rejected the <i>Kruskal–Wallis</i> test hypothesis at 80% level of confidence indicating that two populations (bed depths) have different means.</p> <p>The <i>Mann-Kendal</i> test rejected the hypothesis at 95% level of confidence indicating a decreasing K_v trend with depth.</p> <p>The hyporheic processes could affect streambed K_v distribution patterns for about 9 m below the channel surface.</p>	
Cheng et al. (2011) Platte River, USA	<ul style="list-style-type: none"> Jarque–Bera (J-B) test Kolmogorov–Smirnov (K-S) test Lilliefors test Shapiro–Wilk (S-W) test <i>t</i>-test 	Exponential-semivariogram model	<p><i>(J-B)</i>, <i>(K-S)</i>, <i>(S-W)</i> and <i>Lilliefors</i> tests determine whether streambed K_v at each test site is normally distributed.</p> <p><i>S–W</i> test requires sample size N ($7 \leq N \leq 2,000$). The <i>K–S</i> and <i>Lilliefors</i> require sample size N ($N \geq 2,000$).</p> <p>A <i>t-test</i> with unequal variance determines whether streambed K_v differs significantly between different test sites.</p>	<p>The sites where the normal distribution of streambed K_v was observed suggested sediments were well distributed and belong to a single population of K_v. For sites where normality tests failed, the sediments deposited belong to different hydrogeological processes, including geological conditions, geomorphic history, and physical transport processes.</p> <p>A part of the population of samples was reduced to independent samples by drawing out the spatially correlated samples by using an exponential-semivariogram model.</p>

Dong et al. (2012) Two point bars locations in Clear Creek, Nebraska	Kruskal–Wallis test	The Kruskal–Wallis test determines whether the K_v values from the point bars and from the streambed statistically belong to different populations.	The streambed and point bar K_v values were heterogeneous. The smaller K_v values in the point bar locations result due to a weaker hydrodynamic condition that deposits fine materials at the point bar edge.
Lu et al. (2012) Platte River, USA	Kolmogorov–Smirnov (K-S) test Sign test	<i>K-S</i> test to determine for normal distribution, log-normal distribution, uniform distribution, and exponential distribution respectively. Sign test - nonparametric test to determine if one group tends to produce different values from another group.	The K_s value and kinematic coefficient of viscosity of water had an inverse relationship. Since, K_s is a complex function of sediment packing, structure, heterogeneity, and several other factors, the K_s values determined from grain size analysis and empirical formulas don't represent any specific direction (anisotropic).
Min et al. (2013) Donghe River, China	Shapiro–Wilk Test Spearman Bivariate Correlation analysis	<i>Shapiro–Wilk</i> Normality Test determines whether K_s or $\ln K_s$ is normally or lognormally distributed. <i>Spearman Bivariate Correlation analysis</i> determines whether two non-normal distributed variables are significantly correlated at the 95% confidence level.	K_s values determined from Standpipe Permeameter were normally distributed, at the 95% confidence level. However, the K_s determined using Falling-head Permeameter was log-normally distributed although not normally distributed. There was neither a statistical correlation nor difference between the K_s values of the upper and lower layers.

Chen et al. (2013) Platte River and its tributaries, USA	Measures of Central Tendency and Variability Kruskal–Wallis test	<i>Kruskal–Wallis</i> test to determine if there are statistically significant differences between two or more groups of K_v .	A decreasing trend of K_v was realized in the gaining streams. Higher K_v values occurred in the parts of the channels with greater water depth. Opposite vertical K_v distribution patterns was perceived in gaining and losing streams. The <i>Kruskal–Wallis</i> test indicated that K_v of the gaining streams differs from K_v of the losing streams. In the losing streams, K_v increased downward from the channel surface to depth of about 5 to 10 m. In the gaining streams, K_v values showed a decreasing trend due to the upward flux of suspended sediments, which enhanced the pore spacing and elevated the K_v values in the top layers of the streambed.
Datry et al. (2015) 101 river reaches of French river monitoring network	Mann–Whitney–Wilcoxon test Wilcoxon signed-rank test	Mann–Whitney–Wilcoxon test to compare the mean of K_s values between a priori clogged and reference reaches. Wilcoxon signed-rank tests for assessing seasonal differences in reach-scale K_s and to assess potential observer’s bias.	The distribution of streambed K_s was not normal across 101 stream reaches, and a large proportion of the values were null. The variability in K_s within-reach was high and influenced by penetrating depth and hyporheic exchanges. No significant influence of season on reach-averaged K_s values and bias in measures by two different observers

Wu et al. (2015) Dawen River, China	Kruskal-Wallis (K-W) test Kolmogorov–Smirnov (K-S) test	K-W test determines whether two groups of the K_v values belong to the same population. K-S test determines whether a set of measurements come from the hypothesized distribution such as the uniform, the normal or the lognormal distribution.	The sediment K_v values of the upper four layers before the flood season were distributed normally, while the K_v values of the fifth layer were lognormally distributed. The K_v values before and after the flood season statistically differed. The difference in K_v and its distribution patterns before and after the flood season were attributed to the infiltration of fine-grained particles.
Wang et al. (2016a) Weihe River, the largest tributary of the Yellow River, China	Kruskal-Wallis (K-W) test Shapiro-Wilk test Kolmogorov-Smirnov (K-S) test Cox-Stuart test Spearman Correlation test	The K-W test determines if streambed K_v values differ significantly between two test sites, between two sampling times or between two different layers. The Shapiro-Wilk test and K-S test were applied to verify the normal and log normal distributions of combined and individual datasets. Cox-Stuart test to detect the trend of median K_v values. Spearman Correlation test to measure the strength of the relationship between K_v values and water depth.	The median K_v values showed no evidence of significant trends with time. K-W tests with the Bonferroni correction suggested no significant differences in the K_v values at each site and weak evidence of differences of K_v between the upper and lower layers. Larger particles of streambed sediments were responsible for higher K_v values while the lower K_v values were observed at locations of fine-grained sediment. The clogging with fine sediments and embedding of substrates with fines along channel margins were observed rather than in the thalweg of the river, perhaps resulting in heterogenous streambed hydraulic conductivity.

Kriging with semi-variogram models such as spherical, exponential and gaussian models are individually used to quantify the spatial variability of random variables between two sites and describe monotonic features of spatial correlation as the lag distance increases. Cardenas and Zlotnik (2003) generated a 3D hydraulic conductivity field through the application of 3D kriging module of Mining Visualization System where a spherical variogram model is fitted to the field data. Jang and Liu (2004) used Ordinary Kriging and Sequential Gaussian Simulations (mean and individual) to estimate the spatial variability and distribution of the hydraulic conductivity. Chen (2005) observed a positive correlation between vertical hydraulic conductivity (K_v) and the water depth from the variogram fitted using the least squares method. Semi-variograms and contour maps were developed by Genereux et al. (2008) to aid in visualization of the spatial variability in hydraulic conductivity. Cheng et al. (2011) fits an exponential model to the experimental semi-variogram along the flow direction at each test site to identify the horizontal and vertical correlation between independent samples. Kriging with semi-variogram modeling are collectively used to quantify the spatial variability of random variables between two sites and describe monotonic features of spatial correlation as the lag distance increases. The extent of remote sensing, geographic and hydrologic tools continues to expand and offer the potential for new approaches in design and analysis.

2.7 Summary of literature review

The review provides an overview of the factors such as streambed composition, morphology, topography and other hydro-geo-ecological factors contributing to the variability of streambed hydraulic properties. Examples of research were provided that were intended to help inform others by compiling information on the hydraulic, chemical, and meteorologic gradients that help define and determine the fluxes of water, energy, and solutes between streams and aquifers. Many researchers acknowledge that streambeds are intensely heterogeneous in both space and time. Literatures document that flood events change the structure of streambeds through erosion (degradation, aggradation, sediment transport, and/or material washing) resulting in significant differences in streambed K_s patterns. Some indeed mention that stream sinuosity and facets (riffles, runs, pools, and

glides) also process water, erosion, and sediment differently that add spatial complexity in association to the topographic position and scale, from headwaters, to stream or river valley, to outlet. A large portion of field researchers express that it is very challenging to identify, stratify, and characterize the erosion/sedimentation events deterministically. Some researchers conclude that the streambed hydraulic conductivity study should probably favor rivers or streams in equilibrium as controls, not actively aggrading or degrading, before attempting to compare with modifications or activities that bring on unstable conditions where change may be ongoing. Some literatures mention that studies in persistent stream bed such as bedrock with stability controls (stable systems), may not offer as much to the subject of variability of streambed conductance as one with a continuous supply of sediment materials.

2.8 Research gaps identified based on literature review

The hydraulic conductivity of the dynamic stream bed is difficult to predict and research. However, the in situ measurement of K_s values and other physical properties (such as streambed porosity, viscosity, water temperature, and particle size analysis) at regular interval for longer time periods could help in developing seasonal time series models which help to interpret the spatio-temporal variations of streambed K_s . At this stage, most of the experimental design and sampling is aimed at the understanding of the variability, processes, and functions that connect streams, hyporheic zones, and groundwater. Putting these components together to help identify and model stream network and landscape processes are still at an early stage of consideration.

The effects of in-stream structures on river/stream functions and their influences on the variability of streambed composition and hydraulic properties is seldom considered or known in the past. Channel morphology changes due to aggradation, degradation, and sediment storage. With clean water releases from dams, downstream erosion, substrate flushing, and sorting are the processes contributing to K_s variability with some potential to change with time. Researchers are expected to continue to consider, add, and expand their ability to characterize the spatial and temporal variability of streambed hydraulic

conductivity as a means to increase understanding of water interchange, channel filtering, etc.

2.9 Problem formulation

In the Western Ghats of Indian peninsula, the hydrological activity under the influence of south-west monsoon is more intensive. High variability in the stream flows consequent to the prevailing monsoon is a characteristic of the rivers in this humid zone (Venkatesh et al., 2009). Flash floods occur in the entire belt of foothills of the Himalayas and Western Ghats. The Western Ghats of India in folds numerous ephemeral and intermittent flashy streams having bed material predominantly composed of sand, gravel and large cobbles. The physics of these flashy streams is quite distinct from that of alluvial streams, viz; steep bed slopes, drainage basins are small, peak flows during monsoon season, high rates of sediment transport causing abrupt changes in bed profile, etc. (Putty and Prasad, 2000). Small reservoirs erected on the mountainous rivers are often beset with the danger of rapid siltation (Zhao et al., 2013). Even though, forests serve as a temporary barrier by with-holding storm water and preventing sheet erosion, the soil erosion from hillsides and silt flows from upland watershed may accumulate along valley sides and channel bed over time. These flashy streams fan out into the plains during times of abnormal floods which drives and spread out deposits into streambeds (Adams, 1989).

The Pavanje River located in Western Ghats of India experiences flash floods during the monsoon seasons. Torrential rain washes down the soil and weathered substrate materials, and deposit them in the valleys and streams. The streamflow appears brownish red due to the dispersion of colloidal clay matter. The laterites of this area have variable consistency limits attributed from their distinct mineralogy. Plenty of sand, gravel and fine clayey soil leached out during surface water flow is deposited into streambeds and swampy areas.

Hence, there exists a need for a study to address the spatial and temporal patterns of K_s along a dynamic streambed over relatively short distances (relative to the vented dams) and short time period (relative to the frequent high magnitude events). How does

streambed K_s vary along the reach, upstream and downstream of a vented dam? Additionally, one has to verify whether the streambed K_s will increase due to the hydraulic pressure exerted by head of water behind the vented dams, or else decline due to settlement of very fine sediments and organics into the bed substrate. Each situation may pose varying complexities to consider, and call for representative studies.

In-situ measurement of streambed hydraulic conductivity all along the length of the stream may not be an ideal and cost-effective way. Hence, the applicability of the soft computing approaches could be tested to induce a rule based relationship for estimating the values of streambed hydraulic conductivity at unmeasured locations using representative georeferenced neighborhood data. No study exists in the literature related to the artificial intelligence (AI) based spatial modeling schemes to predict the spatial patterns of *streambed hydraulic conductivity*. Additionally, the potential of several AI approaches to predict streambed K_s could be evaluated comparatively.

2.10 Objectives of the study

Based on the literature gaps mentioned above, the following objectives were proposed:

- Assessment of spatio-temporal variability of streambed hydraulic conductivity over the stream reach regulated by a series of vented dam.
- Geostatistical analysis for spatial representation of the streambed hydraulic conductivity data.
- Development and evaluation of artificial intelligence (AI) approaches for spatial modeling of streambed hydraulic conductivity.

CHAPTER 3

STUDY AREA AND DATA COLLECTION

3.1 General

The study pertains to a part of the Pavanje river originating in the Western Ghats of India. The study is focused on the stream reach obstructed by two vented dams in sequence for assessing the spatial and temporal variations in streambed hydraulic conductance. The sections below explain in detail the physiography and geological details of the basin along with streambed sampling scheme and frequency.

3.2 Pavanje river basin

About three-fourths of the area of Pavanje river basin consists of mountainous and undulating land; its geological structure consist of laterite, dolerite, biotite hornblende granite, banded biotite gneiss and charnockite; and, on the whole, its topography is steep which accounts for the swiftness of river (Avinash et al., 2014). The watershed receives very heavy rainfall (around 3,900mm annually) from the southwest monsoon during the months of June to October (CGWB, 2012). The Pavanje River originates in the foothills of Western Ghats and flows towards the west to join the Arabian Sea. It lies between North latitudes $13^{\circ}07'30''$ to $12^{\circ}57'30''$ and East longitudes $74^{\circ}45'00''$ to $75^{\circ}02'30''$. The basin lies within the Dakshina Kannada district of Karnataka State, India (Figure. 3.1). Drainage frequency values of the basin range from 0.25 to 6.5 m/m². The basement rocks of the basin

predominantly consist of granitic gneiss of the Archean age, one of the oldest rocks of the peninsular India. These basement rocks are overlaid by ferruginous laterites which cover up about 55–60% area of the basin. They are highly porous and permeable. The thickness of laterite cap varies in the order of 3m to 20 m. Lateritic mounds underlain by thin beds of clay, granites and gneiss; patches of dolerite dykes, charnockites, quartzite and chlorite schist's are also noticed in some parts. Coastal alluvium and lateritic soils are predominant in the landscape formed by the weathering of underlying rocks and due to the marine and river processes (Gajendragad et al., 1986).

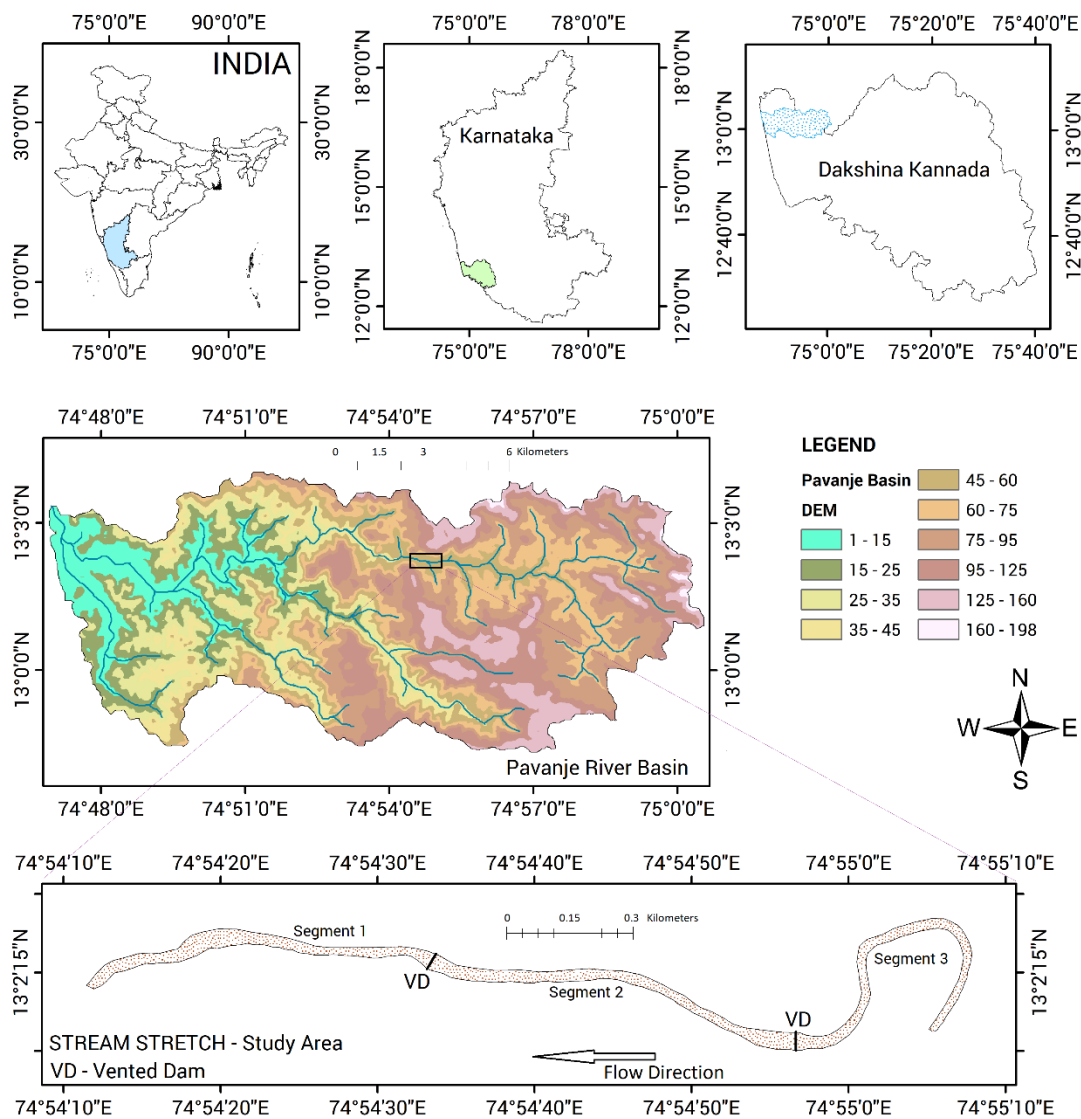


Figure 3.1 Study Area - an intermittent stream of Pavanje River

The lateritic hills do not retain soil moisture and only thick vegetation and grassland is observed in these regions. Torrential rain washes down the soil and weathered substrate materials, and deposit them in the valleys and streams. The water appears brownish red due to the dispersion of colloidal clay matter. The laterites can have variable consistency limits attributed from their distinct mineralogy. Plenty of sand, gravel and fine clayey soil leached out during surface water flow is deposited into streambeds and swampy areas (Shwetha and Varija, 2013).

3.3 Selection of study reach

A series of vented dams (around 8) exist along the Pavanje river across the third and fourth order streams preferentially for recharge of water during non-monsoon periods. The sediment deposition and transportation takes place during the operation of vented dams and the elevation of the streambed varies from 3m to 63m above mean sea level over the entire river, hence there is possibility of significant variation in the streambed soil properties due to sediment transport during the rainy season. The reason for the selection of this particular stretch of the stream is that two vented dams are located (Figure. 3.1) in the span of around 750 meters and is an ideal site wherein we come across all the upstream, midstream and downstream environments with respect to vented dams. As already mentioned earlier, average rainfall over the basin is quite high and stream velocity is observed to be more during the monsoon period which aids in the sediment variation activity. The Pavanje river is dynamic and periodically alter the streambed morphology, besides bringing regular events such as inundation, bank erosion etc. Therefore, this part of stream stretch presents an ideal area for studying the sediment dynamics and their impact on streambed hydraulic conductivity, which is the major thrust of this study.

3.4 Field experiments and data collection

The stream shown in Figure 3.2 was considered for streambed hydraulic conductivity (K_s) estimation at a depth of 0.3m using Guelph Permeameter (GP). The K_s was measured in-situ during the months of February to May of two consecutive years (2016

and 2017) over a 1.829 km stream reach of Pavanje river, where the stream comes across two Vented Dams in sequence. Sampling of K_s was done as per the procedure followed by Chen (2004). The GP tests were conducted along 40 transects across the channel (see Figure 3.2) during dry periods covering the upstream and downstream reaches of each vented dam. The spacing between each transect was 50m and in each transect, for every 5 meter distance, K_s was determined. A total of 187 K_s test samples were collected from the sampling spots every year. For the comparative evaluation of variability of K_s over the upstream and downstream of vented dams, the stream reach considered was divided into three segments (see Figure 3.2); the segment 1 is downstream of vented dam 1, segment 2 is the mid-section which includes both the upstream and downstream environments, and lastly the segment 3 is upstream of vented dam 2. The longitudinal extent of segments 1, 2 and 3 was approximately about 500, 729 and 600m respectively. Before the study began, the channel physiognomies like the type of substrate particles and width of the stream at each transect were surveyed. The sediments deposited in the stream were poorly sorted and composed of loamy sand, silt and fine- to medium-grained sand. The stream reach considered is a sinuous channel with a meander bend in the upstream. The width of stream varied from 18 to 50 m. Table 3.4.1 summarizes the channel characteristics of study reach.

Table 3.4.1 Channel configuration and streambed characteristics at the study reach.

Test Site	Textural class	Structure	Channel geometry	Floodplain connection & Length
Segment 1	Silt loam, loam, sandy loam	Poorly sorted, rippled	Sinuous	Yes, 500 m
Segment 2	Sandy loam, loam, loamy gravels	Cross-stratified, horizontally stratified	Sinuous	No, 729 m
Segment 3	Sandy clay loam, fine sand	Cross-bedded, graded with 'fines upward'	Meander	No, 600 m

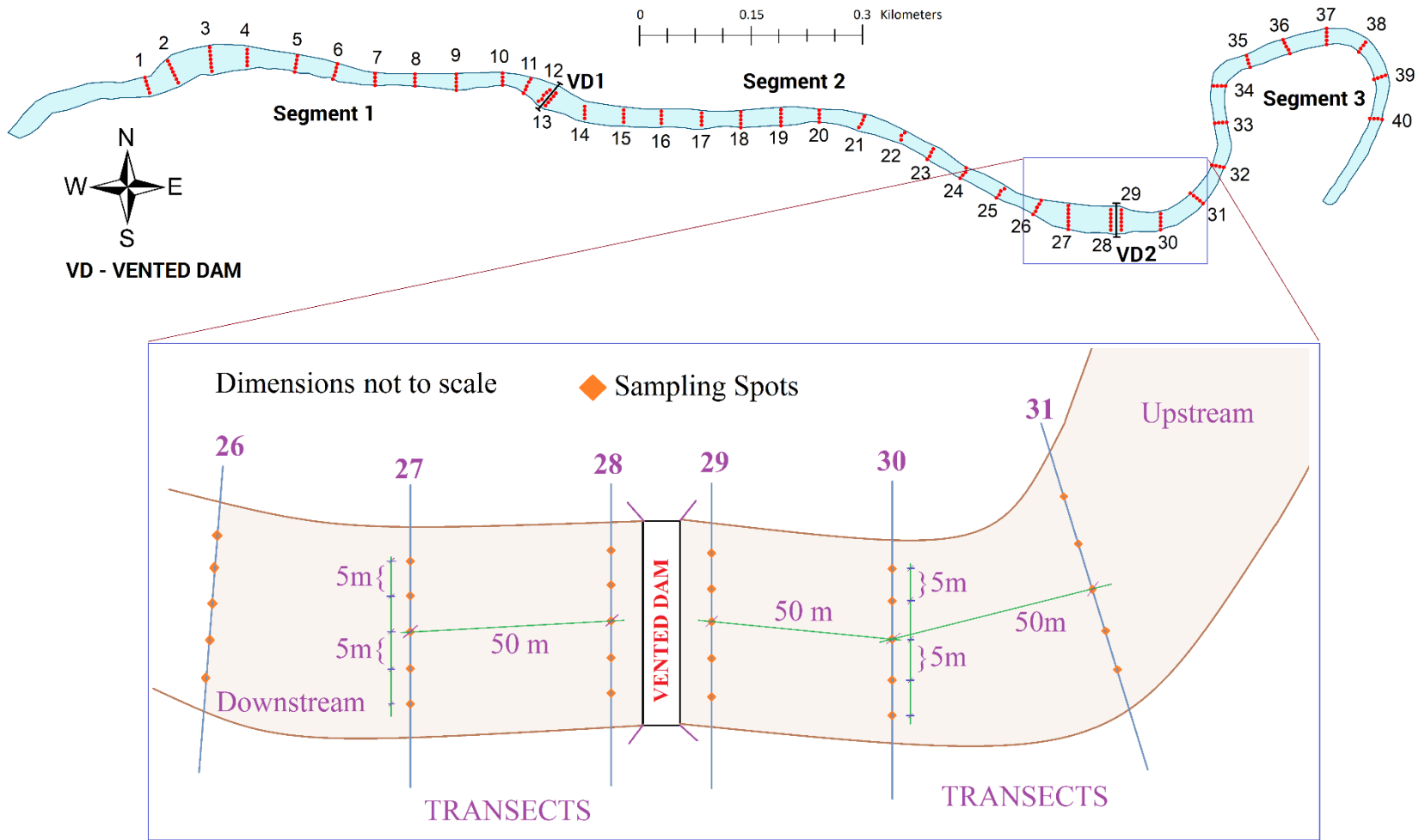


Figure 3.2 Experimental sampling scheme.

3.5 GUELPH Permeameter

Guelph Permeameter designed by Reynolds and Elrick (1985), is a constant head permeameter based on well/auger-hole method and ‘Marriotte’ principle for precise measurements of in situ saturated hydraulic conductivity. The procedure involves measuring the consistent rate of water flow into saturated stream sediments from a cylindrical well hole, in which a constant depth (head) of water is maintained. The K_s measurements are made when a ‘bulb’ of saturated soil is formed around the auger hole due to flow along both vertical (gravity) and lateral (capillary) directions. Depending on the soil type, K_s tests could be made within 30 min to 2 h utilizing just 3.0 to 4.0 liters of water. The two head procedure was followed to get more accurate K_s estimates. The K_s is calculated using the equations given below (Elrick and Reynolds, 1992; Permeameter, G.U.E.L.P.H., 2012).

$$K_s = G_2 \cdot Q_2 - G_1 \cdot Q_1 \quad (3.1)$$

$$Q_1 = \bar{R}_1 \times 35.22 \quad (3.2)$$

$$Q_2 = \bar{R}_2 \times 35.22 \quad (3.3)$$

$$G_1 = \frac{H_2 \cdot C_1}{\pi(2H_1H_2(H_2 - H_1) + a^2(H_1C_2 - H_2C_1))} \quad (3.4)$$

$$G_2 = \frac{H_1 \cdot C_2}{\pi(2H_1H_2(H_2 - H_1) + a^2(H_1C_2 - H_2C_1))} \quad (3.5)$$

where, \bar{R} is steady-state rate of fall of water in reservoirs (cm/s), K_s is sediment saturated hydraulic conductivity (cm/s), a is borehole radius (cm), H_1 is the first head of water established in borehole (cm), H_2 is the second head of water established in borehole (cm) and C_i is dimensionless shape factor that depends primarily on the H/a ratio and according to the soil texture-structure category. MacDonald et al. (2012), Lee et al. (1985) and More and Deka (2017) are few literature examples where Guelph permeameter was used for estimation of K_s in streambed, sandy and sandy loam soils.

3.5.1 Experimental procedure of GUELPH Permeameter

- Before making a measurement using Guelph permeameter, it is necessary to prepare a well hole of required depth in the field using the auger and clean up tools.
- The tripod should be centered over the clean well hole and the water filled Guelph permeameter has to be slowly lowered into the well hole as shown in Figure 3.3. Verify that both the inner and outer reservoirs are connected.
- Thereafter the air inlet tip is raised slowly by gripping the upper air tube so as to establish the initial well head height (H_1) equal to 5 cm.
- Observe the flow rate from the reservoir at fixed time intervals. Monitor the flow rate until it has attained a steady state. Once there is no change in the flow rate at three consecutive time intervals, the reading can be noted down.
- Now, refill the water to inner reservoir if needed and establish the second well head height (10 cm) by slowly raising the air inlet tip again. Make a reading by following the same procedure as mentioned above.
- Based on the steady flow rate readings noted down, and by mentioning the category of soil texture as observed in the field, one could easily calculate the saturated hydraulic conductivity by using “Guelph Permeameter Calculator” spreadsheet.



Figure 3.3 GUELPH Permeameter

3.6 Grain size analysis

Grain size analysis of sediments provides the information on grain size distribution required for classification of the soil or sediment. In the present study, the grain size characteristics of sediments was analyzed that were collected from different transects of the streambed subjected to various degree of erosion, transportation and deposition mechanisms. Sieve analysis was performed on follows:

- The sediment sample was removed by grab samplers. The sediment samples were properly labelled and brought to the laboratory. The samples were oven dried for 24 hours before sieving.
- The procedure given in IS 2720-4 (1985) has been followed. The sieves used for sediment tests were 4.75mm, 3.35mm, 2.36mm, 1.18mm, 600 μ m, 300 μ m, 150 μ m and 75 μ m.
- The sediment sample was placed the sieve stack and kept over the mechanical shaker for 10 minutes. Soon after that, the stacks were removed carefully to weigh and record the weight of samples in each sieve with its retained soil including the bottom pan.
- Particle Size D50 also known as median diameter or median value of particle size distribution was found. It is the value of the particle diameter at 50% in the cumulative distribution. For example, if D50 is 3.5 mm, then 50% of the particles in the sample are larger than 3.5 mm, and 50% are smaller than 3.5 mm. D50 is normally used to characterize the particle size of group of particles.

CHAPTER 4

METHODOLOGY

4.1 General

This chapter presents the statistical and geostatistical methods adopted in the present study in relation to the analysis of the streambed hydraulic conductivity data. An outline of descriptive and inferential statistics used for data analysis is presented. It also includes an overview of the artificial intelligence methods adopted for spatial modeling of streambed hydraulic conductivity.

4.2 Statistical analysis

4.2.1 Normality tests

An evaluation of the normality of data is essential for some statistical tests since, normal data is a basic presumption in parametric testing. The Kolmogorov-Smirnov (K-S) test (Massey Jr, 1951), Lilliefors corrected K-S test (Lilliefors, 1967), Shapiro-Wilk test (Shapiro and Wilk, 1965) and D'Agostino-Pearson test (D'Agostino et al., 1990) were used to determine whether K_s data are normally distributed or not. The K-S test assesses the goodness of fit by comparing the standard normal distribution against the empirical cumulative distribution. However, K-S test is regarded as less sensitive and is not recommended for testing normality nowadays (Ghasemi and Zahediasl, 2012). The

Lilliefors test (a tailored version of K-S test) adjusts the K-S statistic for small values at the tails of probability distribution and examines for a significant difference between the empirical CDF and the specified distribution. Shapiro-Wilk (S-W) test is another similar normality test that effectively assesses the correlation between sample data and the corresponding ideal normal scores, and is an unbiased estimator of goodness-of-fit to the standard normal distribution. The D'Agostino -Pearson test is a versatile and powerful test against non-normality arising from skewness and kurtosis. Its test statistic is based on a comparative evaluation of kurtosis and skewness coefficients of the sample data with that of the moments of a normal distribution, quantified by Pearson's coefficients. The common null hypothesis of all these statistical tests is that the K_s data has been drawn at random from a normal distribution. As with most statistical tests, a statistically significant p-value (typically ≤ 0.05) exhibits a strong evidence against the null hypothesis i.e., the sample distribution is non-normal.

a. Kolmogorov-Smirnov (K-S) test

The Kolmogorov-Smirnov test is defined by:

$$D = \max_{1 \leq i \leq N} \left(F(Y_i) - \frac{i-1}{N}, \frac{i}{N} - F(Y_i) \right) \quad (4.1)$$

H_0 : The data follow a normal distribution

H_a : The data do not follow the specified distribution

where, H_0 is null hypothesis, H_a is alternate hypothesis, F is the theoretical cumulative distribution of the normal distribution of N ordered data points Y_1, Y_2, \dots, Y_N . The hypothesis regarding the distributional form is rejected if the test statistic, D , is greater than the critical value obtained from a K-S table.

b. Lilliefors corrected K-S test

Lilliefors corrected K-S test is an improvement on the Kolmogorov-Smirnov test intended for correcting the K-S for small values at the tails of probability distributions. The K-S test is appropriate when the parameters of the hypothesized distribution are completely

known. However, in real time, it is difficult to specify the parameters of the distribution of any unknown data. In such case, the parameters are to be estimated based on the sample data. Given a sample of n observations, the Lilliefors statistic is defined as:

$$D = \max_x (F^*(X) - S_n(X)) \quad (4.2)$$

where, $S_n(X)$ is the sample cumulative distribution function and $F^*(X)$ is the cumulative normal distribution function with $\mu = \bar{X}$, the sample mean. Even though, the Lilliefors statistic is same as the $K-S$ statistic, the table for the critical values is different which leads to different conclusion about the normality of the data.

c. Shapiro-Wilk (S-W) test

The $S-W$ test was originally designed to test univariate distributions for normality. Given a univariate data $Y = (y_1, \dots, y_n)$ arranged in ascending order, the Shapiro-Wilk test statistic is:

$$W = \frac{\left(\sum_{i=1}^n a_i y_i \right)^2}{nS^2} \quad (4.3)$$

where, the a_i are the Shapiro-Wilk coefficients, and S^2 is the statistical variance of the sample. The W statistic requires that the sample size ≤ 7 and $\geq 2,000$ (Shapiro and Wilk, 1965).

d. D'Agostino-Pearson test

The $D'Agostino-Pearson$ test statistic combines the advantages of tests of skewness and kurtosis to generate an omnibus normality test. Here omnibus refers to the capability to detect deviations from normality due to either skewness or kurtosis. The test statistic is:

$$K^2 = Z^2(\sqrt{b_1}) + Z^2(b_2) \quad (4.4)$$

where, $Z(\sqrt{b_1})$ and $Z(b_2)$ are the normal approximations to test of skewness ($\sqrt{b_1}$) and test of kurtosis (b_2). The K^2 statistic has approximately a chi-squared distribution, with two degrees of freedom when the population is normally distributed (D'Agostino et al., 1990).

4.2.2 Test for equality of variances

The non-parametric tests – Levene's Test (Levene, 1960) for assessing homogeneity of variance and Welch's t-test (Welch, 1947) for analyzing sample means were used to determine if streambed K_s values differ significantly between two segments (i.e., the upstream and downstream of Vented dams) of the river and between two sampling times. The Kruskal-Wallis test is advantageous when the data are not normally distributed. However, while using it to test whether the medians of two data groups are different, it assumes that the observations in each group are from samples of same distribution, so if the data of two groups have dissimilar distribution (for instance, the observations of one group is skewed to the left and another is skewed to the right and have different variances), the results of Kruskal-Wallis test may be unreliable. If the distributions are heteroscedastic, it is better to use Levene's Test or Welch's t-test for two groups instead of Kruskal-Wallis test (Kao and Green, 2008). Whenever the sample sizes are small or unequal and the standard deviations of the two groups are substantially different or unequal, Welch's t-test is recommended. Under the null hypothesis that the difference between two population means is equal, the Welch's t-test calculates a t-statistic by adjusting the number of degrees of freedom even when the population variances are unequal. The Levene's test examines for homogeneity of variances under the null hypothesis that variances are equal across each set of samples.

a. Levene's Test

Levene's test (Levene, 1960) is used to test if k samples have equal variances. Equal variances across samples is called homogeneity of variance. For a variable Y of sample size

N divided into k subgroups, where N_i is the sample size of the i^{th} subgroup, the Levene test statistic is defined as:

$$W = \frac{N - k}{k - 1} \frac{\sum_{i=1}^k N_i (\bar{Z}_i - \bar{Z})^2}{\sum_{j=1}^{N_i} (Z_{ij} - \bar{Z}_i)^2} \quad (4.5)$$

where, Z_{ij} can have one of the following three definitions:

- i. $Z_{ij} = |Y_{ij} - \bar{Y}_i|$ where, \bar{Y}_i is the mean of the i^{th} subgroup.
- ii. $Z_{ij} = |Y_{ij} - \tilde{Y}_i|$ where, \tilde{Y}_i is the median of the i^{th} subgroup.
- iii. $Z_{ij} = |Y_{ij} - \hat{Y}_i|$ where, \hat{Y}_i is the 10% trimmed mean of the i^{th} subgroup.

\bar{Z}_i are the group means of the Z_{ij} and \bar{Z} is the overall mean of the Z_{ij} .

The null hypothesis, $H_o : \sigma_1^2 = \sigma_2^2 = \dots = \sigma_k^2$ for Levene's test is that the variances are equal across all samples. The alternate hypothesis, $H_a : \sigma_1^2 \neq \sigma_2^2 \neq \dots \neq \sigma_k^2$ is that the variances are not equal for at least one pair. The Levene test rejects the hypothesis that the variances are equal if $W > F_{\alpha, k-1, N-k}$. The $F_{\alpha, k-1, N-k}$ is the upper critical value of the F distribution with $k-1$ and $N-k$ degrees of freedom at a significance level of α .

b. Welch's t-test

The *Welch's t-test* for unequal variances is a modification of a *Student's t-test* to check if two sample means are significantly different. The modification made is with respect to the degrees of freedom employed in the test. The Welch's t-test statistic is defined as:

$$t = \frac{\bar{X}_1 - \bar{X}_2}{\sqrt{\frac{s_1^2}{N_1} + \frac{s_2^2}{N_2}}} \quad (4.6)$$

where, X_1 and X_2 represent the two groups to compare and \overline{X}_1 and \overline{X}_2 represent the means of two groups. N_1 and N_2 represent the size of groups and s_1 and s_2 are the standard deviation of the two groups. Soon after the determination of t value, from the 't table' the critical value of Student's t distribution corresponding to the significance level (5%) is evaluated. The null hypothesis, $H_o : \mu_1 = \mu_2$ for the test is that the means are equal and the alternate hypothesis, $H_a : \mu_1 \neq \mu_2$ is that means are not equal.

4.3. Geostatistical analysis

4.3.1 Spatial autocorrelation: Moran's I

Finding the spatial autocorrelation using Moran's I (Index) (Moran, 1948) aids to examine whether the pattern of a phenomenon is clustered, dispersed, or random. When analyzing spatial data, Moran's I index finds the correlation between the neighborhood values of a variable which are scattered in space in two or more dimensions. The Moran's I index is a parametric test which exhibits the spatial autocorrelation value in between -1 and $+1$, and generates a Z-score and p-value to evaluate the level of autocorrelation. A positive index value indicates that the data is spatially clustered while a negative index indicates dispersion. In the present study, the Moran's I for different lags was determined to know the range of autocorrelation values as a function of distance. The Moran's I is calculated as:

$$I = \frac{n}{W} \frac{\sum_{i=1}^n \sum_{j=1}^n W_{ij} \cdot z_i z_j}{\sum_{i=1}^n z_i^2} \quad (4.7)$$

where, n is number of observations, $z_i = x_i - \overline{x}$, x is the value of the variable at location ' i ' and \overline{x} is the mean value of the variable of interest, W is the sum of weights w_{ij} for all pairs in the system (Cliff and Ord, 1981). The inferential Local *Moran's I* statistic is represented as slope in the scatter plot which signposts the type and strength of spatial autocorrelation of a variable.

4.3.2 Spatial interpolation schemes: Deterministic approach

In the present study, two deterministic spatial interpolation methods namely the Inverse Distance Weighting (IDW) and Radial Basis Functions (RBF) were employed to generate the spatial distribution maps of streambed K_s.

The IDW scheme estimates the magnitude of a variable/phenomenon at non-sampled locations by taking the advantage of ‘weighting’ (i.e., the weight of any known point differs with the inverse square of its distance from the estimated point) (Shepard, 1968). The IDW is a moving average interpolator based on search neighborhood strategy which doesn’t account for spatial structure (i.e., arrangement) of the sampled points. Hence, the efficiency of interpolation is dependent on spacing and density of the samples. Inverse Distance Weighting is arrived at using the formula (Johnston et al., 2001):

$$\hat{Z}(s_o) = \sum_{i=1}^n \lambda_i Z(s_i) \quad (4.8)$$

where, $\hat{Z}(s_o)$ is the estimated value for unknown location (s_o), N is the number of measured sample points, $Z(s_i)$ is the measured value at the location s_i , λ_i are the weights assigned to each measured points which are determined by:

$$\lambda_i = \frac{d_{io}^{-p}}{\sum_{i=0}^N d_{io}^{-p}} \text{ with } \sum_{i=1}^N \lambda_i = 1 \quad (4.9)$$

where, d_{io} represents the distance between estimated location s_o and each of the measured location s_i , ‘ p ’ is the weighting power, the rate of which falls off as the distance becomes larger.

The Radial basis functions (RBF) belong to the category of exact interpolation technique with an ability to generalize scattered data to several space dimensions by expanding a linear combination of the basis functions with radial symmetry, (i.e., same

span in all dimensions) (Baxter, 1992). RBF is established in terms of radial distance from a point:

$$Z(x, y) = w\phi\left(\sqrt{(x - x_c)^2 + (y - y_c)^2}\right) = w\phi\|x - c\| = w\phi(r) \quad (4.10)$$

where, w is the weight of RBF determined from interpolation conditions; $c = (x_c, y_c)$ are the coordinates of the point, or center; and r is the spatial distance from neighborhood point in the xy -plane to the center, $\phi(r)$, $r \geq 0$ may be any one of the basis functions. There exists several options of RBFs namely, thin plate spline, completely regularized spline, spline with tension, multi-quadratic and inverse multi-quadratic spline whose shapes are different from one another and result in non-identical interpolation surface. The RBF estimated values could be above the maximum and below the minimum measured values whilst, the values estimated from IDW interpolation never crosses the upper and lower limits of measured values (Buhmann, 2003).

4.3.3 Spatial interpolation schemes: Geostatistical approach

Kriging is the universally accepted best linear unbiased estimator, since it takes regionalization into consideration. The procedure involves exploratory statistical data analysis, fitting suitable semivariogram model, generation of prediction surface map, and (optionally) provides some measures of certainty or accuracy by exploring a variance surface (Johnston et al., 2001). The semivariogram models used in Ordinary Kriging (OK) are the mathematical forms used to describe the inherent spatial correlation structure in the data. Kriging weights for the neighborhood measured points are assigned based on the concept of spatial stationarity of the data quantified through semivariogram model. The variance of estimation error is a resultant of the variogram type and the spatial scattering of measured neighborhood points. The experimental variogram is generally composed with irregular scatter of neighborhood points due to large lag distance and tolerance; and is different from that of ‘theoretical variogram’ which is a plot of variance against lag fitted with a model curve (Goovaerts, 1999). In the present study, OK involving circular, spherical, pentaspherical, exponential and gaussian variogram models were tested to

describe the semivariance. The OK estimator for point estimation is arrived based on the mathematical relations given below:

$$Z(p) = \mu + \varepsilon(p) \quad (4.11)$$

where, $p = (x,y)$ is one of the sample location and $Z(p)$ is the value of the random variable of interest at that particular location; μ is the fixed unknown mean for the data; and $\varepsilon(p)$ is the random error representing the variation around the mean which is intrinsically stationary. When provided with N measurements $Z(p_1), \dots, Z(p_n)$ at known locations p_1, \dots, p_n the estimate \hat{Z} at an unsampled location p_o is given as a weighted sum of the data,

$$\hat{Z}(p_o) = \sum_{i=1}^n \lambda_i Z(p_i) \quad (4.12)$$

where, λ_i is an unknown weight for the measured value at the i th location. To ensure unbiasedness condition for the unknown measurement, the sum of the weights λ_i must be equal to 1. i.e., $\sum_{i=1}^N \lambda_i = 1$ with the expected error: $E[\hat{Z}(p_o) - Z(p_o)]$ and measurement variance:

$$\begin{aligned} \text{var}[\hat{Z}(p_o)] &= E\left[\left\{\hat{Z}(p_o) - Z(p_o)\right\}^2\right] \\ &= 2 \sum_{i=1}^N \lambda_i \gamma(p_i, p_o) - \sum_{i=1}^N \sum_{j=1}^N \lambda_i \lambda_j \gamma(p_i, p_j) \end{aligned} \quad (4.13)$$

where, $\gamma(p_i, p_j)$ is the semivariance of Z between the data points p_i and p_j ; $\gamma(p_i, p_o)$ is the semivariance between the i^{th} data point and the target point p_o . For comprehensive details related to geostatistics and the mathematical concepts of OK and semivariogram modeling one can refer to the following literatures (Webster and Oliver, 2007; Kitanidis, 1997; Goovaerts, 1997).

4.4 Artificial Intelligence Paradigms

4.4.1 Artificial Neural Network

The Multi-layer Perceptron (MLP) Neural Network is one of the most versatile algorithm that has proven capable to simulate highly complex and nonlinear relationships between a set of input variables (predictors) and the output data (predictand). A three layered perceptron network with one hidden layer is as shown in Figure 4.1. The network is trained on a set of reference data by adjusting the parameters of MLP network with the assistance of a Levenberg-Marquardt Back Propagation (BP) algorithm. The network architecture involving a set of processing units (neurons), a specific topology of weighted links connecting the neurons and the learning paradigm that updates the connection weights determine the efficiency of MLP neural network.

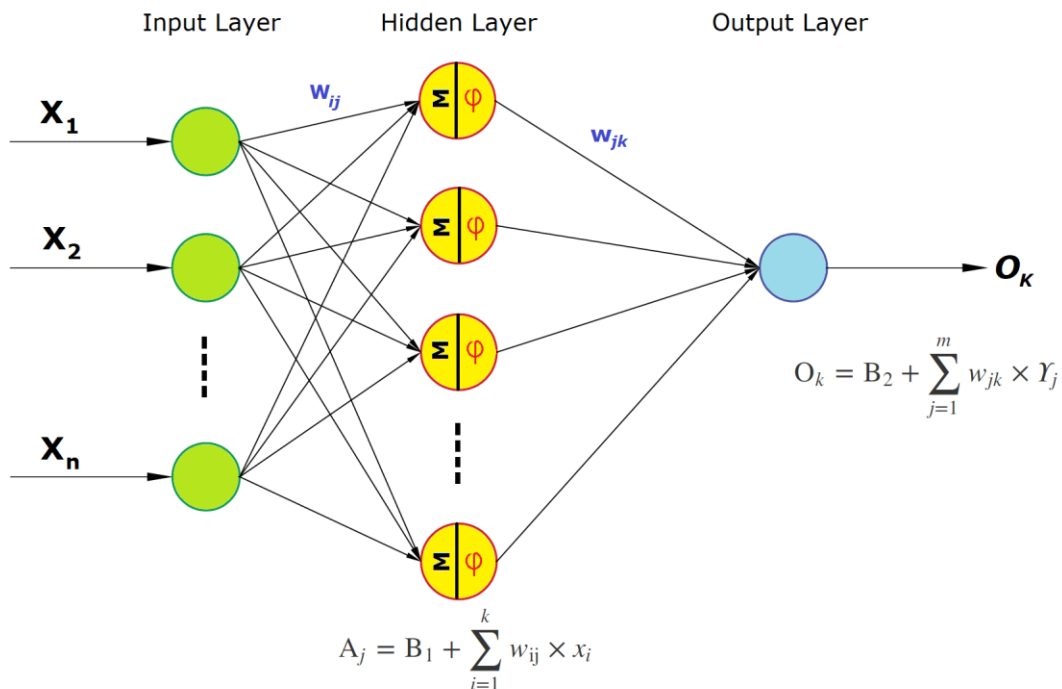


Figure 4.1 Multi-layer Perceptron (MLP) Neural Network architecture

Every single input (X_n), weighted by an element (w_{ij}) of the weight matrix (W) are summated and provided to the transfer function or activation function (ϕ) along with a bias (B) term. The activation function constructs a non-linear decision boundary via linear combinations of the weighted inputs and then applies a threshold to transform the net inputs from all the neuronal unit into an output signal. The Levenberg-Marquardt back propagation learning rule incrementally adjusts the weight and bias terms to minimize the mean square error (MSE) of the network. The quantum of progressions made in adjusting the synaptic weights and biases at every epoch is determined by the learning rate parameter. Smaller learning rates end up in longer training time however, warrant stability that steers to minimum errors.

4.4.2 Adaptive Neuro-Fuzzy Inference System

Adaptive neuro-fuzzy inference system (ANFIS) introduced by Jang, (1993) is a hybrid machine learning approach which involves a fuzzy inference system (FIS) assisted with back propagation algorithm to tune the membership function parameters of FIS. Depending on the complexity of the problem addressed, sometimes the back propagation gradient descent method in combination with a least squares method is used to adjust the parameters of FIS (Jang et al., 1997). The fuzzy inference system, based on the number of input parameters encompasses a set of fuzzy IF–THEN rules or conditional statements to approximate nonlinear functions. ANFIS is a multilayer feedforward five layer architecture as illustrated in Figure 4.2. The fixed nodes are represented by circular outline and the square outlines are adaptive nodes presided by parameter settings. Each node performs a particular function on incoming signals. Every node in the layer 1 (adaptive node) is associated with a node function governed by premise parameters. The output of every single node of layer 2 (fixed node) represents the firing strength of a rule which is nothing but the product of all incoming signals. Similarly, the output of every single node of layer 3 (fixed node) represents the normalized firing strength. Every node in the layer 4 is an adaptive node associated with a node function governed by consequent parameters. The final fixed node in layer 5 labeled as (Σ) computes the overall output as the summation of all incoming signals (Abraham, 2005). The premise and consequent parameters of ANFIS

are tuned in the learning process by means of a hybrid technique which involves the gradient descent back propagation method coupled with a least squares optimization algorithm to provide optimal outputs. Soon after the training converges, the values of the premise parameters of membership function are fixed in the search space and the overall output is expressed as a linear combination of the consequent parameters (Jang, 1992). Herein, grid-partitioning (GP) type of the ANFIS model was employed in the streambed hydraulic conductivity modeling scheme. The performance of ANFIS model is greatly affected by the type and number of membership functions, which are usually ascertained by trial and error procedure.

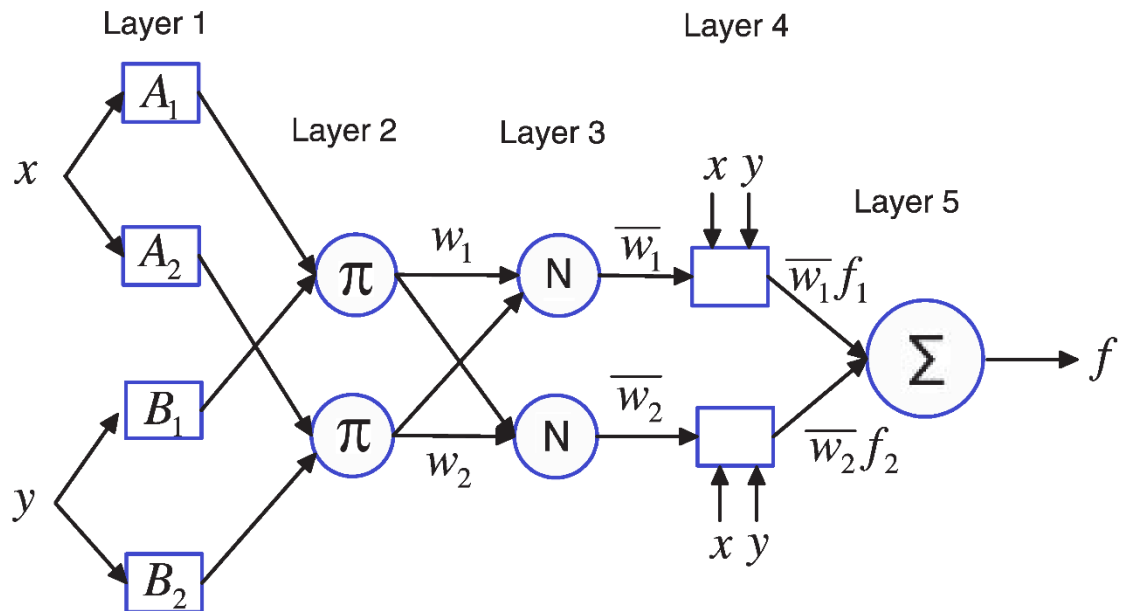


Figure 4.2 ANFIS architecture

4.4.3 Support Vector Machine

SVM one of the supervised learning method was introduced in 1992 by Vladimir Vapnik and his co-workers (Vapnik 1995). Basically, SVM is a machine learning technique for linear and non-linear classification as well as regression. In the case of non-linear data, SVM maps the data-sets of input space into a higher dimensional feature space, using kernel functions which have the ability to convert them into linear ones. In the high dimensional feature space, simpler and linear hyper plane classifiers that have a maximal

margin between the classes are obtained. SVM provides maximum predictive accuracy automatically either by avoiding/minimizing over fitting of data. SVM is based on Structural Risk Minimization principle and includes convex optimization algorithm wherein the empirical risk and the confidence interval of the learning machine are simultaneously minimized by maximizing the geometric margin. SVM can efficiently perform nonlinear regression by utilizing Kernel trick. The computation is critically dependent upon the length of the training patterns/data-set, selection of hyper-parameters and finding out their optimal values while modeling. The details regarding SVM and its theory could be found in the following literatures (Cortes and Vapnik 1995; Cristianini and Shawe-Taylor 2000; Vapnik, 1999).

Let us consider a simple linear regression problem trained on data set $\chi = \{u_i, v_i; i = 1, \dots, n\}$ with input vectors u_i and linked targets v_i . A function $g(u)$ has to be formulated approximately in order to link up inherited relations between the data sets and thereby it could be used in the later part to infer the output v for a new input data u .

Standard SVM regression uses a loss function $L_\epsilon(v, g(u))$ which describes the deviation of the estimated function from the original one. Several types of loss functions can be mined in the literature e.g., linear, quadratic, exponential, Huber's loss function etc. In the present context the standard Vapnik's $-\epsilon$ insensitive loss function is used which is defined as

$$L_\epsilon(v, g(u)) = \begin{cases} 0 & \text{for } |v - g(u)| \leq \epsilon \\ |v - g(u)| - \epsilon & \text{otherwise} \end{cases} \quad (4.14)$$

Using ϵ -insensitive loss function, one can find $g(u)$ that can better approximate the actual output vector ' v ' and has the at most error tolerance ϵ from the actual incurred targets v_i for all training data, and concurrently as flat as possible. Consider the regression function defined by

$$g(u) = w \cdot u + b \quad (4.15)$$

where, $w \in \chi$, χ is the input space; $b \in \mathbb{R}$ is a bias term and $(w \cdot u)$ is dot product of vectors w and u . Flatness in Equ. (4.15) refers to a smaller value of parameter vector w . By

minimizing the norm $\|w\|^2$, flatness can be ascertained along with model complexity. Thus regression problem can be stated as the following convex optimization problem.

$$\begin{aligned}
\min_{w, b, \xi, \xi^*} \quad & \frac{1}{2} \|w\|^2 + C \sum_{i=1}^n (\xi_i + \xi_i^*) \\
\text{subject to} \quad & v_i - (w \cdot u_i + b) \leq \varepsilon + \xi_i \\
& (w \cdot u_i + b) - v_i \leq \varepsilon + \xi_i^* \\
& \xi_i, \xi_i^* \geq 0, \quad i = 1, 2, \dots, n
\end{aligned} \tag{4.16}$$

where, ξ_i and ξ_i^* are slack variables introduced to evaluate the deviation of training samples outside ε -insensitive zone. The trade-off between the flatness of g and the quantity up to which deviations greater than ε are tolerated is depicted by $C > 0$. C is a positive constant influencing the degree of penalizing loss when a training error occurs. Underfitting and overfitting of training data are avoided by minimization of the regularization term $w^2/2$ along with the training error term $C \sum_{i=1}^n (\xi_i + \xi_i^*)$ in Equ. (4.16).

The minimization problem in Equ. (4.16) represents the primal objective function.

Now the problem is dealt by constructing a Lagrange function from the primal objective function by introducing a dual set of variables, $\underline{\alpha}_i$ and $\bar{\alpha}_i$ for the corresponding constraints. Optimality conditions are exploited at the saddle points of a Lagrange function leading to the formulation of the dual optimization problem:

$$\begin{aligned}
\max_{\underline{\alpha}_i, \bar{\alpha}_i} \quad & -\frac{1}{2} \sum_{i,j=1}^n (\underline{\alpha}_i - \bar{\alpha}_i) (\underline{\alpha}_j - \bar{\alpha}_j) \langle u_i \cdot u_j \rangle - \varepsilon \sum_{i=1}^n (\underline{\alpha}_i + \bar{\alpha}_i) + \sum_{i=1}^n v_i (\underline{\alpha}_i - \bar{\alpha}_i) \\
\text{subject to} \quad & \sum_{i=1}^n (\underline{\alpha}_i - \bar{\alpha}_i) = 0 \\
& 0 \leq \underline{\alpha}_i \leq C, \quad i = 1, 2, \dots, n \\
& 0 \leq \bar{\alpha}_i \leq C, \quad i = 1, 2, \dots, n
\end{aligned} \tag{4.17}$$

After determining Lagrange multipliers, $\underline{\alpha}_i$ and $\bar{\alpha}_i$; the parameter vectors w and b can be evaluated under Karush–Kuhn–Tucker (KKT) complementarity conditions (Fletcher, 1987), which are not discussed herein. Therefore, the prediction is a linear regression function that can be expressed as

$$g(\mathbf{u}) = \sum_{i=1}^n (\alpha_i - \bar{\alpha}_i) \langle \mathbf{u}_i, \mathbf{u} \rangle + b \quad (4.18)$$

Thus SVM regression expansion is derived; where w is depicted as a linear combination of the training patterns v_i and b can be found using primary constraints. For $|g(\mathbf{u})| \geq \varepsilon$ Lagrange multipliers may be non-zero for all the samples inside the ε -tube and these remaining coefficients are termed as support vectors.

Now for making SVM regression to deal with non-linear cases; pre-processing of training patterns u_i has to be done by mapping the input space χ into some feature space \mathfrak{S} using nonlinear function $\varphi = \chi \rightarrow \mathfrak{S}$ and then apply to the standard support vector algorithm. Let u_i be mapped into the feature space by nonlinear function $\varphi(u)$ and hence the decision function is given by

$$g(w, b) = w \cdot \varphi(u) + b \quad (4.19)$$

This nonlinear regression problem can be expressed as the following optimization problem. Figure 4.3 depicts the concept of nonlinear support vector regression corresponding to Equ. 4.20.

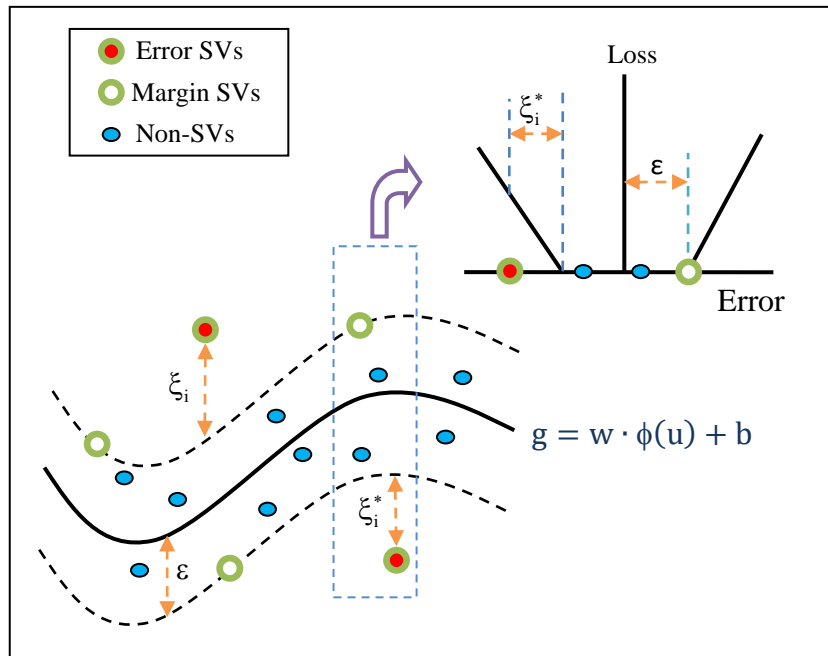


Figure 4.3 Nonlinear SVM with Vapnik's ε -insensitive loss function.
(Adapted from Yu et al. 2006)

$$\begin{aligned}
& \min_{w, b, \xi, \xi^*} \quad \frac{1}{2} \|w\|^2 + C \sum_{i=1}^n (\xi_i + \xi_i^*) \\
& \text{subject to} \quad v_i - (w \cdot \varphi(u_i) + b) \leq \varepsilon + \xi_i \\
& \quad \quad \quad (w \cdot \varphi(u_i) + b) - v_i \leq \varepsilon + \xi_i^* \\
& \quad \quad \quad \xi_i, \xi_i^* \geq 0, \quad i = 1, 2, \dots, n
\end{aligned} \tag{4.20}$$

where w is the vector of coefficients, ξ_i and ξ_i^* are the distances of the training data set points from the region where the errors less than ε are ignored and b is a constant. The index i labels the ‘ n ’ training cases. The $y \in \pm 1$ is the class labels and u_i is the independent variable. Then, the dual form of the nonlinear SVR can be expressed as

$$\begin{aligned}
& \max_{\underline{\alpha}, \bar{\alpha}} \quad -\frac{1}{2} \sum_{i,j=1}^n (\underline{\alpha}_i - \bar{\alpha}_i) (\underline{\alpha}_j - \bar{\alpha}_j) \langle \varphi(u_i) \cdot \varphi(u_j) \rangle - \varepsilon \sum_{i=1}^n (\underline{\alpha}_i + \bar{\alpha}_i) + \sum_{i=1}^n v_i (\underline{\alpha}_i - \bar{\alpha}_i) \\
& \text{subject to} \quad \sum_{i=1}^n (\underline{\alpha}_i - \bar{\alpha}_i) = 0 \\
& \quad \quad \quad 0 \leq \underline{\alpha}_i \leq C, \quad i = 1, 2, \dots, n \\
& \quad \quad \quad 0 \leq \bar{\alpha}_i \leq C, \quad i = 1, 2, \dots, n
\end{aligned} \tag{4.21}$$

The “kernel trick” $K(u_i, u_j) = \langle \varphi(u_i), \varphi(u_j) \rangle$ is used for computations in input space χ to fetch the inner products into feature space \mathfrak{F} . Any function satisfying Mercer’s theorem (Vapnik, V, 1999) should be used as kernels. Finally, the decision function of nonlinear SVM regression with the allowance of the kernel trick is expressed as follows.

$$g(u) = \sum_{i,j=1}^n (\underline{\alpha}_i - \bar{\alpha}_i) K(u_i \cdot u) + b \tag{4.22}$$

The parameters that impact over the effectiveness the nonlinear SVM are the cost constant C , the radius of the insensitive tube ε , and the kernel parameters. These parameters are mutually dependent over one another and hence altering the value of one parameter affects the other linked parameters also. The parameter C checks for the smoothness/flatness of the approximation function. A smaller value of C yields a learning machine with poor approximation due to underfitting of training data. A greater C value overfits the training data and sets its objective to minimize only the empirical risk making way for more complex learning. The parameter ‘ ε ’ is related with smoothening the complexity of the approximation function and controls the width of the ε -insensitive zone used for fitting the

training data. The parameter ‘ ϵ ’ influences over the number of support vectors, and then both the complexity and the generalization capability of the approximation function is dependent upon its value. It also governs the precision of the approximation function. Smaller values of ϵ lead to more number of support vectors and results in complex learning machine. Greater ‘ ϵ ’ values result in more flat estimates of the regression function. Determining appropriate values of C and ϵ is often a heuristic trial-and-error process. Figure. 4.4 shows the general network architecture of SVM.

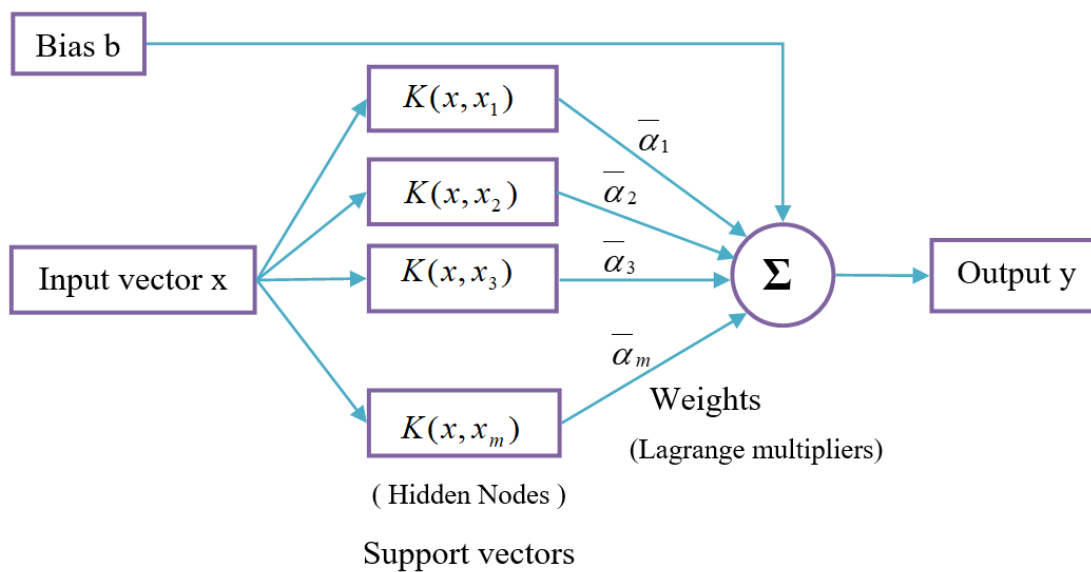


Figure 4.4. Network architecture of SVM. (Adapted from Chen and Yu, 2007)

4.5 Strategies for spatial modeling using AI Paradigms

For spatial modeling of streambed hydraulic conductivity, two diverse schemes/strategies were adopted. As already mentioned, the hydraulic conductivity tests were conducted along 40 transects across the channel covering the upstream and downstream reaches of each vented dam. The spacing between each transect was 50m and in each transect, for every 5 meter interval, K_s was determined. So, in the *first strategy*, the training and testing dataset were chosen in such a pattern that, the K_s data along a transect was estimated by considering the K_s data of two neighborhood transects both upstream and downstream. The Figure 4.5 shows the scheme of selection of training and testing transects

along the study reach. The K_s data measured at transect locations – 2, 3, 5, 6, 8, 9, 11, 12, 13, 15, 16, 18, 19, 21, 22, 24, 25, 27, 28, 30, 31, 33, 34, 36, 37, 39, 40 were considered as training features and the models were calibrated to estimate the K_s values at transects – 1, 4, 7, 10, 14, 17, 20, 23, 26, 29, 32, 35, 38. The predicted K_s values were evaluated against the observed K_s values at those transects. The sample size considered for training and testing of AI models were 134 and 53 K_s point samples in the case of Strategy 1. During model development, the point location details (i.e., the geographical information - latitude and longitude) from where the K_s values were sampled along each transects were considered as model inputs by targeting measured K_s . Specifically, the geographical coordinates were the predictors and the K_s values serve as predictand. The testing transects were considered to be the unknown locations where there is a necessity for prediction. While model testing, the K_s values were estimated at those testing transect locations by entering only geographical coordinates as inputs so that it becomes easier to validate the model predictions based on the observed K_s values. Similarly, in the *second strategy*, the alternate transects - one after the other were considered as training and testing transects. The scheme of Strategy 2 is as shown in Figure 4.6. In this case, the samples of upstream transects are considered for training the models. The sample size considered for training and testing of AI models were 96 and 91 K_s point samples in the case of Strategy 2.

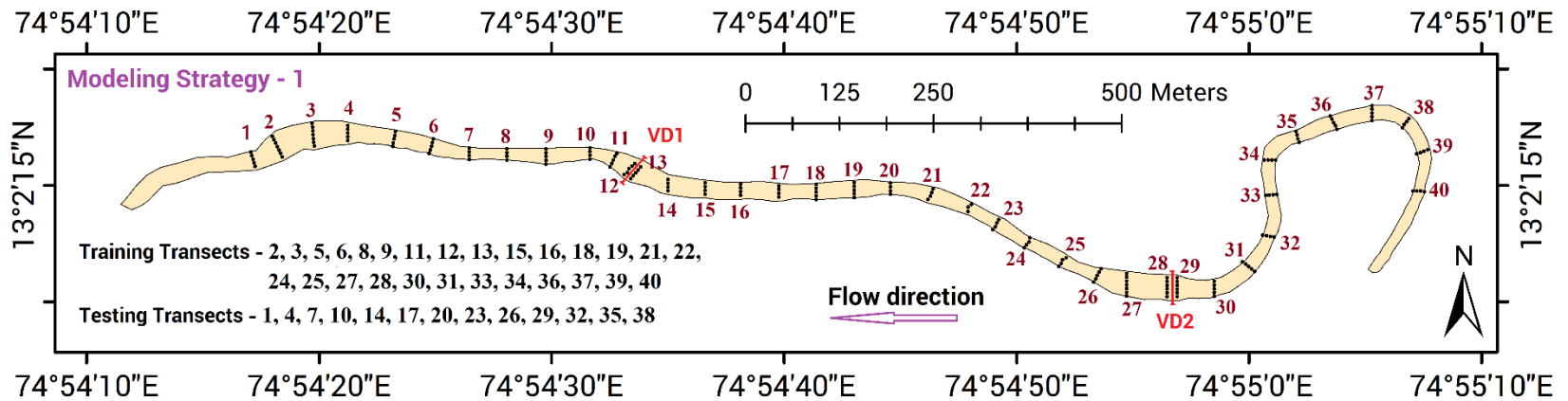


Figure 4.5 Spatial modeling scheme – Strategy 1

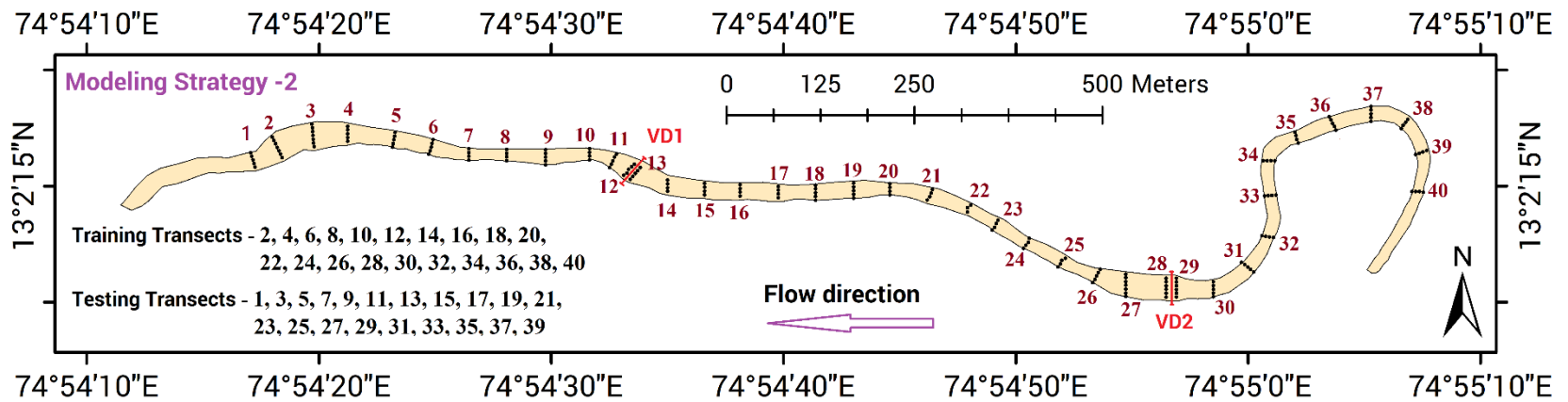


Figure 4.6 Spatial modeling scheme – Strategy 2

4.6 Performance evaluation measures

The spatial prediction performance of all the models were evaluated by computing error and efficiency statistics as given below.

Statistical Criteria	Value	Inference
<p><i>Root Mean Square Error,</i></p> $\mathbf{RMSE} = \sqrt{\frac{\sum_{i=1}^N (O_i - P_i)^2}{N}}$	Value below half the standard deviation	Satisfactory
<p><i>Relative RMSE,</i></p> $\mathbf{RRMSE} = \frac{RMSE}{\sigma_{obs}}$	<p>0.00 ≤ RRMSE ≤ 0.10</p> <p>0.10 ≤ RRMSE ≤ 0.30</p> <p>0.30 ≤ RRMSE ≤ 0.50</p> <p>RRMSE > 0.70</p>	<p>Very Good</p> <p>Good</p> <p>Satisfactory</p> <p>Poor</p>
<p><i>Mean Absolute Error,</i></p> $\mathbf{MAE} = \frac{\sum_{i=1}^N P_i - O_i }{N}$	Value below half the standard deviation	Satisfactory
<p><i>Nash-Sutcliffe Efficiency,</i></p> $\mathbf{NSE} = 1 - \frac{\sum_{i=1}^N (P_i - O_i)^2}{\sum_{i=1}^N (O_i - \bar{O})^2}$	<p>0.75 < NSE < 1.00</p> <p>0.65 < NSE ≤ 0.75</p> <p>0.50 < NSE ≤ 0.65</p> <p>0.4 < NSE ≤ 0.50</p> <p>NSE ≤ 0.4</p>	<p>Very good</p> <p>Good</p> <p>Satisfactory</p> <p>Acceptable</p> <p>Unsatisfactory</p>

<i>Kling-Gupta efficiency,</i>	$0.70 < \text{KGE} < 1.00$	Very good
KGE = $1 - \sqrt{(R-1)^2 + (\beta-1)^2 + (\gamma-1)^2}$	$0.60 < \text{KGE} \leq 0.70$	Good
<i>Correlation Coefficient,</i>	$0.50 < \text{KGE} \leq 0.60$	Satisfactory
$\mathbf{R} = \left[\frac{\sum_{i=1}^N (O_i - \bar{O}) \cdot (P_i - \bar{P})}{\sqrt{\sum_{i=1}^N (O_i - \bar{O})^2 \cdot \sum_{i=1}^N (P_i - \bar{P})^2}} \right]$	$0.4 < \text{KGE} \leq 0.50$	Acceptable
<i>Bias Ratio,</i> $\beta = \frac{\bar{P}}{\bar{O}}$	$\text{KGE} \leq 0.4$	Unsatisfactory
<i>Variability,</i> $\gamma = \frac{CV_p}{CV_o} = \frac{\sigma_p / \bar{P}}{\sigma_o / \bar{O}}$		

where, O and P signpost the observed and predicted K_s values, respectively. \bar{O} and \bar{P} are the mean of observed and forecasted values, σ_o and σ_p are the standard deviation of observed and forecasted values, respectively. N represents the total number of data samples.

CHAPTER 5

RESULTS AND DISCUSSION

5.1 General

This chapter presents the descriptive and inferential statistical results of streambed K_s measurements sampled from the study reach. The obtained statistical measures are thoroughly discussed and comparatively evaluated to provide a major theoretical advance, on the state of the understanding about the processes controlling hydraulic conductivity. The spatial maps of streambed K_s plotted by using deterministic and geostatistical approaches are presented and discussed succinctly. The chapter also includes the results of prediction of K_s using AI based approaches.

5.2 Analysis of streambed hydraulic conductivity values from in-situ GUELPH permeameter tests

The descriptive statistics of in situ measured streambed hydraulic conductivity (K_s) along the three segments of the study reach measured at two different time periods are presented in Table 5.2.1 to illustrate the overall variation in the K_s distribution. The magnitude of K_s with reference to the three segments varied by two orders of magnitude. The streambed K_s along the stream reach varied from 11.634 cm/day – 793.886 cm/day and 16.932 cm/day – 777.989 cm/day during the sampling periods 2016 and 2017, respectively. The longitudinal variability of streambed hydraulic conductivity along every 50m upstream and downstream of vented dams is presented in Figure 5.1. It is evident that, there exists significant differences in mean K_s values of the upstream and downstream segments of vented dams. Progressive decrease and inconsistent mean K_s values can be

observed while getting away from the vented dam 1 towards downstream. Due to lateral accretion deposits spread out by second order stream confluence at around 50m downstream of vented dam 2, an elevated mean K_s is observed at this transect. The mean K_s values of all transects, downstream of vented dam 1 varied between 31.85–188.98 cm/day for 2016 samples and 35.77–192.09 cm/day for 2017 samples; similarly at segment 2 varied between 100.88–535.73 cm/day for 2016 samples and 111.33–504.87 cm/day for 2017 samples. The mean K_s values of all transects upstream of vented dam 2 varied between 473.59–755.39 cm/day for 2016 samples and 377.39–753.31 cm/day for 2017 samples. The streambed K_s samples of segment 3 had reasonable temporal variability due to episodic changes in substrate particles and organic matter inputs at the meander bend of stream which is evident from significant differences in the minimum and extreme values of K_s .

Table 5.2.1 Descriptive statistical analysis of field-scale streambed hydraulic conductivity (K_s) (cm/day)

2016 Data	Min	Max	Mean	S_d	Var	Kurtosis	Skewness
Segment 1	11.634	205.2	87.015	59.339	3521.092	-0.992	0.638
Segment 2	76.871	558.481	328.703	142.222	20227.01	-1.125	-0.444
Segment 3	376.678	793.886	674.809	101.678	10338.47	1.295	-1.358
Full Stretch	11.634	793.886	349.809	255.518	65289.44	-1.337	0.283
2017 Data							
Segment 1	16.932	231.967	93.676	62.386	3892.03	-0.646	0.775
Segment 2	65.86	547.88	332.857	141.238	19948.25	-1.113	-0.426
Segment 3	280.273	777.989	657.485	121.177	14683.98	1.583	-1.503
Full Stretch	16.932	777.989	348.578	249.325	62162.71	-1.301	0.298

Note: S_d – Standard Deviation; Var – Variance

Many varying conditions occur as a result of different geologic and geomorphic characteristics of a river. The stream characteristics that can influence streambed hydraulic conductivity include the configuration of channel geometry, floodplain connection, streambed substrate characteristics like texture, structure etc.

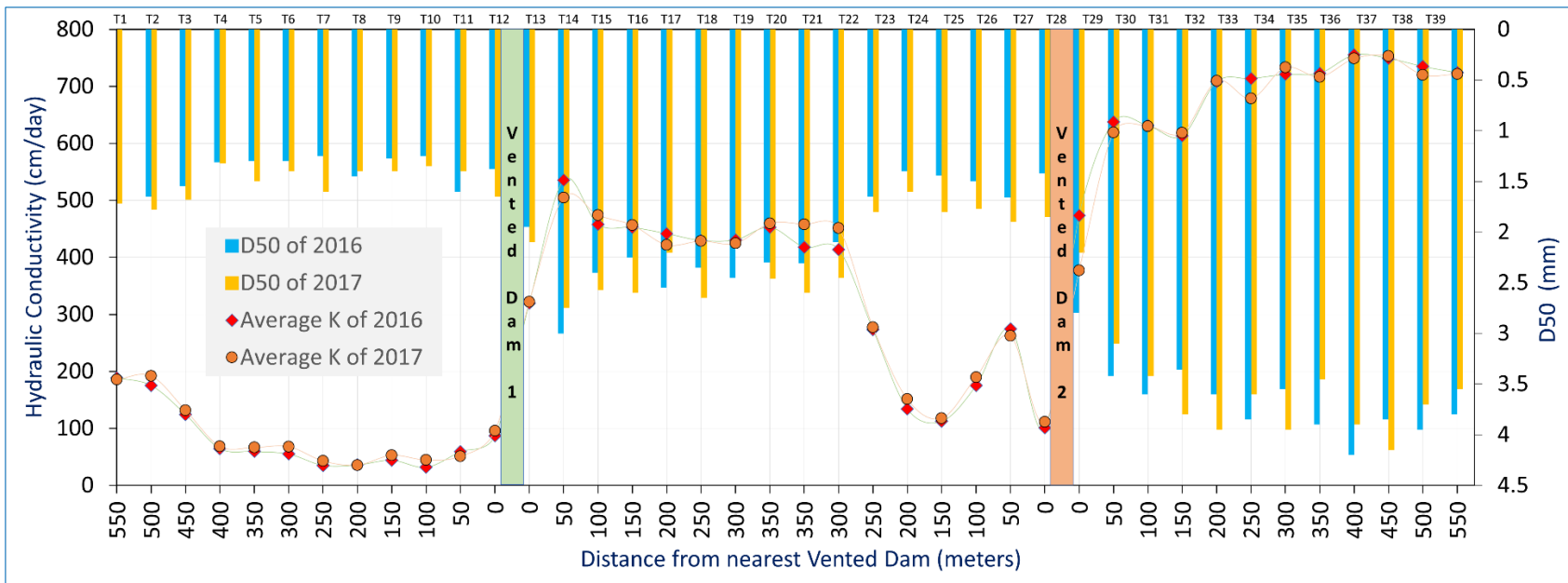


Figure 5.1. D50 and Mean K_s values at transects along the study reach.

The grain size distribution of sediments collected from each transect of the study reach was analyzed in terms of D50 (median diameter), which showed a good correlation with mean K_s values of the corresponding transect. Coarse sediments tend to have a greater percentage of pore space, and hence a lower density, whilst the fine sediments usually contain a greater fraction of clay packed in the pore spaces between larger grains that affects the streambed K_s . As a support to this premise, significant statistical correlation existed between the D50 (median diameter) and mean K_s values of transects along the study reach with $R=0.97$ and 0.96 for samples of 2016 and 2017, respectively. Over the entire study reach, D50 varied between 1.25–4.2 mm with reference to 2016 sediment samples and 1.4–4.15 mm for 2017 samples. As expected, D50 didn't exhibit a static or homogeneous distribution over the reach due to complex patterns of flow and sediment regime instigated by the existence of vented dams. As a result of silt and particulate organic matter inputs from the floodplain and riparian vegetation, the sediments of segment 1 had lower D50 values in the range 1.25–2.25 mm with respect to 2016 samples and 1.4–1.78mm pertaining to 2017 samples. The sediments of segment 2 (sinuous channel) and segment 3 (meandering channel) had moderate D50 values as presented in Figure 5.1.

5.3 Variability of streambed hydraulic conductivity along the study reach

5.3.1 Results of Statistical analysis

The variation of K_s data depicted via box plots (presented in Figure 5.2) allows to analyze the mean, median, range; identify outliers, extreme values and the dispersion represented via interquartile range. The frequency distributions of K_s data is graphically represented by histograms (refer Figures 5.3 and 5.4) wherein a normal distribution is hypothesized and tested through 'Normality tests'. The results of Kolmogorov-Smirnov (K-S), K-S with Lilliefors correction, Shapiro-Wilk and D'Agostino-Pearson tests for K_s measured at two time periods are provided in Table 5.3.1. With reference to the full stretch of stream reach considered, all the normality tests showed a p-value less than 0.05, which signposts a non-normal distribution of both K_s and $\ln(K_s)$ of two different time periods.

Even after transforming the K_s data by using natural log, the distribution remained non-normal due to inherent heterogeneity and significant field scale variability of K_s across the study reach. The K_s data of segment 1 of the year 2016 was observed to have non-normal distribution based on all test statistics. However, the \ln transformed K_s values were found to be normally distributed based on the K-S and D'Agostino-Pearson tests for the same segment.

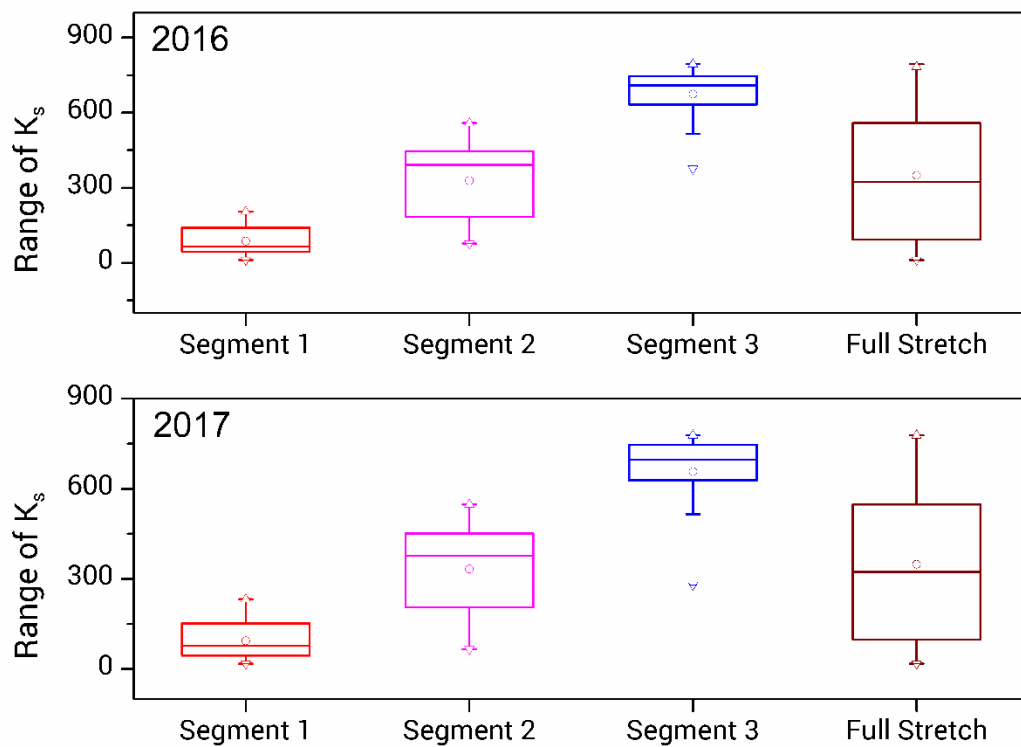


Figure 5.2 Box and whisker plots summarizing K_s measurements of the study reach. The intrabox dots denote medians, triangles denote outliers, whiskers represent minimum and maximum values, and the box edges denote 25th and 75th percentiles.

Table 5.3.1 Comparison among various Normality Tests for checking normal distribution

Normality Tests	K _s data of 2016		K _s data of 2017		lnK _s data of 2016		lnK _s data of 2017	
	Test Statistic	<i>p-value</i>	Test Statistic	<i>p-value</i>	Test Statistic	<i>p-value</i>	Test Statistic	<i>p-value</i>
Segment 1								
Kolmogorov-Smirnov (K-S) Test	1.4814	0.0248	1.5419	0.0172	0.9377	0.3428	0.7887	0.5626
K-S Lilliefors Modification	0.1897	0	0.1974	0	0.1201	0.0289	0.101	0.1961
Shapiro-Wilk Test	0.8825	0	0.888	0	0.9377	0.0039	0.9544	0.0233
D'Agostino-Pearson Test	11.5312	0.0031	7.6412	0.0219	3.0898	0.2133	2.8792	0.237
Segment 2								
Kolmogorov-Smirnov (K-S) Test	1.6903	0.0066	1.2728	0.0783	1.8715	0.0018	1.6047	0.0116
K-S Lilliefors Modification	0.1992	0	0.15	0.0004	0.2206	0	0.1891	0
Shapiro-Wilk Test	0.9105	0.0001	0.9232	0.0003	0.8385	0	0.8524	0
D'Agostino-Pearson Test	17.8104	0.0001	16.9169	0.0002	10.6289	0.0049	12.2018	0.0022
Segment 3								
Kolmogorov-Smirnov (K-S) Test	1.3148	0.063	1.5417	0.0172	1.4682	0.0268	1.7326	0.0049
K-S Lilliefors Modification	0.1789	0.0002	0.2098	0	0.1998	0	0.2358	0
Shapiro-Wilk Test	0.8544	0	0.8161	0	0.7981	0	0.7455	0
D'Agostino-Pearson Test	16.0185	0.0003	18.8866	0.0001	25.509	0	31.0407	0
Full Stretch								
Kolmogorov-Smirnov (K-S) Test	2.0831	0.0003	1.67	0.0076	2.3596	0	2.1546	0.0002
K-S Lilliefors Modification	0.1523	0	0.1221	0	0.1726	0	0.1576	0
Shapiro-Wilk Test	0.9035	0	0.9076	0	0.9001	0	0.9059	0
D'Agostino-Pearson Test	202.9678	0	157.1172	0	17.5491	0.0002	17.6867	0.0001

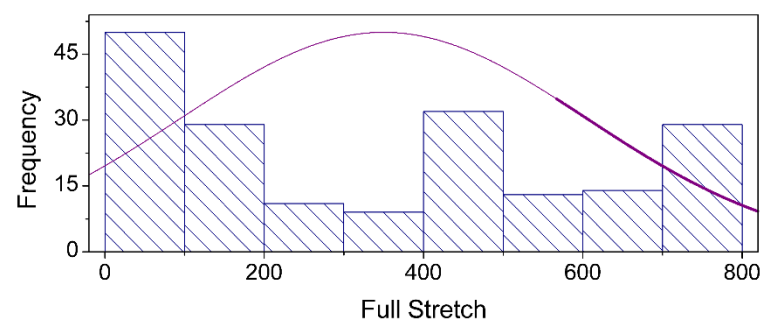
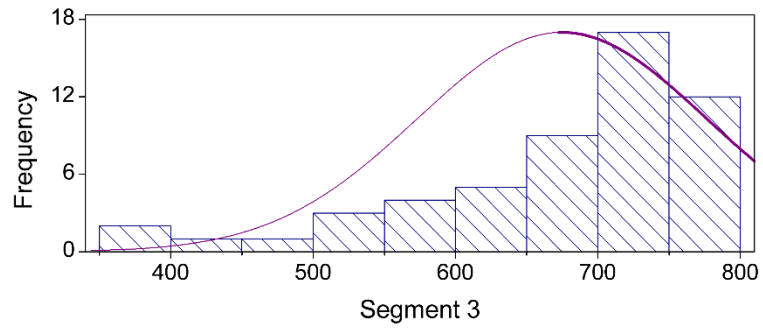
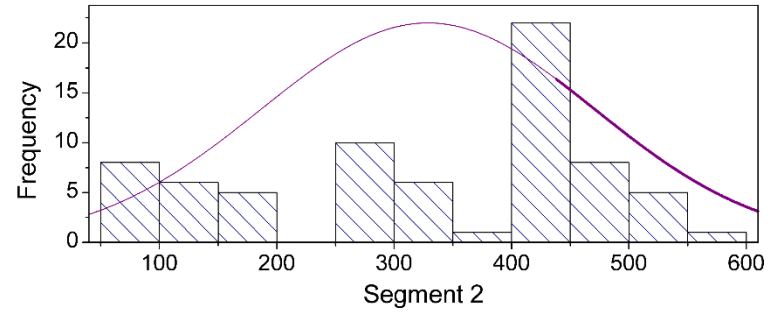
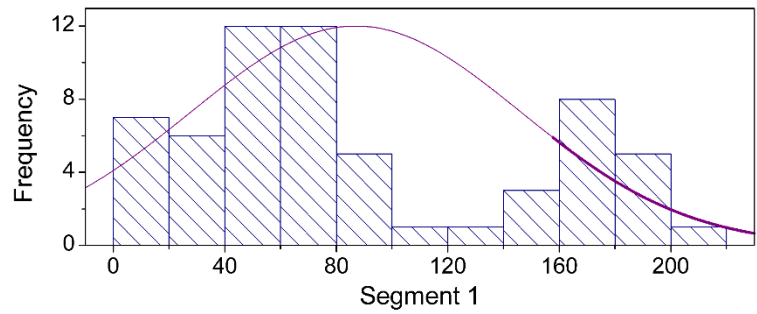
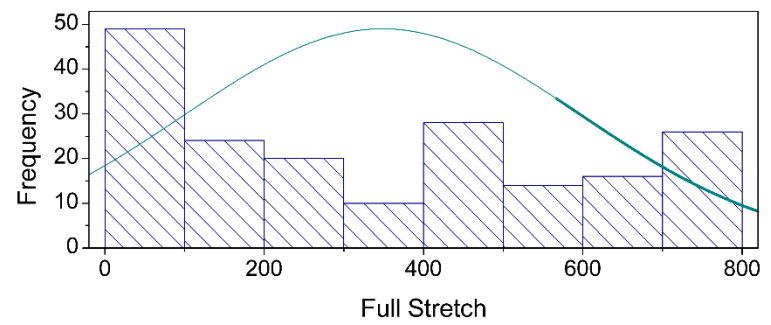
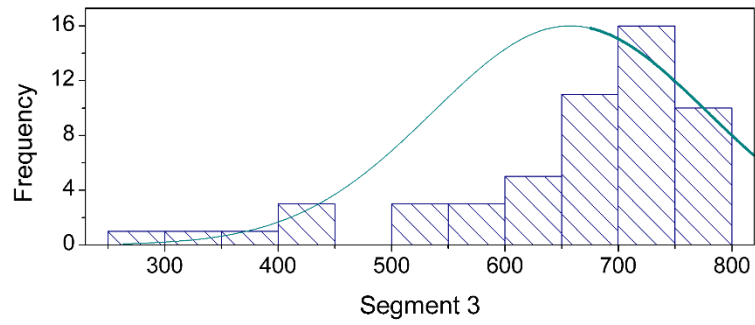
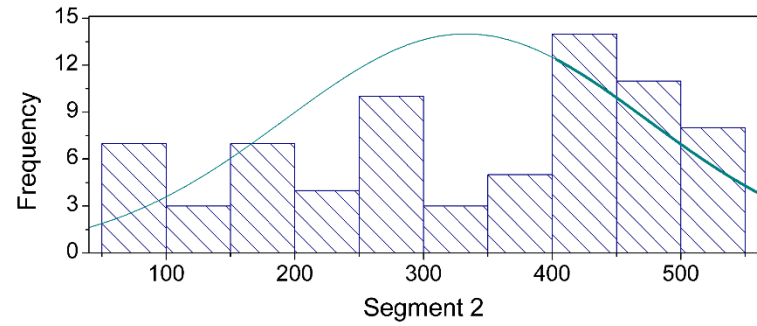
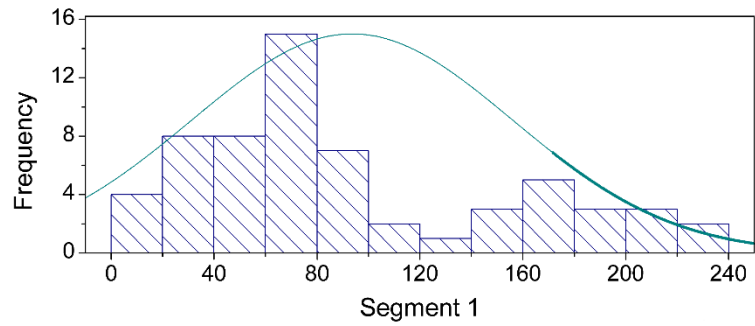


Figure 5.3 Histograms constructed from streambed K_s samples of the year 2016



. Figure 5.4 Histograms constructed from streambed K_s samples of the year 2017

In the 2017 study period, all the normality tests except, Shapiro-Wilk test accepted the null hypothesis of normal distribution of the \ln transformed K_s values at the segment 1 even though, the realistic K_s values were found to be non-normal. The K-S test was the only one to confirm normality of K_s values sampled from segment 2 (during 2017) and segment 3 (during 2016) with a fair p-value > 0.05 . Due to the skewed nature of K_s data of segment 3 during 2017, all the normality tests rejected the null hypothesis of normal distribution of K_s data at a significance level of 0.05. A distribution can deviate from that of normal due to lack of symmetry (skewness), kurtosis and mixture of distributions. The empirical CDF curve of the K-S test and the Q-Q plots presented in Figures 5.5 and 5.6 also portray that K_s data follows a non-normal distribution with reference to K_s data of full stretch.

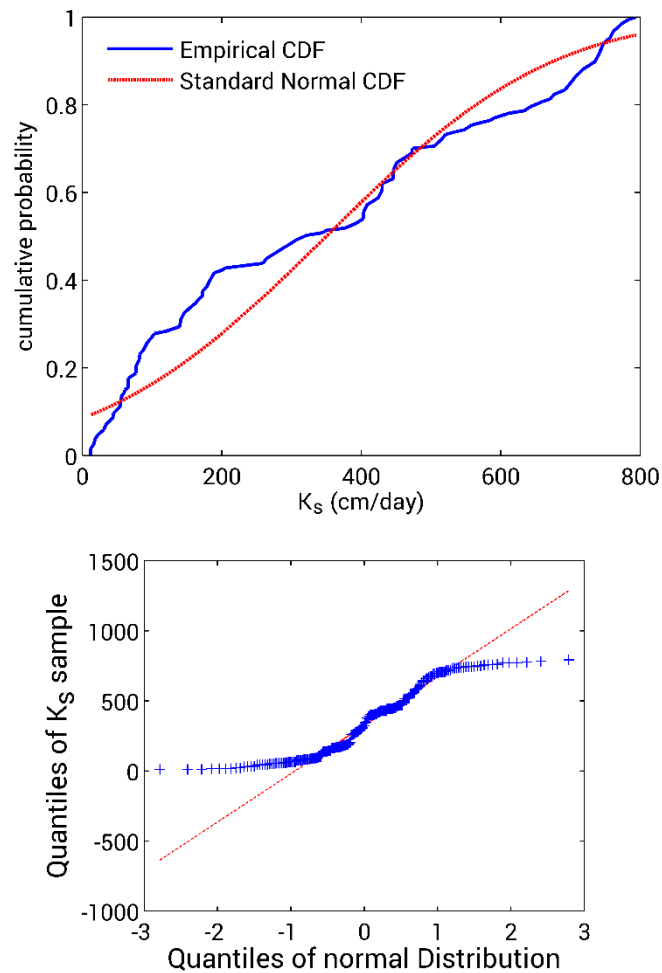


Figure 5.5 Empirical CDF curve of the K-S test and the Q-Q plot of the 2016 K_s data.

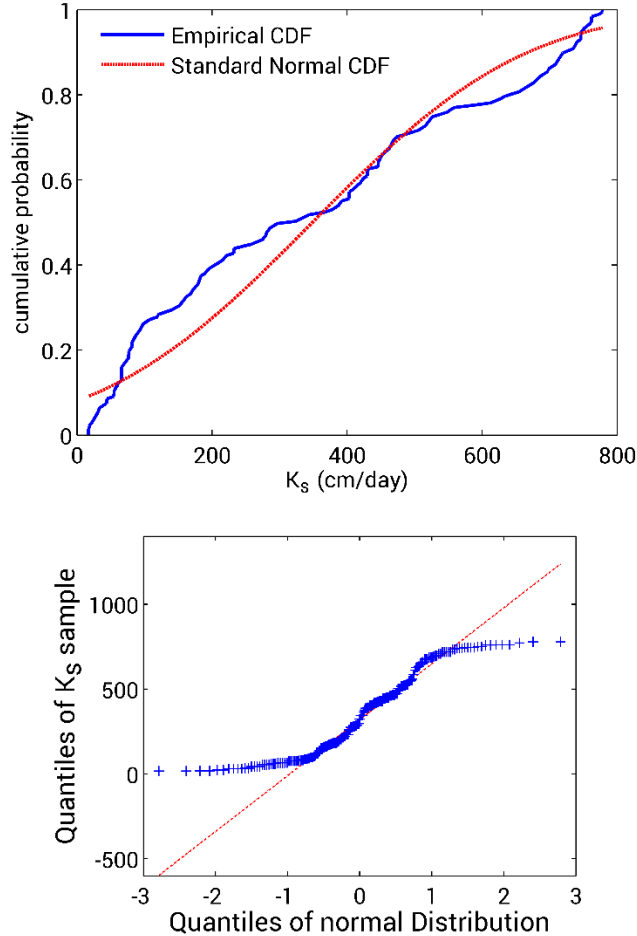


Figure 5.6 Empirical CDF curve of the K-S test and the Q-Q plot of the 2017 K_s data.

The results of Levene's and Welch's t-tests (Table 5.3.2) infer that there exists significant differences in the variance and mean of streambed K_s sampled from the three segments of the study reach. The mean and variance of streambed K_s samples measured at the upstream section of vented dams significantly varied from that of the downstream K_s samples during both the study periods. For instance, the test statistic of Levene's test, conducted for testing equality of variance between samples of segments 1 and 2 of the year 2016, was relatively large with $W=28.92$ and $p=0$. The fluvial sedimentation on the upstream channel of the vented dams, and the bed incision at the downstream which is however compensated during floods accompanied by retrogressive erosion were the main reasons for significant spatial variability of K_s. Various kinds of valley deposits, their physical composition, distinct associations of several deposits, relative distribution and

accumulation places in the streams are some other related factors causing variability in streambed K_s . With respect to streambed K_s of individual segments sampled at different time periods, the Levene's test failed to reject the null hypothesis at the 0.05 significance level (Table 5.3.2) thereby confirming the assumption of temporal homoscedasticity of streambed K_s . The Welch's t-test also accepted the null hypothesis that there was no significant differences in the central tendency of the K_s values sampled between the two time periods in the study reach thereby discarding the rationale of temporal K_s evolution. The negative test statistic (t-values) reflect that the sample mean was smaller than that of the hypothesized mean.

Table 5.3.2 Test results of Levene's and Welch's t-tests.

Between Samples of	Levene's Test		Welch's t-test	
	Test Statistic	<i>p-value</i>	Test Statistic	<i>p-value</i>
Segment 1 & Segment 2 of 2016	28.92	0	-13.13	0
Segment 2 & Segment 3 of 2016	8.41	0.004	-15.92	0
Segment 1 & Segment 3 of 2016	5.37	0.022	-37.24	0
Segment 1 & Segment 2 of 2017	36	0	-12.95	0
Segment 2 & Segment 3 of 2017	5.19	0.024	-13.86	0
Segment 1 & Segment 3 of 2017	7.07	0.009	-30.77	0
Segment 1 of 2016 & 2017	0.03	0.866	-0.6	0.547
Segment 2 of 2016 & 2017	0	0.993	-0.18	0.861
Segment 3 of 2016 & 2017	0.42	0.52	0.8	0.423
Full Stretch of 2016 & 2017	0.27	0.604	0.05	0.962

5.3.2 Results of Geostatistical analysis

The residual spatial autocorrelation between the samples of a variable in the geographical lattice can be detected through 'Spatial correlogram' which is usually a plot of Moran's I as a function of distance or **number** of neighbors. The Moran's I coefficient between P and P_{lag} is simply a slope of the least squares regression line that best fits the

points. Each of the spatial neighborhood sensitivity plots as presented in Figures 5.7, 5.8, 5.9 and 5.10 are distance based (spatial) correlogram revealing the Moran's I across several neighborhood sizes. A significant and positive spatial autocorrelation was observed in the streambed K_s patterns as represented by Moran's I value close to +1. The Moran's I was observed to diminish for the farthest neighbors from that of the reference point representing shrinking of spatial dependence.

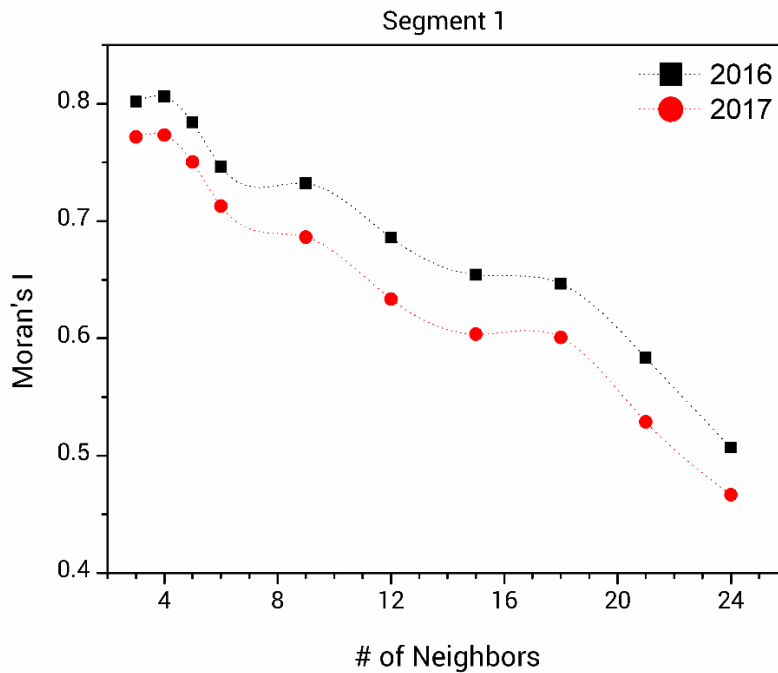


Figure 5.7 Moran's I Spatial Correlogram for streambed K_s patterns of segment 1 which is the downstream of vented dam 1. The dots indicate the values of Moran's I at a significance level of 0.05.

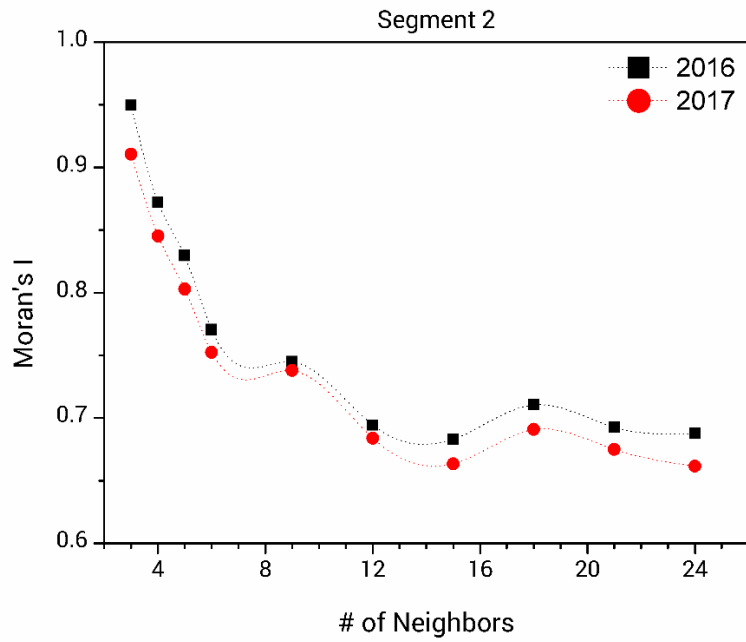


Figure 5.8 Moran's I Spatial Correlogram for streambed K_s patterns of segment 2 which is the streambed between vented dam 1 and 2.

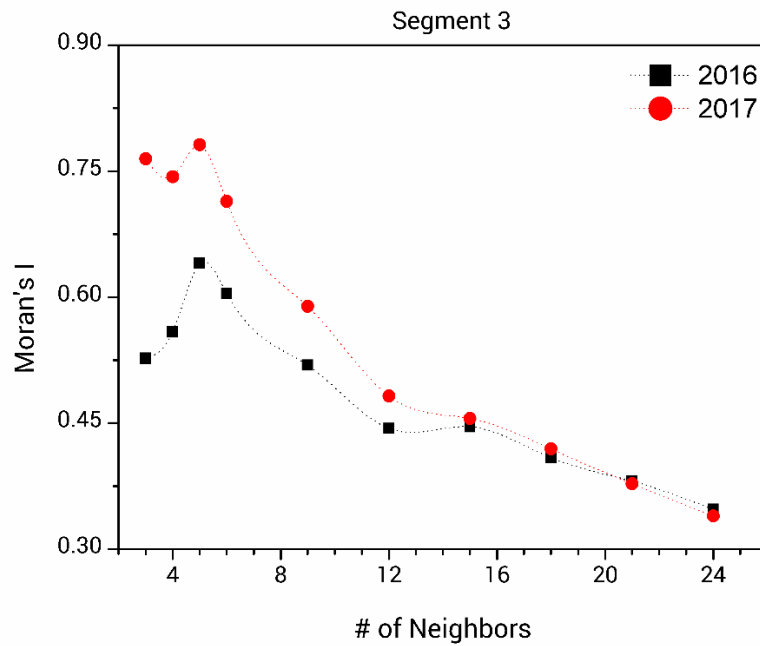


Figure 5.9 Moran's I Spatial Correlogram for streambed K_s patterns of segment 3 which is the upstream of vented dam 2.

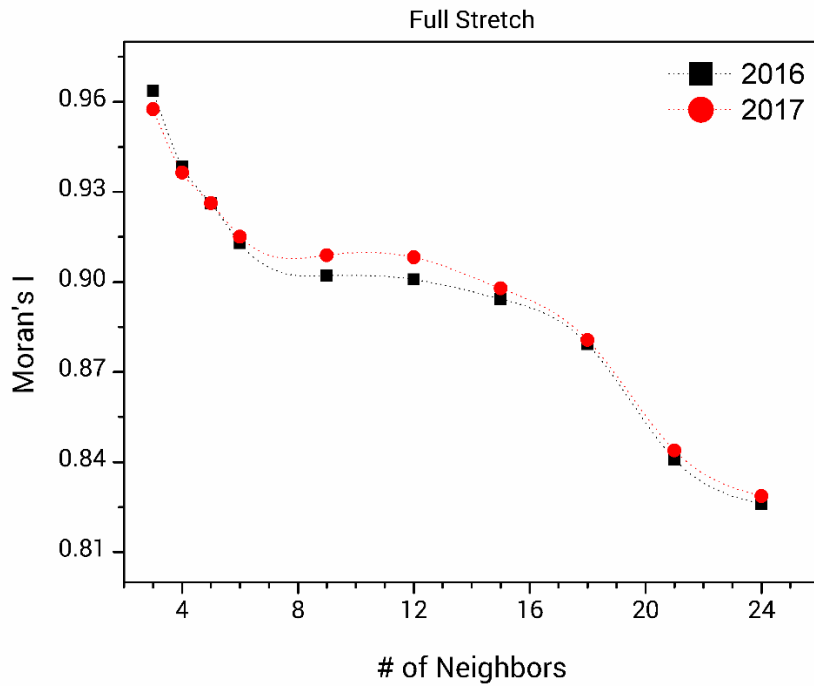


Figure 5.10 Moran's I Spatial Correlogram for streambed K_s patterns considering the entire study reach.

The streambed K_s patterns with reference to segments 1 and 2 showed a reasonable good spatial autocorrelation up to 12 nearest neighbors as per non-directional Moran's I indices. The spatial correlogram of the streambed K_s patterns with respect to full stretch of the study reach had virtuous spatial influence up to 24 nearest neighbors. The streambed K_s patterns at the meandering stream section - segment 3 was seen to have relatively weaker positive spatial auto-correlation with distant neighbors. The local Moran's I scatterplot was used as an exploratory graphical tool for assessing the strength of spatial autocorrelation in the streambed K_s data. In the Figure 5.11, scatter plots of Moran's I are presented, in which the slope of the regression line gives the local Moran's I index. The sign (positive or negative) of the Moran's I index will be simply the sign of the slope of the regression line.

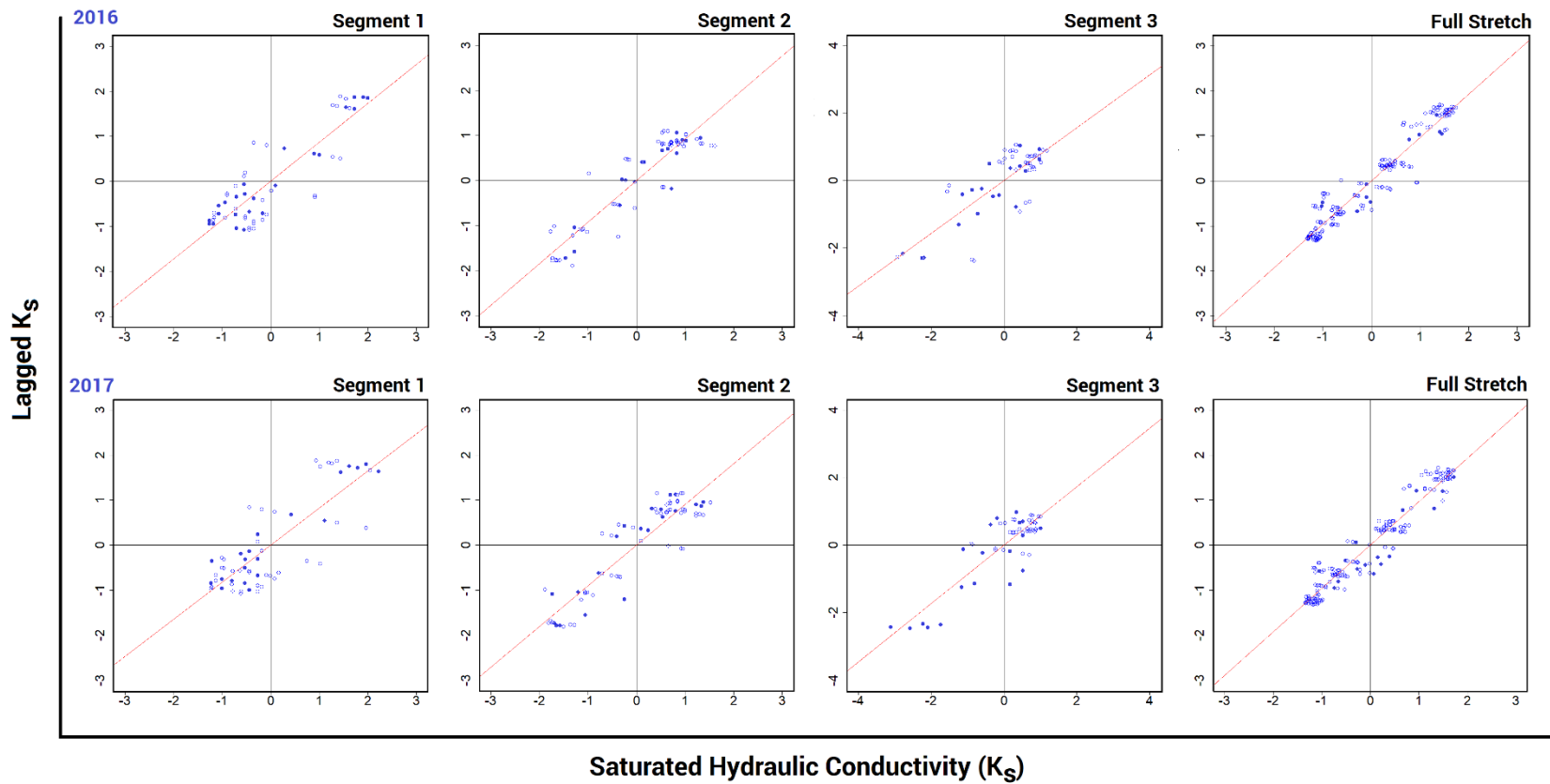


Figure 5.11 The local Moran's I scatterplot for streambed K_s patterns. The upper-right and lower-left quadrants of the scatter plot indicate positive spatial association of values that are higher and lower than the sample mean, respectively. The lower-right and upper-left quadrants include samples that exhibit negative spatial association or spatial outliers; i.e., these sampled values convey little similarity to their neighboring ones.

The streambed K_s samples of two sampling periods were interpolated by incorporating the Standard-IDW and completely regularized spline kernel based RBF interpolation methods using the ‘geostatistical analyst’ wizard of ArcGIS 10.3. The Root Mean Square Error and Kling-Gupta Efficiency (KGE) measures presented in Table 5.3.3 were calculated based on the observed and predicted K_s values assessed through cross-validation by the IDW and RBF methods. The KGE index ranges from $-\infty$ to $+1$ which accounts for all the sources of systematic errors from different components (i.e., bias, correlation and variability) (Gupta et al., 2009). The KGE of RBF estimates (K_s) for the two periods were 0.985 and 0.978, respectively which necessarily represents a robust prediction or spatial interpolation. Figure 5.12 and 5.13 presents the prediction maps of streambed K_s for two time periods using the IDW and RBF methods. With the use of sampled streambed K_s values along the study reach, experimental semivariograms were constructed to characterize the spatial variability of the sampled streambed K_s using Circular, Spherical, Pentaspherical, Exponential and Gaussian semivariogram models. However, the results of only the best-performing semivariograms are reported along with the streambed K_s estimates and their estimation variance at the nodes.

Table 5.3.3 Performance evaluation of IDW and RBF interpolation methods.

Variable	Model	RMSE (cm/day)	KGE
K _s of 2016	IDW -Standard	39.277	0.9812
	RBF - Completely Regularized Spline	33.045	0.9857
K _s of 2017	IDW – Standard	43.982	0.9794
	RBF - Completely Regularized Spline	40.505	0.9785

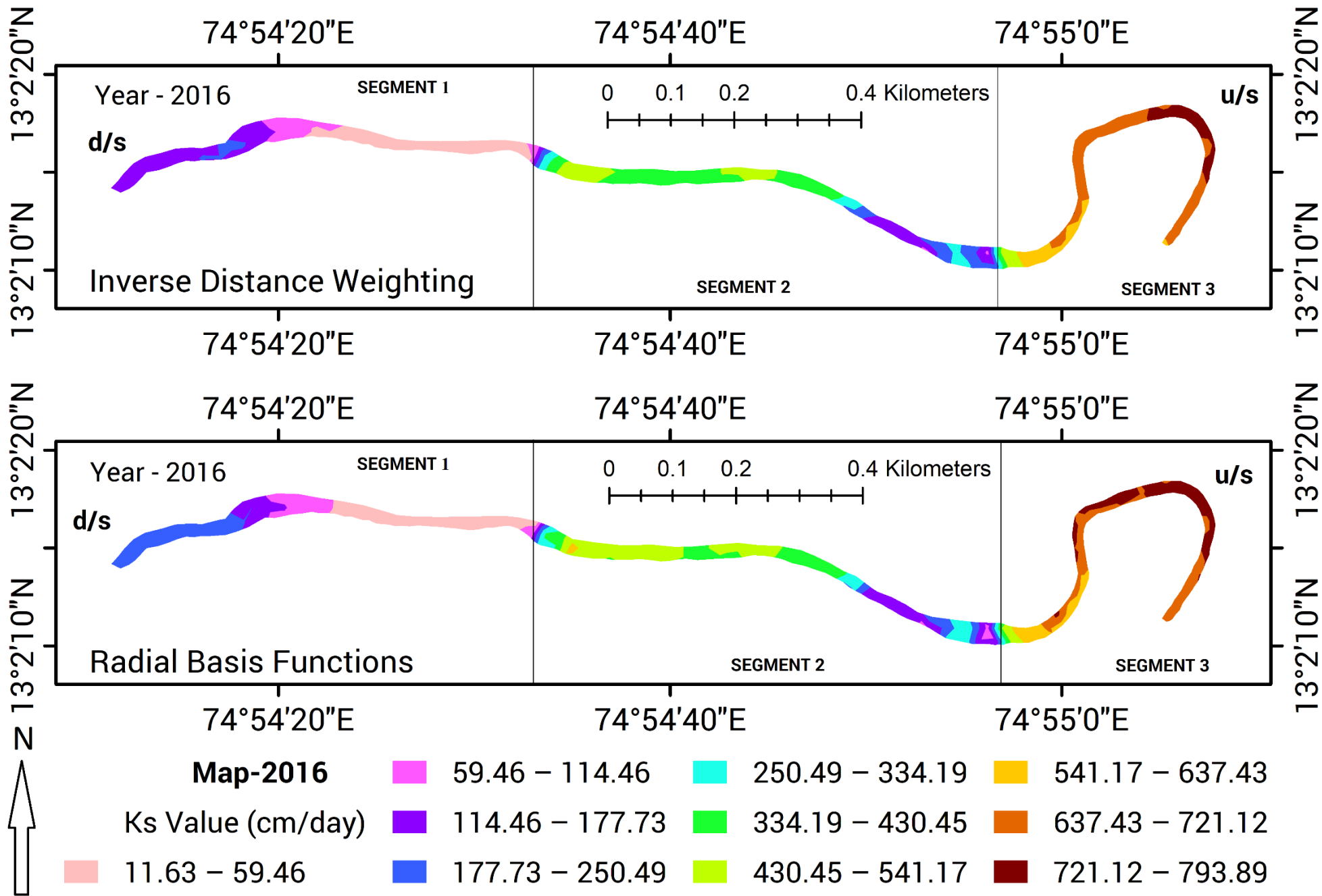


Figure 5.12 Streambed K_s patterns interpolated through IDW and RBF methods with respect to 2016 K_s data

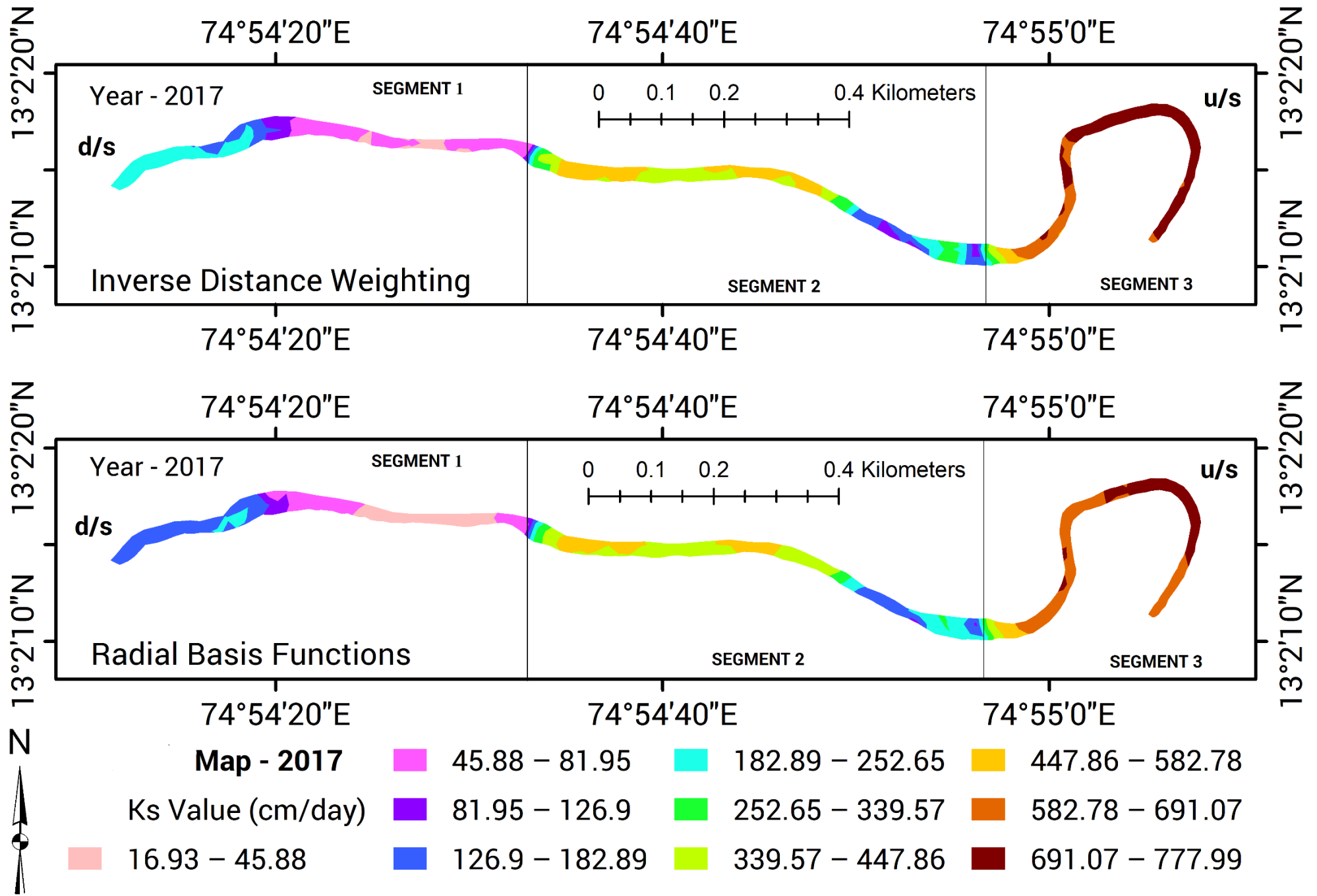


Figure 5.13 Streambed K_s patterns interpolated through IDW and RBF methods with respect to 2017 K_s data

Semivariogram modeling and ordinary kriging analyses were performed in ArcGIS 10.3. Through many simulation trials by using different semivariograms, the best performing experimental semivariograms (presented in Table 5.3.4) of streambed K_s for the study reach were found. The nugget, which represents the small scale variability or the measurement error is selected based on database, and adjusted along with major axis and active lag distance for fitting the semivariogram model that appropriately captures the spatial distribution of K_s data. The lag parameters, including the lag spacing and tolerance of the experimental variograms were tested for 9, 12, 15 and 21 number of nearest neighbors back-to-back. The spatial autocorrelation was observed to drop significantly above 21 neighborhood spacings and, the experimental semivariograms modelled by considering 15 nearest neighbors performed better.

Table 5.3.4 Parameters of semivariogram models fitted to K_s data

Data	Model	Nugget [C₀]	Partial Sill [C]	Range	DR	RMSE (cm/day)	KGE
K _s of 2016	Pentaspherical	1235.441	51758.58	3.95E-03	0.0233	42.9766	0.9725
	Circular	2323.572	51124.07	3.09E-03	0.0434	46.7514	0.966
K _s of 2017	Exponential	544.8727	51366.14	4.45E-03	0.0104	44.5049	0.9747
	Pentaspherical	1578.387	48662.01	4.05E-03	0.0314	46.6615	0.9701

For the K_s samples of the year 2016, Pentaspherical and Circular semivariograms performed better than others tested with an RMSE = 42.976 and 46.751 cm/day respectively; and correspondingly for the K_s data of 2017, the Exponential and Pentaspherical models provided better characterization of the spatial variability of streambed K_s . Figures 5.14, 5.15, 5.16, and 5.17 demonstrates the fitted theoretical semivariograms against the empirical semivariance estimates of streambed K_s . The nugget to sill ratio or dependence ratio (DR) quantifies the degree of spatial autocorrelation and gives an idea of how much variance is successfully accounted in the semivariogram model; a DR of less than 0.25 indicates a strong degree of spatial autocorrelation and, if the DR ratio ranges between 0.25 and 0.75, it is regarded as moderate spatial association; and lastly a DR > 0.75 indicates weak spatial autocorrelation (Aidoo et al., 2015).

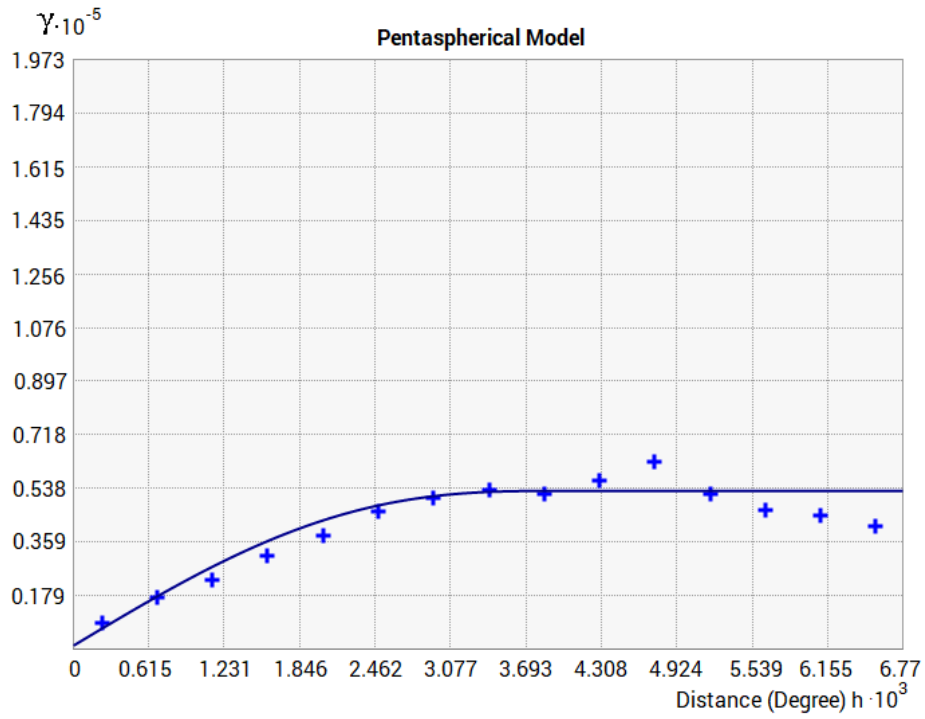


Figure 5.14 Pentaspherical model for streambed K_s samples of 2016

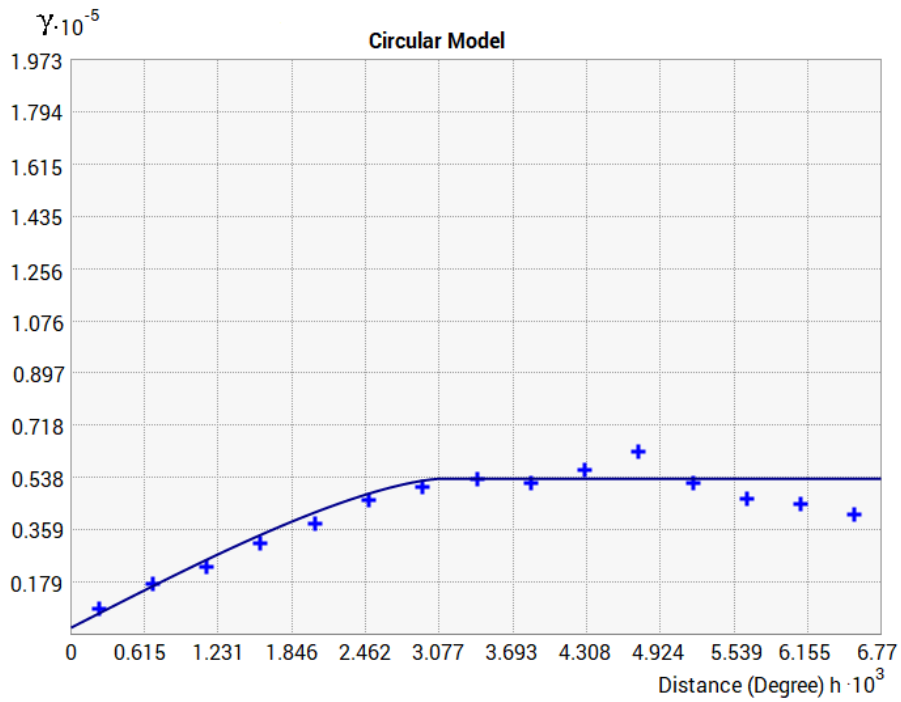


Figure 5.15 Circular model for streambed K_s samples of 2016

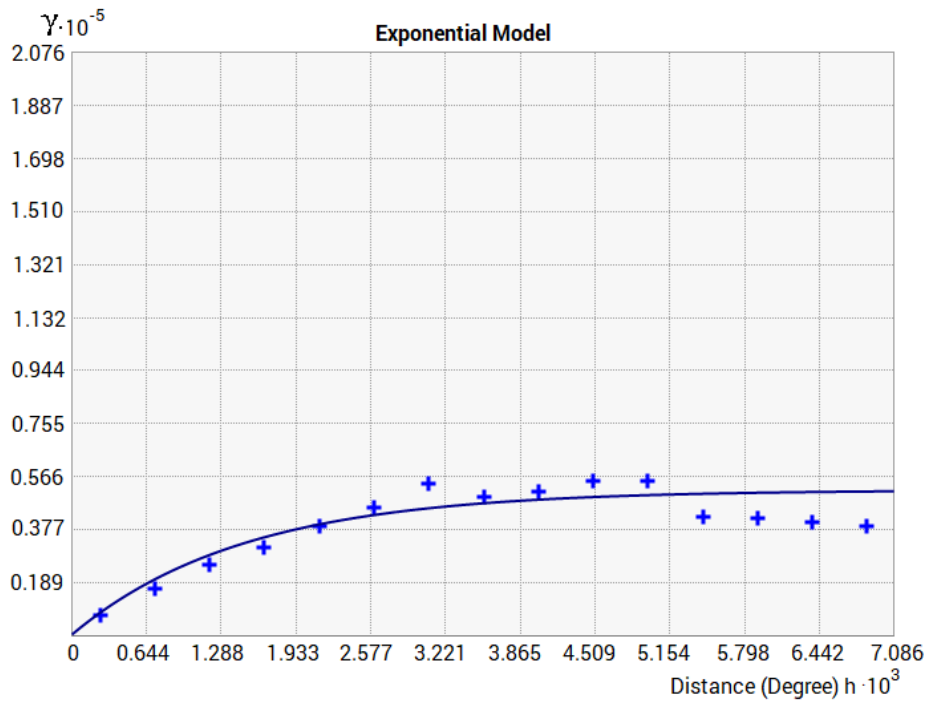


Figure 5.16 Exponential model for streambed K_s samples of 2017

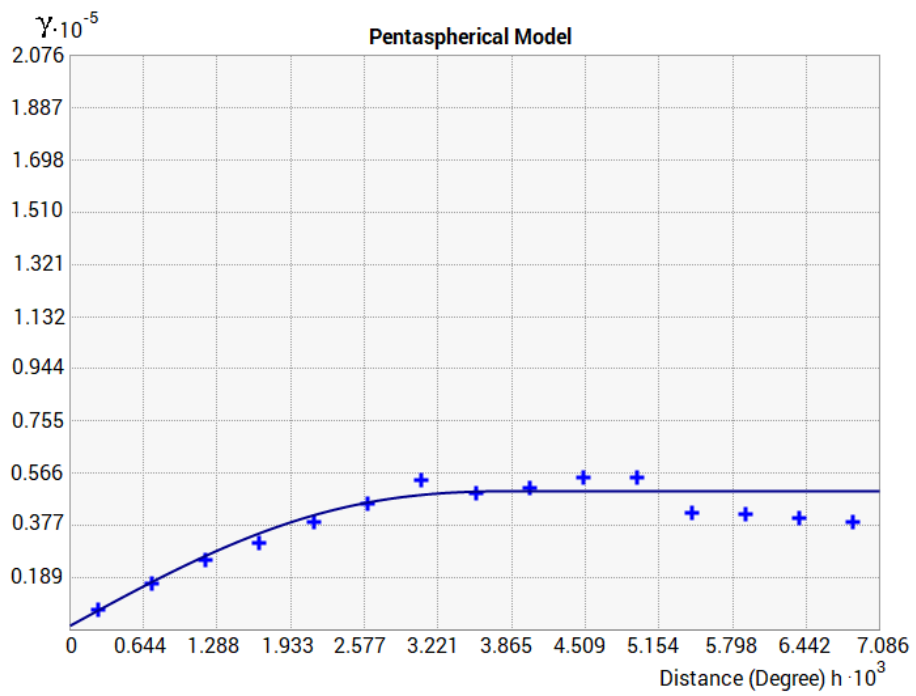


Figure 5.17 Pentaspherical model for streambed K_s samples of 2017.

From the simulated semivariograms (presented in Table 5.3.4) which have very strong dependence ratio's, krigged surface maps of streambed K_s were generated for two time periods (refer Figures 5.18 and 5.19). While applying the ordinary kriging, both anisotropic and isotropic models were fit; nevertheless, the anisotropic models revealed superior fits for interpolating streambed K_s . Among the three interpolation methods tested, the RBF method was the one with lowest RMSE and higher KGE in all the cases. The highly dense homogeneous network of samples contributed for relatively good performance of IDW and RBF methods. According to Li and Heap (2008), while modeling samples of dense homogeneous networks, the geostatistical methods, for instance ordinary kriging doesn't show superior spatial predictions than deterministic methods, such as IDW and RBF, however, the prediction uncertainty will be lower around the sampled values in ordinary kriging estimates compared to deterministic methods. In Figure 5.20 the Taylor diagrams portray the relative performance of individual interpolation methods in simulating the spatial patterns of streambed K_s . The performance of all the three interpolation methods (IDW, RBF and OK) were marginally equal/similar in terms of root mean square difference/error (RMSD), standard deviation and correlation coefficient.

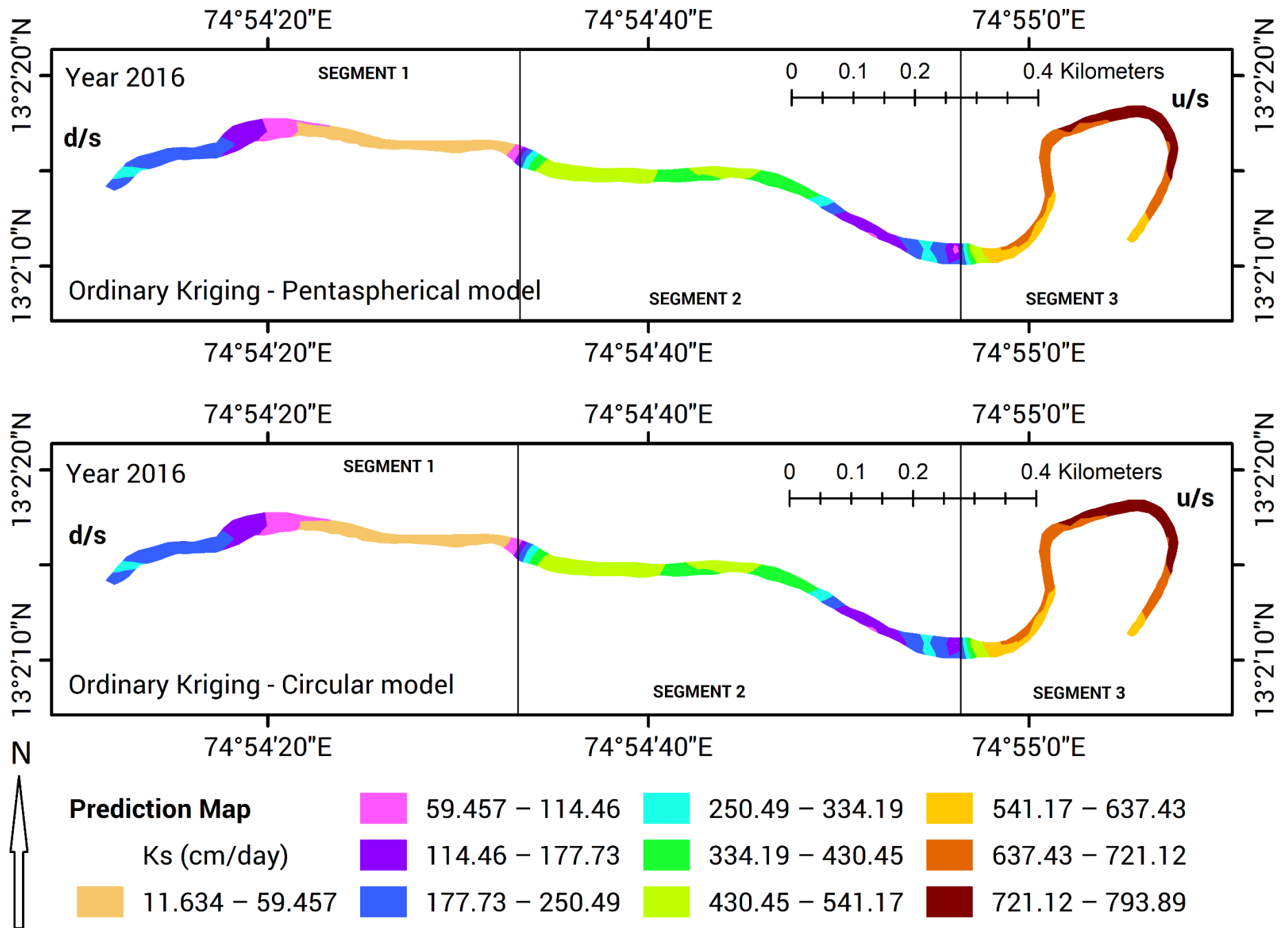


Figure 5.18 Krigged Streambed K_s patterns for the year 2016

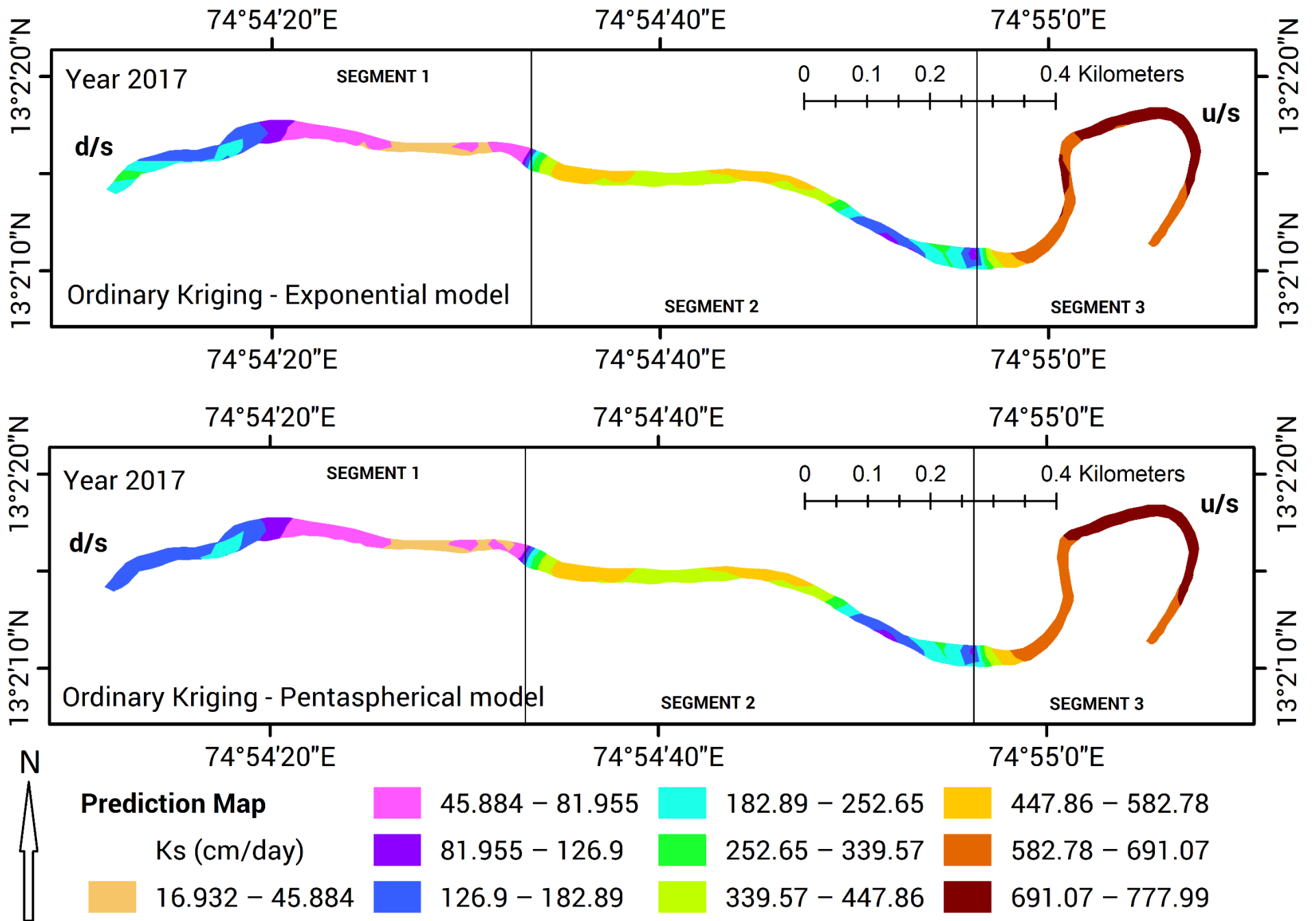


Figure 5.19 Krigged Streambed K_s patterns for the year 2017

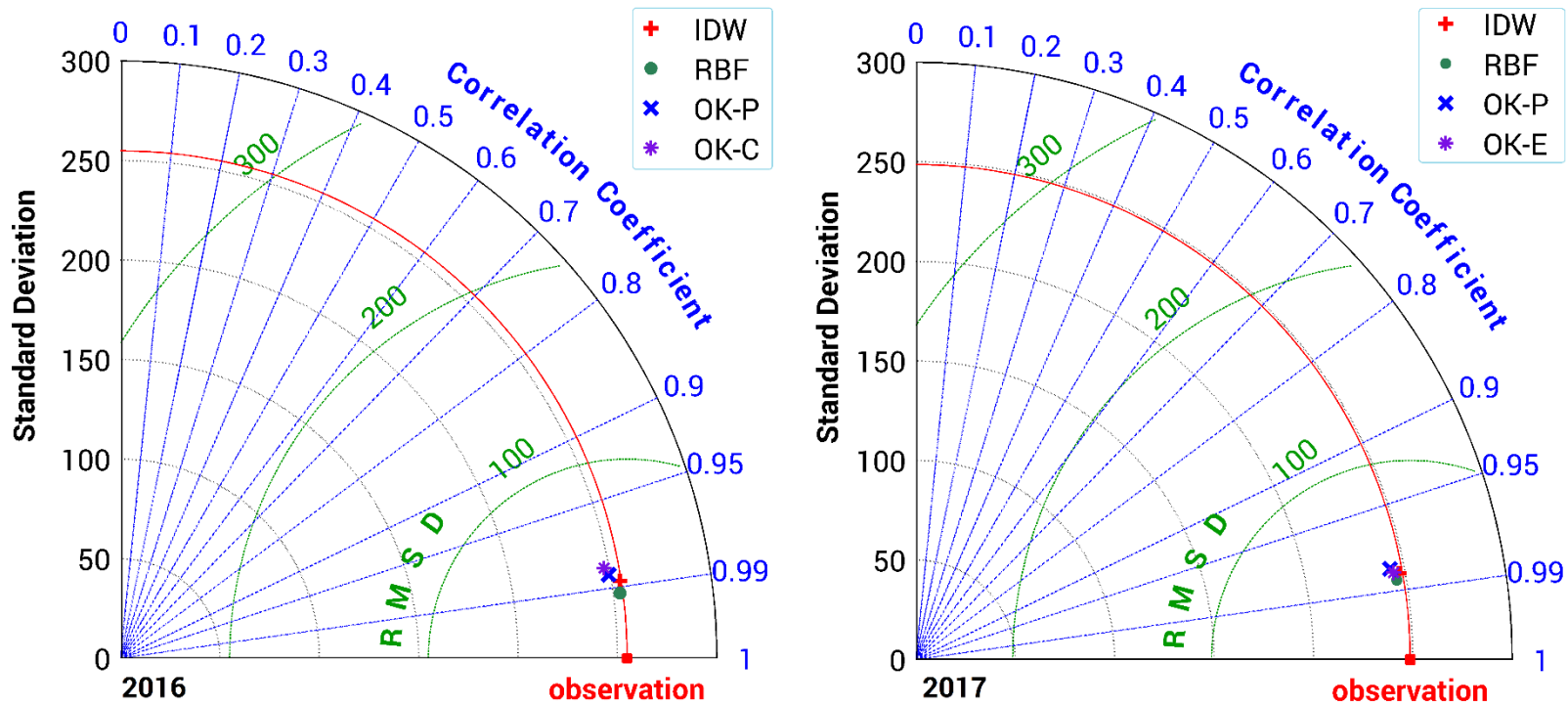


Figure 5.20 Taylor Diagrams for performance evaluation of Interpolation methods.

5.4 Discussion on influence of vented dams on the variability of streambed K_s

It is expected that due to the obstruction caused by vented dams, the coarse sediment load will be held back in the upstream reaches, and the river will dig-in near the tail end of vented dams to get stabilized in its course at the middle reach. The array of channel adjustments that occur both upstream and downstream of vented dams were the factors responsible for the variability of streambed K_s . The presence of series of vented dams imparts particle size heterogeneity all along the direction of the stream and vertically within the bed. Cyclic scour and re-deposition events over time and, intrusion or settlement of fine sediments due to water stagnation behind dams can lead to changes in substrate composition all along the study reach.

Statistically significant differences in streambed K_s and substrate composition subsisted between upstream and downstream sections of vented dams. Significant differences also existed in streambed K_s distribution at different transects within each segment of the study reach. Hydraulic conditions represented by head levels and duration of water storage behind the dams and, the operational strategies were significant factors accounting for within-channel K_s differences. The low- K_s zones at the tail water section downstream of vented dams occur due to the intrusion of fine sediments and organics into the pore spaces of a stable gravel substrate resulting in choking of hyporheic zones and anoxic conditions.

During periods of substrate movement induced by storm peaks, the streambed is extremely dynamic to characterize. A significant volume of bed load is being released and incorporated at the same time period. Anthropogenic disturbances to streambed via in-stream gravel mining, livestock washing, contaminant release from laundry wash, groundwater pumping for agricultural use are some significant factors to consider that lead to variability of K_s . There can be a surge of chemical substances and other nutrients released from anthropogenic activities due to river obstruction.

5.5 Results of AI based spatial models for K_s prediction

The geographical coordinates (i.e., latitude and longitude) of the sampling locations (points) from where the in-situ hydraulic conductivity measurements were made were used as model inputs to predict streambed K_s over spatial scale using artificial neural network (ANN), adaptive neuro fuzzy inference system (ANFIS) and support vector machine (SVM) paradigms. The statistical measures computed by using the actual versus predicted streambed K_s values of individual models are comparatively evaluated.

5.5.1 Performance of ANN prediction models

Based on trial and error scheme, the number of hidden neurons of multi-layer perceptron neural network (ANN) were determined. The *tansig* and *purelin* were employed as input and output transfer functions along with Levenberg-Marquardt back propagation learning rule. The model structure and performance statistics of the ANN model for each strategy are presented in Table 5.5.1 along with the performance statistics of ANN model for each strategy. From the statistical indices, it is evident that the performance of ANN models during the testing phase were satisfactory but not up to the mark. For instance, the MAE of all the models were sufficiently high and the RRMSE values above 0.4 signposts that the spatial K_s predictions were not so accurate but fall under satisfactory category. With reference to Strategy 1 model of 2017, even though the training results were good with an NSE = 0.835, the test performance was merely acceptable with an NSE = 0.75.

Table 5.5.1. Performance indices of ANN modeling

ANN Model	Model structure	Train			Test		
		RRMSE	MAE (cm/day)	NSE	RRMSE	MAE (cm/day)	NSE
Strategy 1 - 2016	2-3-1	0.445	84.67	0.796	0.462	100.63	0.782
Strategy 1 - 2017	2-3-1	0.411	81.22	0.835	0.491	108.72	0.75
Strategy 2 - 2016	2-5-1	0.265	36.41	0.917	0.482	92.36	0.765
Strategy 2 - 2017	2-5-1	0.395	68.26	0.821	0.458	85.82	0.788

5.5.2 Performance of ANFIS prediction models

The adaptive neuro fuzzy inference system (ANFIS) with grid partitioning method was calibrated by selecting the shape and optimal number of membership functions. The optimal ANFIS architectures calibrated based on trial and error approach for spatial modeling of streambed K_s are presented in Table 5.5.2. The ‘hybrid’ training algorithm which includes the back propagation gradient descent method in combination with a least squares method was used for fitting the training data set. The performance statistics of ANFIS model for each strategy are presented in Table 5.5.3.

Table 5.5.2. The optimal ANFIS architectures

ANFIS Models	ANFIS Parameters		
	Membership function		
	Number	Input	output
Strategy 1 - 2016	3	gaussmf	constant
Strategy 1 - 2017	3	gaussmf	constant
Strategy 2 - 2016	3	gbellmf	constant
Strategy 2 - 2017	3	gbellmf	constant

Table 5.5.3. Performance indices of ANFIS modeling

ANFIS Model	Train			Test		
	RRMSE	MAE	NSE	RRMSE	MAE	NSE
		(cm/day)			(cm/day)	
Strategy 1 - 2016	0.206	40.78	0.957	0.247	56.14	0.937
Strategy 1 - 2017	0.216	41.78	0.955	0.222	51.5	0.949
Strategy 2 - 2016	0.279	45.278	0.931	0.372	67.386	0.86
Strategy 2 - 2017	0.294	47.98	0.913	0.335	64.6	0.887

From the statistical indices, it is evident that the performance of all the ANFIS models during the testing phase have acceptable accuracy measures. For instance, the MAE of all the models were sufficiently less and the RRMSE values less than 0.4 and 0.3 signposts that the spatial K_s predictions were decently and highly accurate, respectively. The Strategy 1 model of 2017, had higher prediction accuracy compared to other ANFIS models with a test NSE = 0.949. The gaussian and gbell membership functions were found to provide better prediction accuracy for the spatial modeling strategies 1 and 2, respectively.

5.5.3 Performance of SVM prediction models

The Support Vector Machine (SVM) with radial basis kernel function was employed in this study to predict the spatial streambed hydraulic conductivity. The optimal parameters of SVM (i.e., the cost, kernel and the ε -insensitive loss function) were identified via 3D Grid Search. The Table 5.5.4 presents the optimal values of SVM parameters. Hypothetically, a logarithmic grid ranging between 2^{-12} to 2^{12} is usually sufficient for arriving at the best parameter combination. In the event that the best parameters lie on the limits of the grid, further search could be extended in that direction in a subsequent search. The performance statistics of SVM model for each strategy are presented in Table 5.5.5.

Table 5.5.4. The optimal SVM architectures

SVM Models	SVM Parameters		
	Radial Basis Kernel function		
	Cost 'C'	Gamma ' γ '	Epsilon ' ε '
Strategy 1 - 2016	1024	38	0.0707
Strategy 1 - 2017	1156	44	0.1080
Strategy 2 - 2016	980	52	0.1785
Strategy 2 - 2017	1120	40	0.0967

Table 5.5.5. Performance indices of SVM modeling

SVM Model	Train			Test		
	RRMSE	MAE (cm/day)	NSE	RRMSE	MAE (cm/day)	NSE
Strategy 1 - 2016	0.155	50.45	0.965	0.241	52.56	0.941
Strategy 1 - 2017	0.204	51.67	0.933	0.265	56.41	0.928
Strategy 2 - 2016	0.264	52.567	0.927	0.322	57.66	0.895
Strategy 2 - 2017	0.196	50.96	0.942	0.295	55.3	0.911

From the statistical indices, it is evident that the performance of all the SVM models during the testing phase were of relatively higher accuracy. The MAE of all the model predictions were sufficiently less and the RRMSE values less than 0.3 signposts superior spatial K_s predictions. The Strategy 1 model of 2016, had higher prediction accuracy compared to other SVM models with a test NSE = 0.941.

5.5.4 Comparative evaluation of AI models

The three AI models, namely the ANN, ANFIS and SVM provided more or less satisfactory spatial predictions with respect to both the strategies considered. Both SVM and ANFIS prediction models performed much better than the ANN models and, based on the error indices the SVM models performed relatively better than the ANFIS prediction models. For comparative evaluation of all the models, Table 5.5.6 presents the evaluated statistical indices of test phase. The Figures 5.21 illustrate the scatter plots based on the observed v/s predicted streambed K_s values of the Strategy 1 - ANN, ANFIS and SVM models during the test phase. Similarly, Figure 5.22 illustrate the scatter plots of Strategy 2 - ANN, ANFIS and SVM models during the test phase. The scatter plot displays the strength, direction, and form of the relationship between the observed and predicted streambed K_s . The prediction performance or the relative skill of different AI models is graphically summarized via Taylor diagrams as presented in Figures 5.23 and 5.24.

Table 5.5.6 Comparative evaluation of AI models with respect to test phase results

Statistic	RRMSE	MAE (cm/day)	NSE
Strategy 1 -2016			
ANN	0.462	100.63	0.782
ANFIS	0.247	56.14	0.937
SVM	0.241	52.56	0.941
Strategy 1 - 2017			
ANN	0.491	108.72	0.75
ANFIS	0.222	51.5	0.949
SVM	0.265	56.41	0.928
Strategy 2 -2016			
ANN	0.482	92.36	0.765
ANFIS	0.372	67.386	0.86
SVM	0.322	57.66	0.895
Strategy 2 - 2017			
ANN	0.458	85.82	0.788
ANFIS	0.335	64.6	0.887
SVM	0.295	55.3	0.911

With reference to Strategy 1 model for 2016 K_s data, the SVM model provides relatively better predictions than other two based on the NSE statistic. The RRMSE = 0.24 indicates relatively good spatial K_s predictions. The instances of underestimation and overestimation of observed K_s values were better captured in scatter plots presented in Figure 5.21; wherein the K_s predictions by SVM model was quite closer to the observed values. In Taylor diagram as presented in Figure 5.23, three statistical indices namely the correlation coefficient (R), the standard deviation (σ) and the root-mean-square difference (RMSD) are used to characterize the statistical relationship between the modelled and reference fields. In this case, both ANFIS and SVM predictions were analogous to each other. For comparative evaluation of RRMSE and NSE statistic, the Figure 5.25 presents the pictographic representation via bar chart. The model efficiencies of spatial modeling scheme 1 (i.e., strategy 1) were better compared to strategy 2 due to the incorporation of more number of sampling points in training.

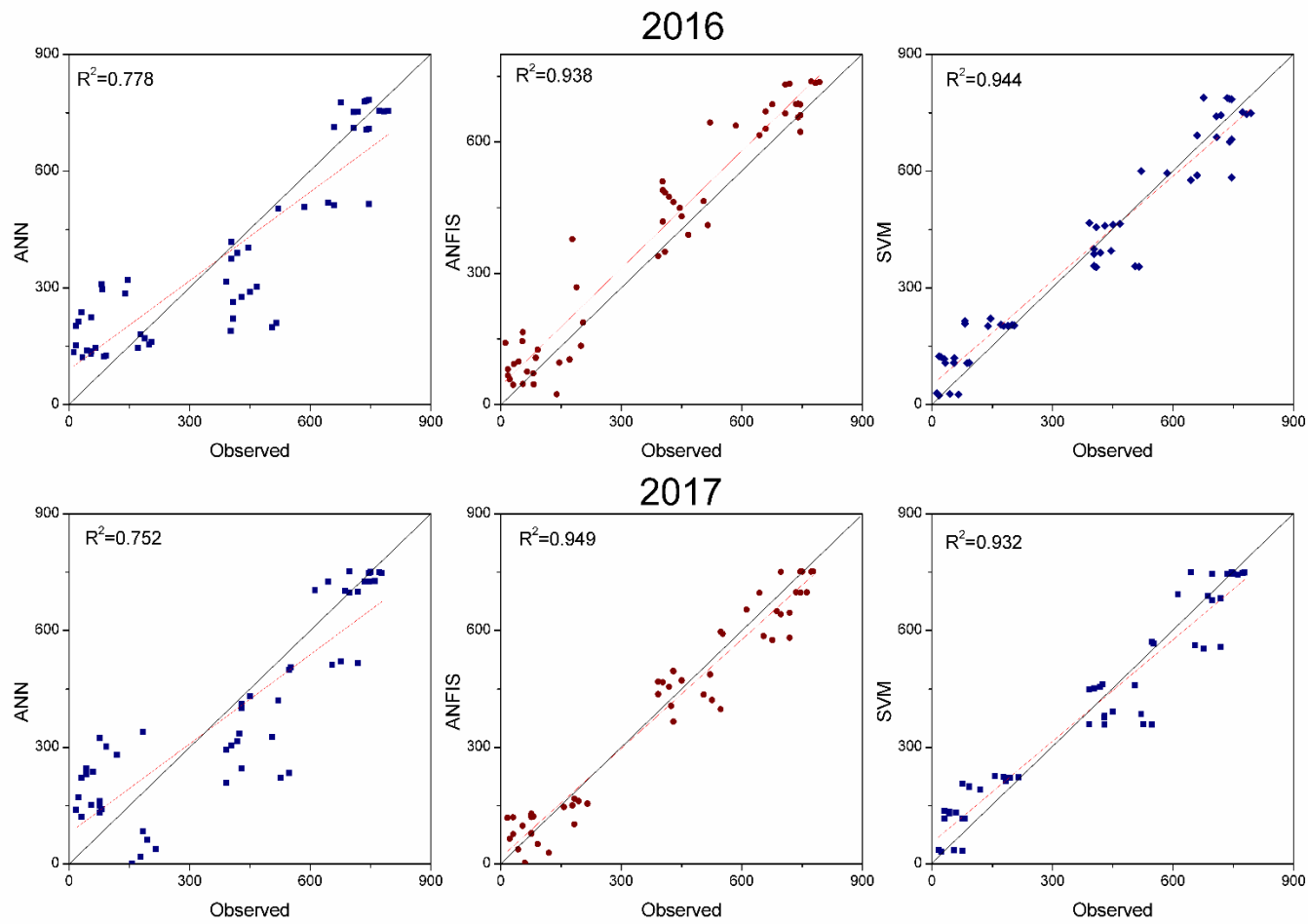


Figure 5.21 Scatter plots of the Strategy 1 – ANN, ANFIS and SVM models during the test period

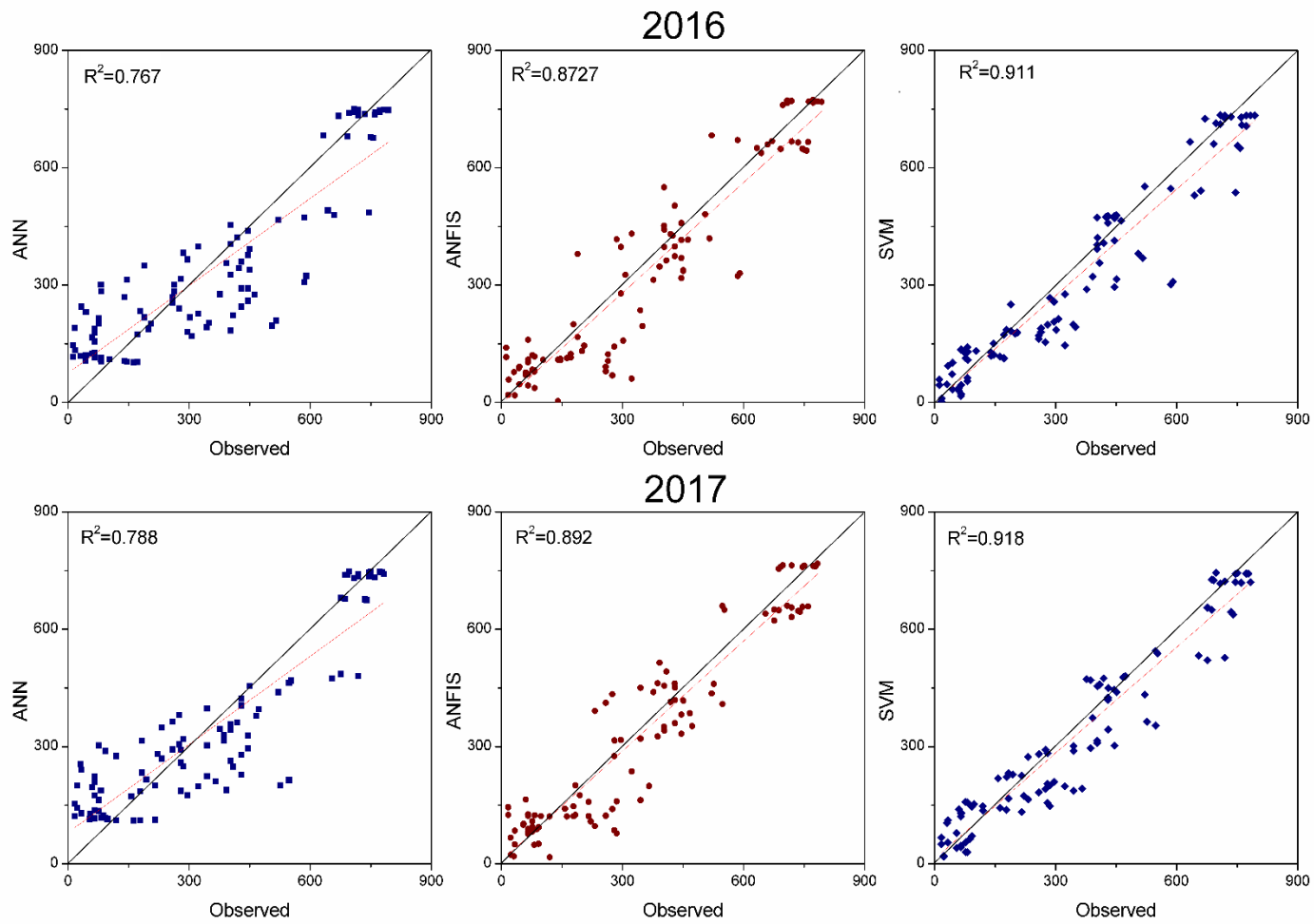


Figure 5.22 Scatter plots of the Strategy 2 – ANN, ANFIS and SVM models during the test period

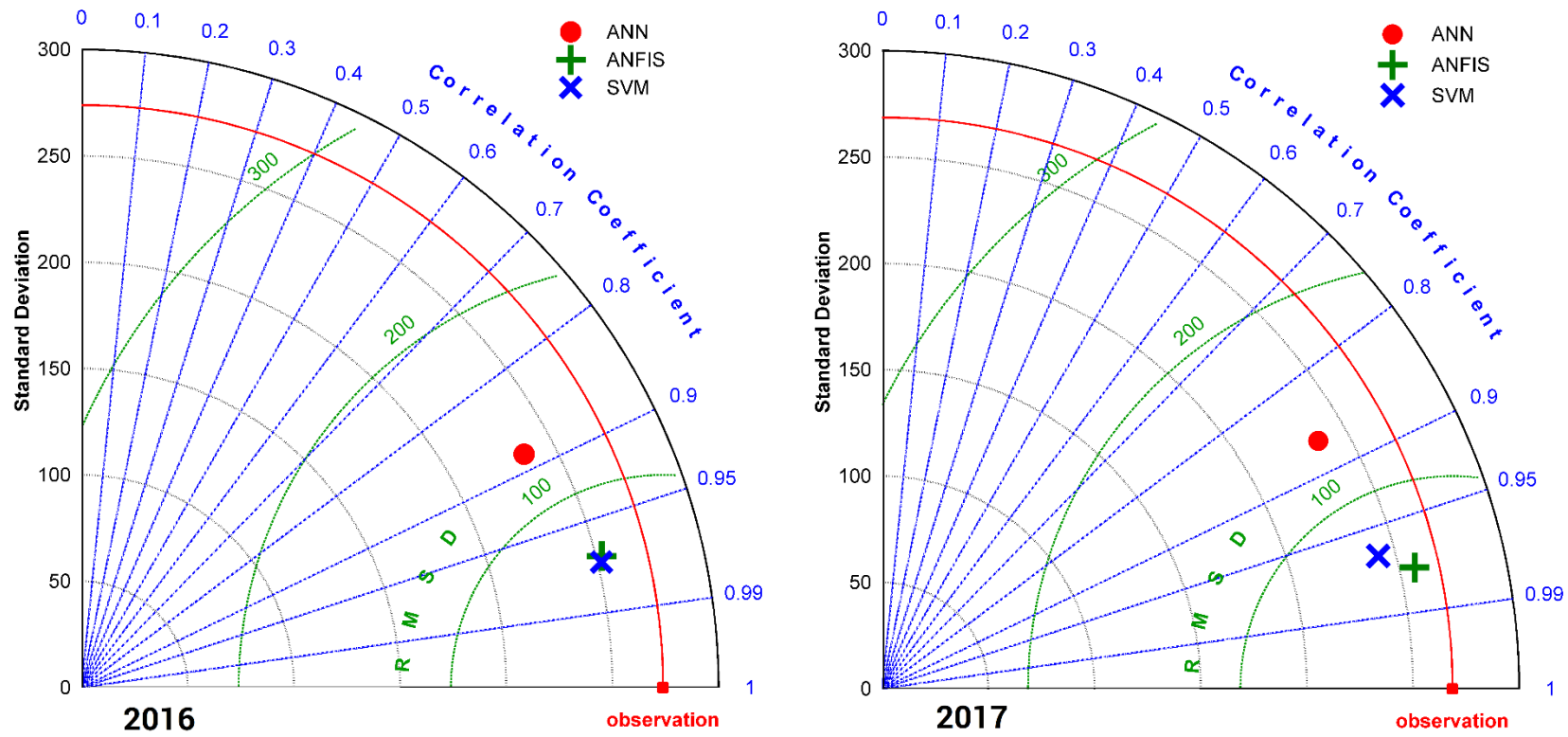


Figure 5.23 Taylor diagrams plotted for comparative evaluation of the Strategy 1 – ANN, ANFIS and SVM models of test phase

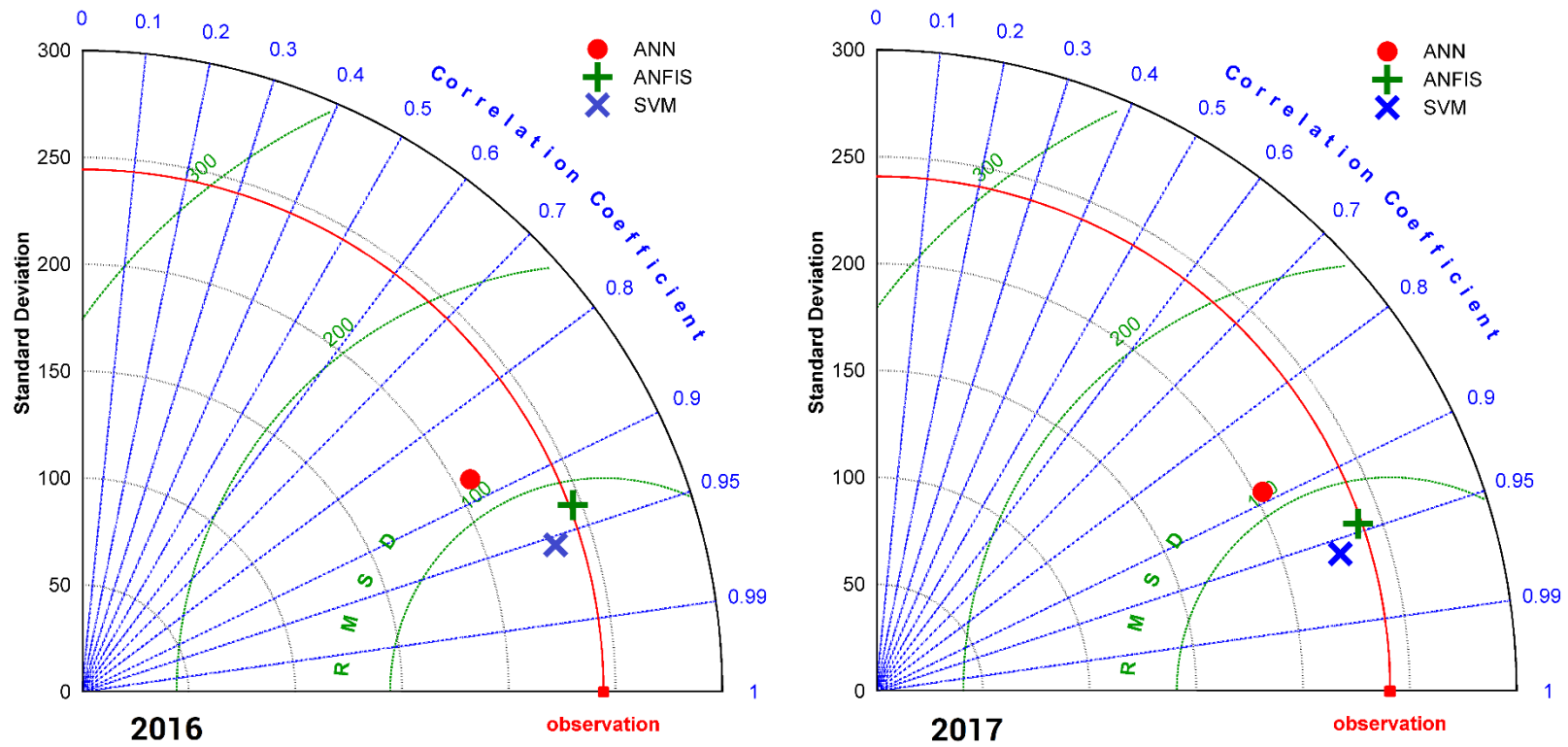


Figure 5.24 Taylor diagrams plotted for comparative evaluation of the Strategy 2 – ANN, ANFIS and SVM models of the test phase

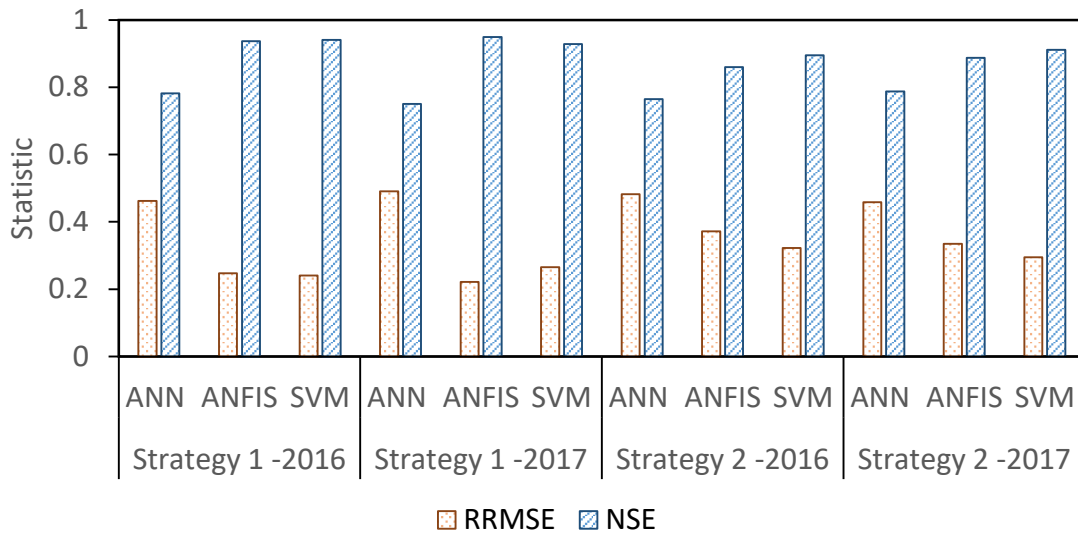


Figure 5.25 Plot of RRMSE and NSE statistic of all the AI models

Pertaining to *Strategy 1 model for 2017 K_s data*, the performance of ANFIS prediction model was found to be relatively superior than the SVM model. The ANN model underperformed as compared to ANFIS and SVM predictions. From the scatter plots presented in Figure 5.21, it can be observed that both ANFIS and SVM models were analogous in capturing the spatial variations of streambed K_s . From the Taylor diagram as presented in Figure 5.23, it can be observed that the standard deviation of ANN predictions significantly differs from that of the observed K_s data. Here, the RMSD, standard deviation and correlation coefficient of ANFIS predictions were superior to SVM predictions.

On comparison of the statistical indices with regard to *Strategy 2 models for 2016 and 2017 K_s data*, it was evident that the SVM predictions outperform than the other two models in terms of all the indices considered. The scatter plots presented in Figure 5.22 portray the ability of individual AI models to fit the observed K_s data. From the Taylor diagrams as presented in Figure 5.24, it could be seen that the standard deviation of ANFIS predictions were closer to the standard deviation curve of observed K_s data. However, the RMSD and correlation coefficient (R) of SVM models were relatively less and higher than the ANFIS predictions, respectively. Henceforth, based on NSE, RMSD and R values, the SVM model predictions were considered to be efficient even though, the ANFIS predictions were less biased compared to SVM predictions.

5.6 Summary

The results of statistical and geostatistical analysis describe the variability of streambed hydraulic conductivity at fine spatial and temporal resolution over a significant length of river and time period. The geostatistical procedures employed for generating interpolated hydraulic conductivity (K_s) fields from a set of K_s measurements aid in visualizing the patterns of streambed K_s and the impact of vented dams on the variability of K_s . The potential of AI based spatial modelling schemes to predict the streambed K_s were comparatively evaluated.

CHAPTER 6

CONCLUSIONS AND RECOMMENDATIONS

6.1 General

The chapter presents the conclusions drawn based on the research insights gained from the experimental study findings along with the limitations of the study. The future recommendations are directed toward researchers in the field of fluvial hydrology, interested to take up and carry out additional research to broaden the scope and findings of this study.

6.2 Conclusions

- The streambed was heterogeneous with regard to hydraulic conductivity distribution with high- K_s zones near the backwater areas of the vented dams and low- K_s zones particularly at the tail water section of vented dams due to an upset of equilibrium between supply and removal of sediments near the vented dam cross section.
- The measures of central tendency and dispersion show that the streambed K_s had reasonable spatial variability within the study reach, with a minimum value of 11.63 cm/day, and the maximum being 793.88 cm/day during the year 2016 and ranged between 16.93 and 777.98 cm/day during the year 2017. The bedrock underlying the streambed and aquifer properties can also be the cause for low hydraulic conductivity at some sections of the stream.

- The Levene's and Welch's t-tests confirm the hypothesis of the significant spatial variability of streambed K_s between the upstream and downstream reaches of the vented dams. However, significant temporal variability of streambed K_s was not observed during the study period across all the three segments.
- Analysis of results demonstrates a strong influence of vented dam presence, particularly on grain size and streambed K_s distribution. The spatial variability of streambed K_s can be because of factors such as accretion or depletion of streambed elements, local anomalies in substrate materials derived from river network.
- The sediments of segment 2 (sinuous channel) and segment 3 (meandering channel) showed moderate to slightly higher D50 values due to the retention of coarse sediment load derived from the upland watershed. However, the sediments of some of upstream transects of segment 2 and segment 1 had lower D50 values as a result of settlement of suspended silt and particulate organic matter inputs from the floodplain and riparian vegetation. The variability of particle sizes resulting from erosion and deposition processes influence streambed hydraulic conductivity.
- The Moran's I index approved the presence of spatial dependence in the heterogeneous streambed K_s samples.
- The IDW and RBF interpolation maps were found more accurate than the krigged surface maps; however, the prediction uncertainty was lower around the sampled values in ordinary kriging estimates compared to deterministic methods.
- The AI based spatial models provided more or less satisfactory spatial K_s prediction efficiencies with respect to both the strategies/schemes considered.
- Although ANN and ANFIS models provided satisfactory level of predictions, the SVM model was found to provide more accurate streambed K_s patterns due to its inherent capability to adapt to input data that are non-monotone and non-linearly separable.
- The tuning of SVM parameters via 3D grid search was responsible for higher efficiencies of SVM models.

6.3 Contributions from the Study

- This study verified the premise that due to the obstruction caused by vented dams, the coarse sediment load will be held back in the upstream reaches, and the river will dig-in near the tail end of vented dams to get stabilized in its course at the middle reach. The array of channel adjustments that occur both upstream and downstream of vented dams are the factors responsible for the variability of streambed K_s .
- With clean water releases from dams, downstream erosion, substrate flushing, and sorting are the processes contributing to K_s variability with some potential to change with time.
- The impact of vented dams on the variability of streambed K_s was better revealed via virtuous maps of deterministic and geostatistical spatial interpolation schemes.
- Even with limited field experimental data, the study discloses the potential of data driven models to predict streambed K_s patterns by presenting two spatial modeling schemes.
- The spatial modelling schemes/strategies proposed were found suitable for predicting streambed K_s patterns. With such spatial modeling schemes that incorporate the neighborhood data to predict the variable of interest, one can easily predict at unknown point locations with significant confidence level.

6.4 Limitations and Future Scope

- This study was based on streambed K_s data sampled during two consecutive years 2016 and 2017. In future, a multi-year sampling of streambed K_s can be conducted to confirm or modify findings of this study.
- In the present study, the in-situ streambed K_s samples were collected at a solitary depth of 30 cm. For testing at greater depths, removing streambed substrate is difficult and also requires purchase of extension tubes. In future, one can conduct experiments at assorted depths to study the K_s variations with depth.
- Some of the limitations of Guelph permeameter include measurement time of several hours at few locations where the bedrock is nearby.

- The variability of streambed hydraulic conductivity is assessed at fine spatial and temporal resolution. Future efforts should involve longer study durations and expanded stream corridor profile to better characterize temporal and spatial variations of streambed K_s . Such efforts would permit better understanding of hyporheic exchanges under variable flow conditions
- Individual impacts of anthropogenic disturbances to streambed and its K_s via instream gravel mining, contaminant releases, groundwater pumping for agricultural use etc. are some of the significant factors to consider.

REFERENCES

- Abbott, B. W., Baranov, V., Mendoza-Lera, C., et al. (2016). “Using multi-tracer inference to move beyond single-catchment ecohydrology”. *Earth- Science Rev*, 160:19–42.
- Abt, S. R., Clary, W. P., and Thornton, C. I. (1994). “Sediment Deposition and Entrapment in Vegetated Streambeds”. *J Irrig Drain Eng*, 120(6):1098–1111.
- Adams, W. M. (1989). “Dam construction and the degradation of floodplain forest on the Turkwel River, Kenya”. *L Degrad Dev*, 1(3):189–198.
- Aidoo, E. N., Mueller, U., Goovaerts, P., and Hyndes, G. A. (2015). “Evaluation of geostatistical estimators and their applicability to characterize the spatial patterns of recreational fishing catch rates”. *Fish. Res.*, 168:20–32.
- Allan, J. D. and Castillo, M. M. (2007). “*Stream Ecology: Structure and function of running waters*”. Springer Netherlands, Dordrecht.
- Arnold, J., Muttiah, R., Srinivasan, R., and Allen, P. (2000). “Regional estimation of base flow and groundwater recharge in the Upper Mississippi river basin”. *J Hydrol*, 227(1):21–40.
- ASTM D653-14 (2014). “*Standard Terminology Relating to Soil, Rock, and Contained Fluids*”. Standard, ASTM International, West Conshohocken, PA.
- Avinash, K., Deepika, B., and Jayappa, K. S. (2014). “Basin geomorphology and drainage morphometry parameters used as indicators for groundwater prospect: Insight from geographical information system (GIS) technique”. *J Earth Sci*, 25(6):1018–1032.
- Baker, A. and Lamont-Black, J. (2001). “Fluorescence of Dissolved Organic Matter as a Natural Tracer of Ground Water”. *Groundwater*, 39(5):745–750.
- Barth, J., Steidle, D., Kuntz, D., Gocht, T., Mouvet, C., von Tümpling, W., Lobe, I., Langenhoff, A., Albrechtsen, H.-J., Janniche, G., Morasch, B., Hunkeler, D., and Grathwohl, P. (2007). “Deposition, persistence and turnover of pollutants: First

- results from the EU project AquaTerra for selected river basins and aquifers”. *Sci Total Environ*, 376(1-3):40–50.
- Baveye, P., Vandevivere, P., Hoyle, B. L., DeLeo, P. C., and de Lozada, D. S. (1998). “Environmental Impact and Mechanisms of the Biological Clogging of Saturated Soils and Aquifer Materials”. *Crit Rev Environ Sci Technol*, 28(2):123–191.
- Baxter, B. J. C. (1992). “*The Interpolation theory of Radial Basis Functions*”. Ph.D Thesis, Trinity College.
- Biggs, T. W., Dunne, T., Domingues, T. F., and Martinelli, L. A. (2002). “Relative influence of natural watershed properties and human disturbance on stream solute concentrations in the southwestern Brazilian Amazon basin”. *Water Resour Res*, 38(8):25–1–25–16.
- Blasch, B. K. W., Constantz, J., and Stonestrom, D. A. (2007). “Thermal Methods for Investigating Ground-water Recharge”. In Stonestrom, D., ed., *Ground-water recharge in the arid and semiarid southwestern United States*: U.S. Geological Survey Professional Paper 1703. U.S. Geological Survey.
- Boadu, F. K. (2000). “Hydraulic Conductivity of Soils from Grain-Size Distribution: New Models”. *J Geotech Geoenvironmental Eng*, 126(8):739–746.
- Bridge, J. S. (2003). “*Rivers and floodplains: forms, processes, and sedimentary record*”. Wiley-Blackwell, Cornwall.
- Brunke, M. (1999). “Colmation and depth filtration within streambeds: Retention of particles in hypohelic interstices”. *Int Rev Hydrobiol*, 84(2):99–117.
- Buhmann, M. (2003). “*Radial basis functions: theory and implementations*”. Cambridge University Press, Cambridge.
- Cardenas, M. B. and Wilson, J. L. (2007a). “Effects of current-bed form induced fluid flow on the thermal regime of sediments”. *Water Resour Res*, 43(8):W08431.

- Cardenas, M. B. and Wilson, J. L. (2007b). “Thermal regime of dune-covered sediments under gaining and losing water bodies”. *J Geophys Res Biogeo*, 112:G04013.
- Cardenas, M. B. and Zlotnik, V. A. (2003). “Three-dimensional model of modern channel bend deposits”. *Water Resour Res*, 39(6):1141.
- Casas-Mulet, R., Lakhanpal, G., and Stewardson, M. J. (2018). “The relative contribution of near-bed vs. intragravel horizontal transport to fine sediment accumulation processes in river gravel beds”. *Geomorphology*, 303:299–308.
- Castro, N. M. and Hornberger, G. M. (1991). “Surface-subsurface water interactions in an alluviated mountain stream channel”. *Water Resour Res*, 27(7):1613–1621.
- Cey, E. E., Rudolph, D. L., Parkin, G. W., and Aravena, R. (1998). “Quantifying groundwater discharge to a small perennial stream in Southern Ontario, Canada”. *J Hydrol*, 210(1):21–37.
- CGWB (2012). “*Ground Water Information Booklet, Dakshina Kannada District, Karnataka*”. Technical report, Central Ground Water Board, South Western Region, Bangalore.
- Chen, X. (2000). “Measurement of streambed hydraulic conductivity and its anisotropy”. *Environ Geol*, 39(12):1317–1324.
- Chen, X. (2004). “Streambed Hydraulic Conductivity for Rivers in South-Central Nebraska”. *J Am Water Resour Assoc*, 40(3):561–573.
- Chen, X. (2005). “Statistical and geostatistical features of streambed hydraulic conductivities in the Platte River, Nebraska”. *Environ Geol*, 48(6):693–701.
- Chen, X. (2011). “Depth-dependent hydraulic conductivity distribution patterns of a streambed”. *Hydrol Process*, 25(2):278–287.
- Chen, X., Burbach, M., and Cheng, C. (2008). “Electrical and hydraulic vertical variability in channel sediments and its effects on streamflow depletion due to groundwater extraction”. *J Hydrol*, 352(3-4):250–266.

- Chen, X., Dong, W., Ou, G., Wang, Z., and Liu, C. (2013). "Gaining and losing stream reaches have opposite hydraulic conductivity distribution patterns". *Hydrol Earth Syst Sc*, 17(7):2569–2579.
- Cheng, C., Song, J., Chen, X., and Wang, D. (2011). "Statistical Distribution of Streambed Vertical Hydraulic Conductivity along the Platte River, Nebraska". *Water Resour Manag*, 25(1):265–285.
- Chestnut, T. J. and McDowell, W. H. (2000). "C and N dynamics in the riparian and hyporheic zones of a tropical stream, Luquillo Mountains, Puerto Rico". *J North Am Benthol Soc*, 19(2):199–214.
- Clarkin, K. (2008). "*Stream Simulation: An Ecological Approach to Providing Passage for Aquatic Organisms at Road-Stream Crossings*". U.S. Department of Agriculture, San Dimas, California.
- Clément, P. and Piégay, H. (2005). "Statistics and Fluvial Geomorphology". In *Tools in fluvial geomorphology*, pp. 597–630. John Wiley & Sons, Ltd, Chichester, UK.
- Cliff, A. D. and Ord, J. K. (1981). "*Spatial processes: models and applications*". Pion, London.
- Constantz, J. (2008). "Heat as a tracer to determine streambed water exchanges". *Water Resour Res*, 44(4):W00D10.
- Constantz, J., Su, G., and Hatch, C. (2004). "Heat as a Tracer to examine hydraulic Conductance near the Russian River Bank Filtration Facility, Sonoma County, CA". In *NATO Advanced Research Workshop on Riverbank Filtration*, USGS Collaboration, Slovakia Republic.
- Constantz, J., Thomas, C. L., and Zellweger, G. (1994). "Influence of diurnal variations in stream temperature on streamflow loss and groundwater recharge". *Water Resour Res*, 30(12):3253–3264.
- Constantz, J. E., Niswonger, R. G., and Stewart, A. E. (2008). "Analysis of temperature gradients to determine stream exchanges with ground water. In: Rosenberry DO,

- LaBaugh JW (eds.) *Field techniques for estimating water fluxes between surface water and ground water*. U.S. Geological Survey, Virginia, pp 117–126
- Cox, M. H., Su, G. W., and Constantz, J. (2007). “Heat, Chloride, and Specific Conductance as Ground Water Tracers near Streams”. *Groundwater*, 45(2):187–195.
- D’Agostino, R. B., Belanger, A., and D’Agostino Jr, R. B. (1990). “A suggestion for using powerful and informative tests of normality”. *Am Stat*, 44(4):316–321.
- Dai, F., Zhou, Q., Lv, Z., Wang, X., and Liu, G. (2014). “Spatial prediction of soil organic matter content integrating artificial neural network and ordinary kriging in Tibetan Plateau”. *Ecolog Indi*, 45:184–194.
- Dale, V. H., Swanson, F. J., and Crisafulli, C. M. (2005). *Ecological Responses to the 1980 Eruption of Mount St. Helens*. Springer, New York.
- Datry, T., Lamouroux, N., Thivin, G., Descloux, S., and Baudoin, J. M. (2015). “Estimation of sediment hydraulic conductivity in river reaches and its potential use to evaluate streambed clogging”. *River Res Appl*, 31(7):880–891.
- Domenico, P. A. and Schwartz, F. W. (1990). *Physical and Chemical Hydrogeology*. Second edition. John Wiley and Sons, Inc., New York.
- Dong, W., Ou, G., Chen, X., and Wang, Z. (2014). “Effect of temperature on streambed vertical hydraulic conductivity”. *Hydrol Res*, 45(1):89.
- Duwelius, R. F. (1996). *Hydraulic Conductivity of the Streambed, East Branch Grand Calumet River, Northern Lake County, Indiana*. Technical report, U.S. Geological Survey Water Resources Investigations Report 96-4218.
- Elrick, D. and Reynolds, W. (1992). “Methods for analyzing constant-head well permeameter data”. *Soil Sci Soc Am J*, 56(1):320–323.
- Erskine, L. (2002). *The relationship between riparian vegetation, bank erosion and channel pattern, Magela Creek, Northern Territory*. B.Sc.(Hons.) Thesis, University of Wollongong, Australia.

- Erskine, W. D. and Webb, A. A. (2003). “Desnagging to resnagging: new directions in river rehabilitation in southeastern Australia”. *River Res Appl*, 19(3):233–249.
- Everest, F. H., McLemore, C. E., and Ward, J. F. (1980). “*An Improved Tri-Tube Cryogenic Gravel Sampler*”. Technical report, U.S. Department of Agriculture, Forest Service, Pacific Northwest Forest and Range Experiment Station, Portland, OR.
- Fanelli, R. M. and Lautz, L. K. (2008). “Patterns of Water, Heat, and Solute Flux through Streambeds around Small Dams”. *Groundwater*, 46(5):671–687.
- Fares, A., Alva, A. K., Nkedi-Kizza, P., and Elrashidi, M. A. (2000). “Estimation of soil hydraulic properties of a sandy soil using capacitance probes and Guelph permeameter”. *Soil Sci*, 165(10):768–777.
- Fleckenstein, J. H., Stefan, K., Hannah, D. M., and Boano, F. (2010). “Groundwater surface water interactions: New methods and models to improve understanding of processes and dynamics”. *Adv Water Resour*, 33(11):1291–1295.
- Forkuor, G., Hounkpatin, O. K., Welp, G., and Thiel, M. (2017). “High resolution mapping of soil properties using remote sensing variables in South-Western Burkina Faso: a comparison of machine learning and multiple linear regression models”. *PLoS One*, 12(1):e0170478.
- Forsman, K. J. (2000). “*Contaminant Transport in Non-Uniform Streams and Streambeds*”. Ph.D Thesis, Uppsala University, Villavägen, Sweden.
- Fox, A., Laube, G., Schmidt, C., Fleckenstein, J. H., and Arnon, S. (2016). “The effect of losing and gaining flow conditions on hyporheic exchange in heterogeneous streambeds”. *Water Resour Res*, 52(9):7460–7477.
- Fox, G. A. and Durnford, D. S. (2003). “Unsaturated hyporheic zone flow in stream/aquifer conjunctive systems”. *Adv Water Resour*, 26:989–1000.
- Gajendragad, M., Naganna, C., Ranganna, G., Gurappa, K., Nayak, I., and Handrakantha, G. (1986). “Saltwater intrusion and related problems in South Kanara - A case study”.

- In Gorelick, S., eds, *Conjunctive water use* (Proceedings of the Budapest Symposium), pp. 231–239, Oxfordshire. IAHS.
- Garde, R. J. and Raju, K. G. R. (2010). “*Mechanics of Sediment Transportation and Alluvial Stream Problems*”. New Age International, New Delhi, third edition.
- Garrett, C. G., Vulava, V. M., Callahan, T. J., and Jones, M. L. (2012). “Groundwater surface water interactions in a lowland watershed: source contribution to streamflow”. *Hydrol Process*, 26(21):3195–3206.
- Gates, T. K., Cody, B. M., Donnelly, J. P., Herting, A. W., Bailey, R. T., and Mueller Price, J. (2009). “Assessing Selenium Contamination in the Irrigated Stream-Aquifer System of the Arkansas River, Colorado”. *J Environ Qual*, 38(6):2344.
- Genereux, D. P., Leahy, S., Mitasova, H., Kennedy, C. D., and Corbett, D. R. (2008). “Spatial and temporal variability of streambed hydraulic conductivity in West Bear Creek, North Carolina, USA”. *J Hydrol*, 358(3-4):332–353.
- Gerecht, K. E., Cardenas, M. B., Guswa, A. J., Sawyer, A. H., Nowinski, J. D., and Swanson, T. E. (2011). “Dynamics of hyporheic flow and heat transport across a bed-to-bank continuum in a large regulated river”. *Water Resour Res*, 47(3).
- Ghasemi, A. and Zahediasl, S. (2012). “Normality tests for statistical analysis: a guide for non-statisticians”. *Int J Endocrinol*, 10(2):486.
- Ghorbani, H., Kashi, H., Hafezi Moghadas, N., and Emamgholizadeh, S. (2015). “Estimation of soil cation exchange capacity using multiple regression, artificial neural networks, and adaptive neuro-fuzzy inference system models in Golestan Province, Iran”. *Commun soil sci plant analy*, 46(6):763–780.
- Goovaerts, P. (1997). “*Geostatistics for natural resources evaluation*”. Oxford University Press, New York.
- Goovaerts, P. (1999). “Geostatistics in soil science: state-of-the-art and perspectives”. *Geoderma*, 89(1):1–45.

- Gordon, N. D., McMahon, T. A., Finlayson, B. L., Gippel, C. J., and Nathan, R. J. (2004). “*Stream Hydrology: An Introduction for Ecologists*”. second edition, John Wiley and Sons, West Sussex, England.
- Gowda, C. C. and Mayya, S. (2015). “Evaluation of the Small Storage Reservoirs during its Operation in Series for Non Monsoon Periods”. *Aquatic Proc.*, 4:1150 – 1154.
- Grekousis, G., Manetos, P., and Photis, Y. N. (2013). “Modeling urban evolution using neural networks, fuzzy logic and GIS: The case of the Athens metropolitan area”. *Cities*, 30:193–203.
- Gu, C., Hornberger, G. M., Mills, A. L., Herman, J. S., and Flewelling, S. A. (2007). “Nitrate reduction in streambed sediments: Effects of flow and biogeochemical kinetics”. *Water Resour Res*, 43(12):W12413.
- Gunduz, O. (2007). “The influence of stream bed hydraulic conductivity on sustaining baseflow in rivers”. *Water Sci. Technol.*, 56(1):259–266.
- Gupta, H. V., Kling, H., Yilmaz, K. K., and Martinez, G. F. (2009). “Decomposition of the mean squared error and NSE performance criteria: Implications for improving hydrological modelling”. *J Hydrol*, 377(1):80–91.
- Hamill, L. and Bell, F. G. (2013). “Groundwater resource development”. Butterworth, London.
- Hannula, S. and Poeter, E. (1995). “*Temporal and spatial variations of hydraulic conductivity in a streambed in Golden Colorado*”. Technical report, Colorado State University, Fort Collins.
- Hansen, W. F. (1987). “Some Applications of Flood Frequency and Risk Information in Forest Management”. In *Application of frequency and risk in water resources*, pp. 219–226. Springer Netherlands, Dordrecht.
- Happ, S. C., Rittenhouse, G., and Dobson, G. (1940). “*Some principles of accelerated stream and valley sedimentation*”. Technical report, U.S Department of Agriculture, Washington D. C.

- Harvey, J. W. and Bencala, K. E. (1993). “The Effect of streambed topography on surface-subsurface water exchange in mountain catchments”. *Water Resour Res*, 29(1):89–98.
- Hatch, C. E., Fisher, A. T., Ruehl, C. R., and Stemler, G. (2010). “Spatial and temporal variations in streambed hydraulic conductivity quantified with time-series thermal methods”. *J Hydrol*, 389(3-4):276–288.
- Heritage, G. L., Birkhead, A. L., Broadhurst, L. J., and Harnett, B. R. (2009). “The Influence of Flooding on the Erodibility of Cohesive Sediments along the Sabie River, South Africa”. In Smith, N. D. and Rogers, J., editors, *Fluvial Sedimentology VI*, pp 131–145. Blackwell Publishing Ltd., Oxford, UK.
- Hester, E. T. and Doyle, M. W. (2008). “In-stream geomorphic structures as drivers of hyporheic exchange”. *Water Resour Res*, 44(3):W03417.
- Holland, J. F., Martin, J. F., Granata, T., Bouchard, V., Quigley, M., and Brown, L. (2004). “Effects of wetland depth and flow rate on residence time distribution characteristics”. *Ecol Eng*, 23(3):189–203.
- Huang, Y., Zhou, Z., Guo, Q., Tang, Y., and Lu, W. (2014). “Factors affecting the measurement of the vertical hydraulic conductivity of a streambed sediment using standpipe tests”. *Hydrol Process*, 28(20):5204–5211.
- Hvorslev, M. J. (1951). “*Time lag and soil permeability in ground-water observations*”. Technical report, US Army Corps of Engineers, Waterways Experimental Station, Vicksburg, Mississippi.
- Irvine, D. J., Cranswick, R. H., Simmons, C. T., Shanafield, M. A., and Lautz, L. K. (2015). “The effect of streambed heterogeneity on groundwater-surface water exchange fluxes inferred from temperature time series”. *Water Resour Res*, 51(1):198–212.
- ISO/TS.17892-11 (2004). “*Geotechnical investigation and testing – Laboratory testing of soil – Part 11: Determination of permeability by constant and falling head*”. Technical report, International Organization for Standardization, Switzerland.

- Iwata, T., Nakano, S., and Inoue, M. (2003). "Impacts of Past Riparian Deforestation on Stream Communities in a Tropical Rain Forest in Borneo". *Ecol Appl*, 13(2):461–473.
- Jackson, W. L. (1981). "*Bed material routing and streambed composition in alluvial channels*". Ph.D thesis, Oregon State University, Corvallis, USA.
- James, L. A., Watson, D. G., and Hansen, W. F. (2007). "Using LiDAR data to map gullies and headwater streams under forest canopy: South Carolina, USA". *Catena*, 71(1):132–144.
- Jana, R. B., Mohanty, B. P., and Springer, E. P. (2008). "Multiscale Bayesian neural networks for soil water content estimation". *Water Resour Res*, 44(8).
- Jang, C.-s. and Liu, C.-W. (2004). "Geostatistical analysis and conditional simulation for estimating the spatial variability of hydraulic conductivity in the Choushui River alluvial fan, Taiwan". *Hydrol Process*, 18(7):1333–1350.
- Jang, C.-S. and Liu, C.-W. (2005). "Contamination potential of nitrogen compounds in the heterogeneous aquifers of the Choushui River alluvial fan, Taiwan". *J Contam Hydrol*, 79(3-4):135–155.
- Jiang, W., Song, J., Zhang, J., Wang, Y., Zhang, N., Zhang, X., Long, Y., Li, J., and Yang, X. (2015). "Spatial variability of streambed vertical hydraulic conductivity and its relation to distinctive stream morphologies in the Beiluo River, Shaanxi Province, China". *Hydrogeol J*, 23(7):1617–1626.
- Jiang, X.-W., Wan, L., Cardenas, M. B., Ge, S., and Wang, X.-S. (2010). "Simultaneous rejuvenation and aging of groundwater in basins due to depth-decaying hydraulic conductivity and porosity". *Geophys Res Lett*, 37(5):L05403.
- Johnston, K., Ver Hoef, J. M., Krivoruchko, K., and Lucas, N. (2001). "*Using ArcGIS geostatistical analyst*". ESRI Redlands.

- Kalbus, E., Reinstorf, F., and Schirmer, M. (2006). “Measuring methods for Groundwater, Surface water and their Interactions: A Review”. *Hydrol Earth Syst Sc*, 10(6):873–887.
- Kao, L. S. and Green, C. E. (2008). “Analysis of variance: is there a difference in means and what does it mean?”. *J. Surg. Res*, 144(1):158–170.
- Katsuyama, M., Tani, M., and Nishimoto, S. (2010). “Connection between streamwater mean residence time and bedrock groundwater recharge/discharge dynamics in weathered granite catchments”. *Hydrol Process*, 24(16):2287–2299.
- Kelly, S. E. and Murdoch, L. C. (2003). “Measuring the Hydraulic Conductivity of Shallow Submerged Sediments”. *Groundwater*, 41(4):431–439.
- King, G. and Wood, R. (1994). “The impact of earthquakes on fluids in the crust”. *Ann Di Geofis*, 37(6):1453–1460.
- Kirkwood, C., Cave, M., Beamish, D., Grebby, S., and Ferreira, A. (2016). “A machine learning approach to geochemical mapping”. *J Geochem Explor*, 167:49–61.
- Kitanidis, P. K. (1997). “*Introduction to Geostatistics*”. Cambridge University Press, Cambridge.
- Kodešová, R., Šimunek, J., Nikodem, A., and Jirku, V. (2010). “Estimation of the Dual-Permeability Model Parameters using Tension Disk Infiltrometer and Guelph Permeameter”. *Vadose Zo J*, 9(2):213.
- Landon, M. K., Rus, D. L., and Harvey, F. E. (2001). “Comparison of Instream Methods for Measuring Hydraulic Conductivity in Sandy Streambeds”. *Groundwater*, 39(6):870–885.
- Lassetre, N. and Harris, R. (2001). “*The geomorphic and ecological influence of large woody debris in streams and rivers*”. University of California, Berkeley.

- Lee, D., Elrick, D., Reynolds, W., and Clothier, B. (1985). "A comparison of three field methods for measuring saturated hydraulic conductivity". *Can J Soil Sci*, 65(3):563–573.
- Lee, J.-Y., Lim, H., Yoon, H., and Park, Y. (2013). "Stream Water and Groundwater Interaction Revealed by Temperature Monitoring in Agricultural Areas". *Water*, 5(4):1677–1698.
- Leek, R., Wu, J. Q., Wang, L., Hanrahan, T. P., Barber, M. E., and Qiu, H. (2009). "Heterogeneous characteristics of streambed saturated hydraulic conductivity of the Touchet River, South Eastern Washington, USA". *Hydrol Process*, 23(8):1236–1246.
- Leuenberger, M. and Kanevski, M. (2015). "Extreme learning machines for spatial environmental data". *Comput Geosci*, 85:64–73.
- Levene, H. (1960). "Robust tests for equality of variances". In Olkin, I., eds, *Contributions to Probability and Statistics: Essays in Honor of Harold Hotelling*, pp 278–292. Stanford University Press, PA, California.
- Li, J. and Heap, A. D. (2008). "A review of spatial interpolation methods for environmental scientists". *Geoscience Australia*, Record 2008/23, 137pp
- Lilliefors, H. W. (1967). "On the Kolmogorov-Smirnov test for normality with mean and variance unknown". *J Am Stat Assoc*, 62(318):399–402.
- Lindgren, R. J. and Landon, M. K. (2000). "*Effects of ground-water withdrawals on the Rock River and associated valley aquifer, eastern Rock County, Minnesota*". Technical report, USGS, Mounds View, MN.
- Liu, D., Zhao, J., Chen, X., Li, Y., Weiyan, S., and Feng, M. (2018). "Dynamic processes of hyporheic exchange and temperature distribution in the riparian zone in response to dam-induced water fluctuations". *Geosci J*, pp 1–11.

- Lu, C., Chen, X., Cheng, C., Ou, G., and Shu, L. (2012). “Horizontal hydraulic conductivity of shallow streambed sediments and comparison with the grain-size analysis results”. *Hydrol Process*, 26(3):454–466.
- MacDonald, A., Maurice, L., Dobbs, M., Reeves, H., and Auton, C. (2012). “Relating in situ hydraulic conductivity, particle size and relative density of superficial deposits in a heterogeneous catchment”. *J Hydrol*, 434:130–141.
- Makaske, B. (2001). “Anastomosing rivers: a review of their classification, origin and sedimentary products”. *Earth-Science Rev*, 53(3-4):149–196.
- Malmon, D. V., Reneau, S. L., and Dunne, T. (2004). “Sediment sorting and transport by flash floods”. *J Geophys Res: Earth Sur*, 109:F02005.
- Massey Jr, F. J. (1951). “The Kolmogorov-Smirnov test for goodness of fit”. *J Am Stat Assoc*, 46(253):68–78.
- Matsuda, I. (2004). “River Morphology and Channel Processes”. In Dooge, J. C., eds, *Fresh Surface Water*. EOLSS, UNESCO.
- Mazumder, S. (2004). “River Behaviour Upstream and Downstream of Hydraulic Structures”. In *Int. Conf. on Hydraulic Engineering: Research and Practice*, pp. 253–263, Roorkee. Dept. of Civil Engineering, IIT, Roorkee.
- McKenzie-Smith, F. J., Bunn, S. E., and House, A. P. N. (2006). “Habitat dynamics in the bed sediments of an intermittent upland stream”. *Aquat Sci*, 68(1):86–99.
- Menció, A., Galán, M., Boix, D., and Mas-Pla, J. (2014). “Analysis of stream–aquifer relationships: A comparison between mass balance and Darcy’s law approaches”. *J Hydrol*, 517:157–172.
- Messina, A. and Biggs, T. (2016). “Contributions of human activities to suspended sediment yield during storm events from a small, steep, tropical watershed”. *J Hydrol*, 538:726–742.

- Moran, P. A. (1948). "The interpretation of statistical maps". *J R Stat Soc Ser B*, 10(2):243–251.
- Murdoch, L. C. and Kelly, S. E. (2003). "Factors affecting the performance of conventional seepage meters". *Water Resour Res*, 39(6):n/a–n/a.
- Nie, J., Gang, D. D., Benson, B. C., and Zappi, M. E. (2012). "Nonpoint Source Pollution". *Water Environ Res*, 84(10):1642–1657.
- Niehoff, D., Fritsch, U., and Bronstert, A. (2002). "Land-use impacts on storm-runoff generation: scenarios of land-use change and simulation of hydrological response in a meso-scale catchment in SW-Germany". *J Hydrol*, 267(1-2):80–93.
- Nowinski, J. D., Cardenas, M. B., and Lightbody, A. F. (2011). "Evolution of hydraulic conductivity in the floodplain of a meandering river due to hyporheic transport of fine materials". *Geophys Res Lett*, 38(1):L01401.
- Obana, M., Chibana, T., and Tsujimoto, T. (2014). "Characteristics of subsurface water flow influenced by formation process of gravel bar". In Schleiss, A. J., de Cesare, G., Franca, M. J., and Pfister, M., eds, *River Flow 2014*, pp. 1187–1193. CRC Press.
- Partington, D., Therrien, R., Simmons, C. T., and Brunner, P. (2017). "Blueprint for a coupled model of sedimentology, hydrology, and hydrogeology in streambeds". *Rev. Geophys.*, 55(2):287–309.
- Permeameter, G.U.E.L.P.H (2012). "*Guelph Permeameter – Operating Instructions (2800K1)*". Technical report, Santa Barbara, CA.
- Polyakov, V. O., Nichols, M. H., McClaran, M. P., and Nearing, M. A. (2014). "Effect of check dams on runoff, sediment yield, and retention on small semiarid watersheds". *J Soil Water Conserv*, 69(5):414–421.
- Prince, K. R. (1984). "*Streamflow Augmentation at Fosters Brook, Long Island, New York: A Hydraulic Feasibility Study*". Technical report, U.S. Geological Survey, Virginia.

- Putty, M. and Prasad, R. (2000). "Runoff processes in headwater catchments - An experimental study in Western Ghats, South India". *J Hydrol*, 235(1):63–71.
- Quinn, J. M., Croker, G. F., Smith, B. J., and Bellingham, M. A. (2009). "Integrated catchment management effects on flow, habitat, instream vegetation and macroinvertebrates in Waikato, New Zealand, hill-country streams". *New Zeal J Mar Freshw Res*, 43(3):775–802.
- Rana, S. M., Scott, D. T., and Hester, E. T. (2017). "Effects of in-stream structures and channel flow rate variation on transient storage". *J Hydrol*, 548:157–169.
- Rehg, K. J., Packman, A. I., and Ren, J. (2005). "Effects of suspended sediment characteristics and bed sediment transport on streambed clogging". *Hydrol Process*, 19(2):413–427.
- Reid, C. E., Jerrett, M., Petersen, M. L., Pfister, G. G., Morefield, P. E., Tager, I. B., Raffuse, S. M., and Balmes, J. R. (2015). "Spatiotemporal prediction of fine particulate matter during the 2008 Northern California wildfires using machine learning". *Environ Sci Tech*, 49(6):3887–3896.
- Reid, I. and Frostick, L. E. (1987). "Flow dynamics and suspended sediment properties in arid zone flash floods". *Hydrol Process*, 1(3):239–253.
- Reynolds, W., Bowman, B., Brunke, R., Drury, C., and Tan, C. (2000). "Comparison of Tension Infiltrometer, Pressure Infiltrometer, and Soil Core Estimates of Saturated Hydraulic Conductivity". *Soil Sci Soc Am J*, 64(2):478.
- Reynolds, W. D. and Elrick, D. E. (1985). "In situ measurement of field-saturated hydraulic conductivity, sorptivity, and the [alpha]-parameter using the Guelph permeameter". *Soil Sci*, 140:292–302.
- Ronan, A. D., Prudic, D. E., Thodal, C. E., and Constantz, J. (1998). "Field study and simulation of diurnal temperature effects on infiltration and variably saturated flow beneath an ephemeral stream". *Water Resour Res*, 34(9):2137–2153.

- Rosenberry, D. O. (2000). "Unsaturated-zone wedge beneath a large, natural lake". *Water Resour Res*, 36(12):3401–3409.
- Rosenberry, D. O. (2008). "A seepage meter designed for use in flowing water". *J Hydrol*, 359(1-2):118–130.
- Rosenberry, D. O., Klos, P. Z., and Neal, A. (2012). "In situ quantification of spatial and temporal variability of hyporheic exchange in static and mobile gravel-bed rivers". *Hydrol Process*, 26(4):604–612.
- Rosenberry, D. O. and Pitlick, J. (2009). "Local-scale variability of seepage and hydraulic conductivity in a shallow gravel-bed river". *Hydrol Process*, 23(23):3306–3318.
- Rosenberry, D. O., Toran, L., and Nyquist, J. E. (2010). "Effect of surficial disturbance on exchange between groundwater and surface water in nearshore margins". *Water Resour Res*, 46(6):WR008755.
- Rosgen, D. L. (1994). "A classification of natural rivers". *Catena*, 22(3):169–199.
- Rosgen, D. L. (1996). "Applied River Morphology". Wildland Hydrology Books, Pagosa Springs, CO, second edition.
- Rosgen, D. L. (2001). "The Cross-Vane, W-Weir and J-Hook Vane Structures. their Description, Design and Application for Stream Stabilization and River Restoration". In Wetlands engineering and river restoration, pp. 1–22, Reston, VA. American Society of Civil Engineers.
- Ryan, R. J. and Boufadel, M. C. (2006). "Influence of streambed hydraulic conductivity on solute exchange with the hyporheic zone". *Environ Geol*, 51(2):203–210.
- Ryan, R. J. and Boufadel, M. C. (2007). "Evaluation of streambed hydraulic conductivity heterogeneity in an urban watershed". *Stoch Environ Res Risk Assess*, 21(4):309–16.
- Sabater, F., Butturini, A., Martí, E., Muñoz, I., Romaní, A., Wray, J., and Sabater, S. (2000). "Effects of riparian vegetation removal on nutrient retention in a Mediterranean stream". *J North Am Benthol Soc*, 19(4):609–620.

- Schneidewind, U., Thornton, S., Van De Vijver, E., Ingeborg, J., and Seuntjens, P. (2015). "Spatial Variability of Streambed Hydraulic Conductivity of a Lowland River". In *EGU General Assembly Conference*, page 5363. Copernicus, Vienna.
- Schumm, S. A., Mcwhorter, D. D., Sunada, D. K., and Watson, C. C. (1984). "*Incised Channels: Morphology, Dynamics, and Control*", Water Resources Publications, LLC, Colorado.
- Scott, D. (2000). "Soil wettability in forested catchments in South Africa; as measured by different methods and as affected by vegetation cover and soil characteristics". *J Hydrol*, 231-232:87–104.
- Sehgal, M., Garg, A., Suresh, R., and Dagar, P. (2012). "Heavy metal contamination in the Delhi segment of Yamuna basin". *Environ Monit Assess*, 184(2):1181–1196.
- Shapiro, S. S. and Wilk, M. B. (1965). "An analysis of variance test for normality (complete samples)". *Biometrika*, 52(3/4):591–611.
- Shepard, D. (1968). "A two-dimensional interpolation function for irregularly-spaced data". In *Proceedings of the 1968 23rd ACM National Conference*, pp. 517–524. ACM.
- Shetkar, R. V. and Mahesha, A. (2011a). "Tropical, Seasonal River Basin Development: Hydrogeological Analysis". *J Hydrol Eng*, 16(3):280–291.
- Shetkar, R. V. and Mahesha, A. (2011b). "Tropical, Seasonal River Basin Development through a Series of Vented Dams". *J Hydrol Eng*, 16(3):292–302.
- Shwetha, P. and Varija, K. (2013). "Soil water-retention prediction from pedotransfer functions for some Indian soils". *Arch Agro Soil Sci*, 59(11):1529–1543.
- Simonds, F. W. and Sinclair, K. A. (2002). "*Surface water-ground water interactions along the lower Dungeness River and vertical hydraulic conductivity of streambed sediments, Clallam County, Washington*". Technical report, US Geological Survey, Washington D. C.

- Simpson, S. C. and Meixner, T. (2012). “Modeling effects of floods on streambed hydraulic conductivity and groundwater-surface water interactions”. *Water Resour Res*, 48(2):W02515.
- Skalak, K., Pizzuto, J., and Hart, D. D. (2009). “Influence of small dams on downstream channel characteristics in Pennsylvania and Maryland: Implications for the long-term geomorphic effects of dam removal”. *J Am Water Resour Assoc*, 45(1):97–109.
- Snoussi, M., Haïda, S., and Imassi, S. (2002). “Effects of the construction of dams on the water and sediment fluxes of the Moulouya and the Sebou Rivers, Morocco”. *Reg Environ Change*, 3(1-3):5–12.
- Soares, M., Gunkel, G., and Grischek, T. (2012). “Comparison of established methods to determine infiltration rates in river banks and lake shore sediments”. In Malina, G. eds, *Groundwater Quality Sustainability*, chapter 19, pp. 229–247. CRC Press.
- Song, J., Chen, X., Cheng, C., Summerside, S., and Wen, F. (2007). “Effects of hyporheic processes on streambed vertical hydraulic conductivity in three rivers of Nebraska”. *Geophys Res Lett*, 34(7):L07409.
- Song, J., Chen, X., Cheng, C., Wang, D., Lackey, S., and Xu, Z. (2009). “Feasibility of grain-size analysis methods for determination of vertical hydraulic conductivity of streambeds”. *J Hydrol*, 375(3-4):428–437.
- Song, J., Chen, X., Cheng, C., Wang, D., and Wang, W. (2010). “Variability of streambed vertical hydraulic conductivity with depth along the Elkhorn River, Nebraska, USA”. *Chinese Sci Bull*, 55(10):992–999.
- Sophocleous, M. (2002). “Interactions between groundwater and surface water: the state of the science”. *Hydrogeol J*, 10(1):52–67.
- Springer, A. E., Petrouson, W. D., and Semmens, B. A. (1999). “Spatial and Temporal Variability of Hydraulic Conductivity in Active Reattachment Bars of the Colorado River, Grand Canyon”. *Groundwater*, 37(3):338–344.

- Stewardson, M., Datry, T., Lamouroux, N., Pella, H., Thommeret, N., Valette, L., and Grant, S. (2016). “Variation in reach-scale hydraulic conductivity of streambeds”. *Geomorphology*, 259:70 – 80.
- Su, G. W., Jasperse, J., Seymour, D., and Constantz, J. (2004). “Estimation of hydraulic conductivity in an alluvial system using temperatures”. *Groundwater*, 42(6):890–901.
- Tahmiscioglu, M. S., Nermin, A., Ekmekçi, F., and Durmus, N. (2007). “Positive and negative impacts of dams on the environment”. In *International Congress on River Basin Management*, pp. 759–769.
- Thomas, S. M., Neill, C., Deegan, L. A., Krusche, A. V., Ballester, V. M., and Victoria, R. L. (2004). “Influences of land use and stream size on particulate and dissolved materials in a small Amazonian stream network”. *Biogeochemistry*, 68(2):135–151.
- Tockner, K., Paetzold, A., Karaus, U., Claret, C., and Zettel, J. (2009). “Ecology of Braided Rivers”. In Smith, H. S., Best, J. L., Bristow, C. S., and Petts, G. E., eds, *Braided Rivers*, pp. 339–359. Blackwell Publishing Ltd., Oxford, UK.
- Tonina, D. and Buffington, J. M. (2009). “Hyporheic Exchange in Mountain Rivers I: Mechanics and Environmental Effects”. *Geography Compass*, 3(3):1063–1086.
- Tonina, D. and Buffington, J. M. (2011). “Effects of stream discharge, alluvial depth and bar amplitude on hyporheic flow in pool-riffle channels”. *Water Resour Res*, 47(8):W08508.
- Tonina, D., de Barros, F. P., Marzadri, A., and Bellin, A. (2016). “Does streambed heterogeneity matter for hyporheic residence time distribution in sand-bedded streams?”. *Adv Water Resour*, 96:120–126.
- Tóth, J. (1962). “A theory of groundwater motion in small drainage basins in central Alberta, Canada”. *J. Geophys Res*, 67(11):4375–4388.
- Trimble, S. W. (2008). “*Man-induced erosion on the southern Piedmont: 1700-1970*”. second edition, Soil Conservation Society of America, Ankeny.

- Twarakavi, N. K., Šimnek, J., and Schaap, M. (2009). “Development of pedotransfer functions for estimation of soil hydraulic parameters using support vector machines”. *Soil Sci Soc Am J*, 73(5):1443–1452.
- Ulrich, C., Hubbard, S. S., Florsheim, J., Rosenberry, D., Borglin, S., Trotta, M., and Seymour, D. (2015). “Riverbed Clogging Associated with a California Riverbank Filtration System: An Assessment of Mechanisms and Monitoring Approaches”. *J Hydrol*, 529:1740–1753.
- Valerio, A., Rajaram, H., and Zagona, E. (2010). “Incorporating Groundwater-Surface Water Interaction into River Management Models”. *Groundwater*, 48(5):661–673.
- Wang, W., Li, J., Feng, X., Chen, X., and Yao, K. (2011). “Evolution of stream-aquifer hydrologic connectedness during pumping - experiment”. *J Hydrol*, 402(3-4):401–414.
- Wang, W., Li, J., Wang, W., Chen, X., Cheng, D., and Jia, J. (2014). “Estimating streambed parameters for a disconnected river”. *Hydrol Process*, 28(10):3627–3641.
- Ward, A. D. and Trimble, S. W. (2003). “*Environmental hydrology*”. second edition, CRC Press, UK.
- Webster, R. and Oliver, M. A. (2007). “*Geostatistics for Environmental Scientists*”. second edition, John Wiley and Sons, West Sussex, England.
- Welch, B. L. (1947). “The generalization of student’s problem when several different population variances are involved”. *Biometrika*, 34(1/2):28–35.
- Welsch, D. J. (1991). “*Riparian forest buffers – function and design for protection and enhancement of water resources*”. Technical report, U.S. Dept. of Agriculture, Radnor, PA.
- Whelan, J. L. (2007). “*Hyphoreic zone hydraulic testing: River Tame, Birmingham, UK*”. M.Sc Thesis, University of Birmingham.

- Wohl, E. (2010). “*Mountain Rivers Revisited*”, Volume 19 of Water Resources Monograph. American Geophysical Union, Washington, D. C.
- Wörman, A., Packman, A. I., Marklund, L., Harvey, J. W., and Stone, S. H. (2007). “Fractal topography and subsurface water flows from fluvial bedforms to the continental shield”. *Geophys Res Lett*, 34(7):L07402.
- Wu, G., Shu, L., Lu, C., Chen, X., Zhang, X., Appiah-Adjei, E., and Zhu, J. (2015). “Variations of streambed vertical hydraulic conductivity before and after a flood season”. *Hydrogeol J*, 23(7):1603–1615.
- Wynn, T. and Mostaghimi, S. (2006). “The effects of vegetation and soil type on streambank erosion, southwestern Virginia, USA”. *J Am Water Resour Assoc*, 42(1):69–82.
- Yamada, H., Nakamura, F., Watanabe, Y., Murakami, M., and Nogami, T. (2005). “Measuring hydraulic permeability in a streambed using the packer test”. *Hydrol Process*, 19(13):2507–2524.
- Yule, C. M., Gan, J. Y., Jinggut, T., and Lee, K. V. (2015). “Urbanization affects food webs and leaf-litter decomposition in a tropical stream in Malaysia”. *Freshw Sci*, 34(2):702–715.
- Zhang, K., Wang, Z.-Y., and Liu, L. (2010). “The effect of riverbed structure on bed load transport in mountain streams”. In Dittrich, A., Koll, K., Aberle, J., and Geisenhainer, P., eds, *River Flow 2010*, pp. 863–870, Karlsruhe.
- Zhao, G., Mu, X., Wen, Z., Wang, F., and Gao, P. (2013). “Soil Erosion, Conservation, and Eco-Environment Changes in the Loess Plateau of China”. *L Degrad Dev*, 24(5):499–510.
- Zhou, Y., Ritzi, R. W., Soltanian, M. R., and Dominic, D. F. (2014). “The influence of streambed heterogeneity on hyporheic flow in gravelly rivers”. *Groundwater*, 52(2):206–216.

Zhu, H., Cheng, P., Zhong, B., and Wang, D. (2014). “The mechanisms of contaminants release due to incipient motion at sediment-water interface”. *Sci China Physics, Mech Astron*, 57(8):1563–1568.

Zume, J. and Tarhule, A. (2008). “Simulating the impacts of groundwater pumping on stream–aquifer dynamics in semiarid northwestern Oklahoma, USA”. *Hydrogeol J*, 16(4):797–810.

PUBLICATIONS BASED ON PRESENT RESEARCH WORK

Journal Articles

1. Raghavendra N. S., Deka, P. C., Ch, S., & Hansen, W. F. (2017). Factors influencing streambed hydraulic conductivity and their implications on stream–aquifer interaction: A conceptual review. *Environmental Science and Pollution Research*, 24(32), 24765-24789. DOI: 10.1007/s11356-017-0393-4
2. Raghavendra N. S., & Deka, P. C. (2018). Variability of streambed hydraulic conductivity in an intermittent stream reach regulated by Vented Dams: A case study. *Journal of Hydrology*, 562, 477-491. DOI: 10.1016/j.jhydrol.2018.05.006
3. Raghavendra N. S., & Deka, P. C. (2019). Artificial intelligence approaches for spatial modeling of streambed hydraulic conductivity. *Acta Geophysica*, 67(3), 891-903. DOI: 10.1007/s11600-019-00283-5

Conference Article

1. Raghavendra N. S., Deka, P. C (2016). “Influence of series of Vented Dam intersections on the Channel Processes: A Case Study in the Pavanje River Basin”. 21st International Conference on Hydraulics, Water Resources and River Engineering (ISH - HYDRO 2016 International), CWPRS, Pune.

Appendix



GUELPH Permeameter installed for measurement of hydraulic conductivity of streambed



Setting the reservoir knob of GUELPH permeameter



Recording the water level change in the permeameter column





View of Streambed between Vented dam 1 and 2



View of Streambed upstream of Vented dam 2



View of Vented Dam when gates are open in the month of May 2016



Soil sampling from streambed

CURRICULUM VITAE



Name:	SUJAY RAGHAVENDRA N
Permanent Address:	#25, 1 ST MAIN ROAD, 5 TH CROSS, 1 ST PHASE, BEML LAYOUT 5 TH STAGE, RAJARAJESHWARINAGAR, BANGALORE-560098
EDUCATION:	MASTER OF TECHNOLOGY (2012-14) Discipline: Water Resources Engineering and Management National Institute of Technology Karnataka, Surathkal, India BACHELOR OF ENGINEERING (2007-11) Discipline: Civil Engineering Bangalore Institute of Technology, Bangalore. (2007-2011) Affiliated to: Visvesvaraya Technological University, Belgaum.
Contact No.:	+91-9035219180
Email ID:	sujay.gopan@gmail.com ; sujayraghavendran@ymail.com
ORCID:	0000-0002-0482-1936
